# Anaerobic Digestion Kinetics of Batch Methanogenic and Electrogenic Systems

by

Steven Gregg Hart

A Dissertation Presented in Partial Fulfillment
of the Requirements for the Degree
Doctor of Philosophy

Approved April 2020 by the
Graduate Supervisory Committee:

César I Torres, Chair
Prathap Parameswaran
Bruce E Rittmann
Rosa Krajmalnik-Brown

ARIZONA STATE UNIVERSITY

May 2020

ABSTRACT

Eighty-two percent of the United States population reside in urban areas. The centralized treatment of the municipal wastewater produced by this population is a huge energy expenditure, up to three percent of the entire energy budget of the country. A portion of this energy is able to be recovered through the process of anaerobic sludge digestion. Typically, this technology converts the solids separated and generated during the wastewater treatment process into methane, a combustible gas that may be burned to generate electricity. Designing and optimizing anaerobic digestion systems requires the measurement of degradation rates for waste-specific kinetic parameters. In this work, I discuss the ways these kinetic parameters are typically measured. I recommend and demonstrate improvements to these commonly used measuring techniques. I provide experimental results of batch kinetic experiments exploring the effect of sludge pretreatment, a process designed to facilitate rapid breakdown of recalcitrant solids, on energy recovery rates. I explore the use of microbial electrochemical cells, an alternative energy recovery technology able to produce electricity directly from sludge digestion, as precise reporters of degradation kinetics. Finally, I examine a fundamental kinetic limitation of microbial electrochemical cells, acidification of the anode respiring biofilm, to improve their performance as kinetic sensors or energy recovery technologies.

ACKNOWLEDGMENTS

Completion of this dissertation was only possible through the support and help of many teachers, colleagues, friends, and family members over many years. I first became seriously interested in the biological sciences in Mr. Loveless's classes at Calloway County High School in my hometown of Murray, Kentucky. At Murray State University, under the thoughtful guidance of Dr. Tim Johnston and Dr. Chris Trzepacz, I had the opportunity to conduct my own microbiology research projects. TAing the microbiology lab was one of the highlights of my time as an undergraduate student. I particularly remember the field trip we'd take each semester to the local wastewater treatment plant. I remember being the most excited member of the tour group as a student and, later, an instructor during these trips.

After graduating with my bachelor's degree from Murray State, I worked at the Asian Rural Institute, a training center for integrated organic farming in rural Japan, through the Young Adult Service Corps. I cannot overstate the influence the many incredible people I worked with in Japan had on my values and career goals.

Before starting my graduate education, I was very fortunate to be able to work as a research technician in Dr. Eldon Geisert's lab at the Hamilton Eye Institute in Memphis, TN, studying the genetics of neurodegenerative diseases. In Dr. Geisert's lab I learned many new technical skills. Most importantly, while working with XiangDi, Justin, Joe, and Dr. Geisert, I learned how to be a valuable member of a research team.

I have Dr. Rittmann to thank for bringing me to Arizona State University. I reached out to him while working in Memphis more than a year before I would apply to ASU. He responded immediately and was kind and encouraging. I spent the next several months reading Rittmann and McCarty every day in my favorite coffee shop after work. Throughout my graduate Career, Dr. Rittmann has been an excellent mentor. I particularly appreciate the many opportunities he has given me to develop my teaching skills. When I finally joined the Swette Center, I found an incredibly supportive community working on a huge number of projects directly related to solving concrete problems. I would like to acknowledge a few specific individuals. Dr. Parameswaran patiently taught me the fundamentals of environmental engineering research and played a huge role in the direction of my dissertation research. Dr. Krajmalnik-Brown taught me how to present complex data in intuitive ways that precisely convey information, an extremely valuable skill. Drs. Michelle Young and Dongwon Ki have been invaluable colleagues and friends, and this dissertation would not have been completed without them. I count myself very lucky to have had the support and friendship of Megan Meinel, Carole Flores, Ethan Howley, and Diana Calvo. I appreciate all the effort of the researchers that contributed to the work presented here: Michelle Young, Ethan Howley, Anna Guerrero, Sharad Kumar Vellore Suresh, Michael Waddington, Jimmy Xu, Sarah Brown, Collette Wilson, Kaitlyn Alvarez, Sawyer Routt, Grant Gordon, and Zixuan Wang. I am very appreciative of all the support Diane Hagner and Sarah Arrowsmith have provided during my time in the Swette Center.

A few words are insufficient to express my gratitude to Dr. Torres, my advisor and committee chair. I can only describe some of the qualities that make him such an exceptional mentor. Dr. Torres would always make time to meet when I needed to talk about new results, the next experiment, or the next chapter. He would regularly help troubleshoot issues I had in the lab, such as problems with a new reactor design or a stubborn microbial culture. He encouraged me to "just try things out" in the lab, and would get excited with me when we got an unexpected result. He spent hours looking at confocal scans with me, just as convinced as I was that the next one would be the key we needed to finally understand what was going on. Since I joined his lab, it has always been clear that Dr. Torres was invested in my success. He's the kind of mentor I aspire to be, and I am proud and honored to have been a member of his lab.

I would like to thank my parents, John and Sharon, and my brother, Benjamin for all of their love and support. I'd also like to thank Daniel Roush for his friendship and advice over the years. Most of all, I would like to thank my wife, Olga. Since we first met in Dr. Johnson's groundwater remediation class, Olga has been a constant companion, an invaluable advisor, and my best friend. Her patience and support, more than anything else, is the reason I am here today presenting this dissertation.

I'd also like to acknowledge the financial support of Science Foundation Arizona, the NSF GRFP, the Biodesign Swette Center for Environmental Biotechnology, ASU School of Life Sciences, NSF grant #1335884, ONR grant #N00141512702, and the Center for Bio-mediated and Bio-inspired Geotechnics.

TABLE OF CONTENTS

Page

LIST OF TABLES ..... xii

LIST OF FIGURES ..... xiv

PREFACE ..... xxvi

CHAPTER

1 INTRODUCTION ..... 1

1.1 Urbanization and the Built Environment ..... 1

1.2 Constituents of Municipal Wastewater and Sewage ..... 1

1.3 Wastewater Treatment in the United States ..... 3

1.4 Wastewater Treatment ..... 4

1.5 Sludge Stabilization and Treatment ..... 6

1.6 Anaerobic Digestion ..... 8

1.6.1 Economic Benefits of Anaerobic Digestion ..... 8

1.6.2 The Biochemical Process of Anaerobic Digestion ..... 9

1.6.3 Quantifying Anaerobic Digestion Rates ..... 11

1.6.4 Anaerobic Digestion in Microbial Electrochemical Cells ..... 13

2 TESTS TO MEASURE ANAEROBIC DIGESTION KINETICS ..... 16

2.1 Processes in Anaerobic Digestion ..... 16

CHAPTER Page

2.2 Anaerobic Digestion in Microbial Electrochemical Cells ..... 18

2.3 Batch Tests Used to Quantify Anaerobic Digestion Kinetics..... 20

2.4 Kinetic Expressions Used to Model Hydrolysis ..... 24

2.4.1 First-Order Kinetics ..... 27

2.4.2 Monod Kinetics..... 27

2.4.3 Gompertz Kinetics ..... 28

2.5 Limitations to Simple Kinetic Approaches..... 30

3 THE EFFECTS OF PRE-TREATMENT ON THE KINETICS OF WASTE-ACTIVATED SLUDGE DIGESTION..... 32

3.1 Introduction..... 34

3.2 Materials and Methods..... 37

3.2.1 Municipal Wastewater Sludge and Pretreatment Techniques ..... 37

3.2.2 Modified BMP Assays..... 37

3.2.3 Chemical Analyses..... 39

3.2.4 Calculations..... 40

3.3 Results and Discussion ..... 43

3.3.1 Alkaline Pretreatment Converted the Greatest Proportion of PCOD to SSCOD ..... 43

3.3.2 Thermal Pretreatment Resulted in the Greatest Ultimate Methane Recovery and the Greatest Risk of Inhibition..... 44

CHAPTER Page

3.3.3 Hydrolysis Rate Constants Derived from Methane Alone are Overestimated After Pretreatment ..... 47

3.4 Conclusions ..... 50

4 CALCULATING KINETIC PARAMETERS FROM BATCH ANAEROBIC DIGESTION OF MIXED MUNICIPAL SLUDGES WITH THERMALLY PRE-TREATED WAS ..... 52

4.1 Introduction ..... 54

4.2 Materials and Methods ..... 56

4.2.1 Sludge Sampling and Pretreatment ..... 56

4.2.2 Batch Methanogenic Digestion Loading ..... 57

4.2.3 Gas Measurements ..... 57

4.2.4 Analytical Methods ..... 58

4.2.5 Modeling First-order Hydrolysis Constants and Maximum Rates of Recovery ..... 59

4.3 Results and Discussion ..... 61

4.3.1 Effects of Pretreatment ..... 61

4.3.2 Methane Recovery and Intermediate Hydrolysis Product Accumulation ..... 63

4.3.3 Calculation of First-order Rate Constants ..... 68

4.4 Conclusions ..... 72

CHAPTER Page

5 MODEL SUBSTRATES YIELD COMPLEX RECOVERY PATTERNS DURING METHANOGENIC AND ELECTROGENIC BATCH ANAEROBIC DIGESTION ..... 74

5.1 Introduction ..... 76

5.2 Materials and Methods ..... 80

5.2.1 Inoculum ..... 80

5.2.2 Mineral Medium ..... 81

5.2.3 Batch Methanogenic Digestion Tests ..... 81

5.2.4 Microbial Electrolysis Cell Tests ..... 82

5.2.5 Volatile Fatty Acid Analysis ..... 83

5.2.6 pH Measurements and Adjustments ..... 83

5.2.7 Hydrolysis Modeling ..... 84

5.3 Results and Discussion ..... 84

5.3.1 Multiple Recovery Events are Observed From the Digestion of Casein and Cellulose ..... 84

5.3.2 Most Recovery Events Corresponded to VFA Consumption. ..... 86

5.3.3 Hydrolysis of Particulate Substrates Occurred Rapidly ..... 91

5.3.4 Methane or Current Alone Were Not Good Indicators of the Rate of Particulate Hydrolysis ..... 93

5.4 Conclusions ..... 95

CHAPTER Page

6 KINETICS OF METHANOGENIC AND ELECTROGENIC BATCH ANAEROBIC DIGESTION OF MIXED MUNICIPAL SLUDGES ..... 96

6.1 Introduction ..... 98

6.2 Methods ..... 101

6.2.1 Sludge Sampling ..... 101

6.2.2 MEC Biofilm Growth ..... 101

6.2.3 Methanogenic and Electrogenic Batch Digestions ..... 102

6.2.4 Chemical Analysis ..... 103

6.2.5 First-Order Kinetic Rate Models ..... 104

6.3 Results and Discussion ..... 105

6.3.1 Initial SSCOD and VFA Accumulation Persists Longer in Electrogenic Digestions ..... 105

6.3.2 Particulate Hydrolysis and SSCOD Hydrolysis Occurred at Similar Rates in Methanogenic and Electrogenic Digestions ..... 106

6.3.3 Patterns of Electrogenic and Methanogenic Hydrolysis Rate Show Multiple Events ..... 109

6.3.4 Modeling Sludge Hydrolysis Rates Using Multiple Gompertz Kinetic Expressions ..... 112

6.4 Conclusions ..... 114

7 CHALLENGES TO OPTICALLY QUANTIFYING PH GRADIENTS IN GEOBACTER SULFURREDUCENS BIOFILMS ..... 116

CHAPTER Page

7.1 Introduction ..... 118

7.1.1 pH Limitations in Anode Respiring Biofilms ..... 118

7.1.2 Previous Measurements of *Geobacter* Anode Biofilm pH Gradients ..... 121

7.1.3 C-SNARF-4 as a pH Indicator In and Around Biomass ..... 123

7.2 Materials and Methods ..... 126

7.2.1 ARB cultivation in the Microbial Electrochemical Flow Cell (MEFC) ..... 126

7.2.2 Slide Assays ..... 128

7.2.3 Fluorescent Dyes Used ..... 128

7.2.4 Microscopic Procedure ..... 129

7.3 Results and Discussion ..... 130

7.3.1 Geobacter spp. Biofilm Growth and Imaging ..... 130

7.4 Geobacter sulfurreducens spp. Biomass Distortion Effects on C-SNARF-4 ..... 135

7.4.1 HPTS as a potential pH indicator in Geobacter sulfurreducens biofilms ..... 140

7.5 Conclusions ..... 142

8 SUMMARY AND SIGNIFICANCE ..... 143

8.1 Summary of Presented Work ..... 143

8.2 Significance of Reported Work ..... 146

CHAPTER Page

WORKS CITED ..... 148

APPENDIX

A Supplimentary Figures ..... 161

LIST OF TABLES

Table Page

2.1 Kinetics Used in Selected Batch Anaerobic Digestion Studies.....26

3.1 Ultimate COD Recoveries ($P_{max}$) and Hydrolysis Constants ($K_{hyd}$) Calculated Equation 3 and Equation 4. $P_{start}$ Values Used are Shown for Modeled Product Accumulation. Fitted Non-Biodegradable Solids Fractions, VSSNBD, are Shown for Modeled VSS Destruction. R-Squared Values are Shown for the Measured and Modeled Data.....49

4.1 First-Order Kinetic Parameters for Batch Methanogenic Digestions With and Without Pretreatment and BES. Details About the Modeled and Measured Parameters May be Found in Section 2.5 of the Methods. R-Squared Values are Reported for the Fit Between Modeled and Measured Data.....71

5.1 Initial Loadings of All BMP and MEC Experiments. F/M Loadings are Based Upon the Ratio of the Initial Substrate Concentration In Gcod/L to the ADS Inoculum Mass In Gvss/L. MEC and BMP Experiments Were Conducted Sequentially. The Overall Loadings Vary Due to Slight Differences in the Solids Content of the ADS Used In Each Case. BMPs And MECs Loaded With Casein and Cellulose Contained Equal Concentrations of Each Substrate On a COD Basis.....82

6.1 Calculated Hydrolysis Constants and Ultimate Product Recovery for Methanogenic and Electrogenic Digestions. Values are Calculated for Methane or Current, Methane or Current + SSCOD, Methane or Current + VFA, and VSS Destruction. Error Represents ± One Standard Error (N=3).....109

LIST OF FIGURES

Figure Page

1.1 Process Flow Diagram for a Typical Municipal Wastewater Treatment System With Anaerobic Digestion of Primary and Secondary Sludges.....4

1.2 Schematic Diagram of the Parallel and Sequential Biochemical Conversions During Anaerobic Digestion.....10

2.1 Schematic Diagram of the Sequential and Parallel Reactions Occurring During Anaerobic Digestion. Boxes Indicate the Commonly Measured Quantities Volatile Suspended Solids (Blue), Semi-Soluble Chemical Oxygen Demand (Red), and Volatile Fatty Acids (Green).....17

2.2 Schematic Diagram of a Microbial Electrolysis Cell (MEC).....19

2.3 Example Model Fittings From First-Order, Monod, and Gompertz Kinetics for Methane Accumulation in a BMP Test. Solid Black Points Indicate Cumulative Methane Produced from a BMP Tests. Dashed Black Lines Represent Modeled Cumulative Methane. Gray Lines Represent the Rate of Methane Accumulation. Dashed Gray Lines Represent Modeled Methane Recovery Rates.....30

3.1 Initial Conditions for Inoculated Batch Digestions Fed With Pretreated and Unpretreated WAS. Shown are VSS, SSCOD, and VFA Concentrations, Along With Ph at the Start of Each Experiment. Error Bars Represent ± One Standard Error.....43

Figure Page

3.2 Volatile Suspended Solids, SSCOD, Cumulative CH4 Production, and pH for BMPs of Control, Alkaline Pretreated, or Thermally Pretreated WAS. VSS, SSCOD, and pH Show All Measurements From Four Biological Replicates of Each Condition and Error Bars Represent ± One Standard Error of the Technical Replicates of Each Sample. Cumulative CH4 Shows the Average of Four Biological Replicates; Error Bars Represent ± One Standard Deviation.....45

3.3 The Combined Total Volatile Fatty Acid Concentration as Determined by HPLC Analysis of Samples Taken From All Biological Replicates.....46

3.4 Modeled Product Formation and VSS Solubilization With First-Order Approximations for BMPs With No Pretreatment, Alkaline Pretreatment and Thermal Pretreatment of WAS. Points are Measured Quantities; Dashed Lines are Modeled Data Using Equation 3 (CH4, CH4+SSCOD, CH4+VFA) And Equation 4 (Net VSS).....48

4.1 Distribution of Loaded Substrate Between the Solid and Liquid Fractions of Primary Sludge (PS), Waste Activated Sludge (WAS), and Thermally Pretreated Waste Activated Sludge (T-WAS). Error Bars Represent ± One Standard Error (N=3) .....62

Figure Page

4.2 SSCOD, VSS, Total VFA, and Cumulative Methane for Batch Methanogenic Digestions With and Without Pretreatment. The Insets Show the First 16 Days of the Respective Data. Red Lines Represent Batch Methanogenic Digestions With Thermally Pretreated WAS. Black Lines Represent Batch Methanogenic Digestions With No Pretreatment. Error Bars Represent ± One Standard Error (N=3)..... 64

4.3. SSCOD, VSS, Total VFA, and Cumulative Methane for Batch Methanogenic Digestions With and Without Pretreatment With BES Added to Inhibit Methanogenesis. Red Lines Represent Batch Methanogenic Digestions With Thermally Pretreated WAS. Black Lines Represent Batch Methanogenic Digestions With No Pretreatment. Error Bars Represent ± One Standard Error (N=3)..... 67

4.4 Modeled Product Formation With First-Order Approximations for Batch Methanogenic Digestions. Rates are Shown for VSS Destruction, Methane Accumulation, Methane + SSCOD, and Methane + VFAs. Circles Represent Measured Quantities; Error Bars Indicate ± One Standard Error (N=3). Dashed Lines Represent Modeled First Order Reactions Fitted to the Measured Data; Shaded Areas Represent ± One Standard Error Of Modeled Data (N=3) ..... 70

Figure Page

5.1 Examples of Batch Anaerobic Digestion Experiments Carried Out in MECs. The Top Panel Shows Results From Cellulose Digestion In an MEC With a High Surface Area Carbon Fiber Anode and a High Substrate Loading. The Bottom Panel Shows the Results of Casein Digestion In Mecs At Higher (Black) and Lower (Blue) Loadings. In Both Panels, Dashed Lines Indicate MECs That Were Run Without Substrate to Measure Endogenous Biofilm Decay.....79

5.2 COD Cumulative Recovery and Recovery Rates for MEC and BMP Experiments. Dashed Lines Represent Current or Methane Production Rates In gCOD/L-D (Right Axis). Solid Lines Represent Cumulative COD Recovery as a Fraction of Loaded COD (Left Axis). Values of Control MEC Digestions and BMPs Conducted With Inoculum But Without Substrate Have Been Subtracted From All Datasets.....85

5.3 Individual VFA Concentrations Over Time In MEC and BMP Experiments. Dashed Lines Indicate Acetate, Propionate, Isobutyrate, Butyrate, Isovalerate, and Valerate Concentrations Over Time as gCOD $L^{-1}$ (Left Axis). Solid Black Lines Indicate Current or Methane Recovery Rates In gCOD $L^{-1}d^{-1}$ (Right Axis).....87

5.4 Bulk Liquid pH Measurements for MEC and BMP Experiments. Solid Points With Solid Lines Indicate MEC pH Values. Open Points With Dashed Lines Indicate BMP Experiments.....90

Figure Page

5.5 Recovery of Current, Methane, and VFAs as Fractions of Loaded COD. Dashed Lines Represent Cumulative Coulombs for Mecs and Cumulative Methane for BMPs. Dotted Lines Indicate the Sum of All VFAs Measured By HPLC. Solid Lines Indicate the Sum of Methane or Coulombs and VFAs.....92

5.6 Modeled COD Recovery Assuming First Order Kinetics. Open Circles Indicate Cumulative Coulombs or Methane. Dashed Lines Represent Coulombs or Methane Modeled. Solids Points Are the Sum of Recovered Methane or Coulombs and the Total Measured VFAs. Solid Lines Illustrate the Modeled Coulombs/Methane + VFAs.....94

6.1 VSS, SSCOD, VFA, Methane, and Circuited Electrons Recovery. Negative Control Values Have Been Averaged (N=3) and Subtracted for Each Dataset. Error Bars Represent One Standard Error (N=3 For Each). The Grey Region Accompanying the Cumulative Circuited Electron Graph Also Represents One Standard Error; Continuous Error Calculations are Possible Due to the Very High Number of Data Points (N=3 Reactors, >52,000 Points Each).....106

Figure Page

6.2 Modeled Product Formation With First-Order Approximations for Batch Methanogenic and Electrogenic Digestions. Fittings are Shown for VSS Destruction, Methane or Current Accumulation, Methane or Current + SSCOD, and Methane or Current + VFAs. Circles Represent Measured Quantities; Error Bars Indicate ± One Standard Error (N=3). Dashed Lines Represent Modeled First Order Reactions Fitted to the Measured Data; Shaded Areas Represent ± One Standard Error Of Modeled Data (N=3).....107

6.3 Total Carbohydrate Concentrations From Bulk Samples of Methanogenic and Electrogenic Digestions. ADS Controls are Shown With Dashed Lines. 0.192 gCOD/Mm Carbs as Glucose Was Used to Convert to Units of COD. Error Represents ± One Standard Error (N=3) ..... 111

6.4 Representative Model Fittings of an Individual Methanogenic and Electrogenic Batch Digestions From Cumulative Methane or Charge + VFA. Panels A-B Show Model Fittings for Cumulative Recovery Using Three Gompertz Curves (Yellow, Gray, Blue), The Sum of Individual Fittings (Red), and Results of Single First-Order Fitting (Green). Panels C-D Show Model Fittings for the Rates of Recovery for CH4 or Charge. Shown are Measured Rates (Black), Cumulative Modeled Rates From Three Components in Panels A-B (Red), and the Modeled Rate From a Single First-Order Fitting (Green).....114

7.1 Intermediate and Final Product Accumulation in Batch Methanogenic and Inhibited Electrogenic Reactors..... 119

Figure Page

7.2. Adapted From Marcus et al. 2011. Modeled pH Gradients Within Anode Respiring Biofilms Resulting From Decreasing Buffer Concentrations.....121

7.3. Schematic Diagram of the Microbial Electrochemical Flow Cell (MEFC). A Three-Electrode System is Used. The Anode is an Indium Tin Oxide Doped Glass Slide Positioned at the Top of the Flow Cell, Directly Under the Microscope Objective Lens. The Stainless-Steel Needle Through Which Media Exits the Flow Cell is Used as the Cathode, While an Ag/AgCl Reference Electrode is Ionically Connected With the System Via Another Stainless-Steel Needle. Anode Potentials are Poised With a Potentiostat.....127

7.4. Standard Curve of the pH-Dependent Emission Shift of C-SNARF-4. Measurements Were Performed on a Leica SP8 Using a 543nm Excitation Line With a 63x Oil-Immersion Objective. 30 mM Phosphate Buffers Titrated to Various pH Values Were Used as Standards Without Any Cellular or Matrix Components Present. Error Bars Represent ± One Standard Error (N=3). This Calibration Was Used for Slide Assays (Figure 7.9); A Separate Calibration Was Performed in the MEFC, Without Cellular Or Matrix Components, for Biofilm Imaging.....129

Figure Page

7.5. Biofilm Growth in the Microbial Electrochemical Flow Cell. (Top) Transmitted Light Images of Geobacter Sulfurreducens Biofilm Growing on an Indium Tin Oxide-Coated Glass Electrode at Two Different Current Densities. (Bottom Left) Current Produced During Biofilm Growth. (Bottom Right) Imaging Biofilms With the Leica TCS SP5 AOBS Spectral Confocal System in The W.C. Keck Bioimaging Lab.....131

7.6. High-Resolution Images of an Anode Respiring Biofilm Taken With the Leica TCS SP5 AOBS Spectral Confocal System in the W.C. Keck Bioimaging Lab With 63x a Dipping Objective at Different Distances From the Anode Surface. Fluorescence Probes for DNA (DAPI, Blue) and Plasma Membrane (F/M 4-64, Red) Were Used.....132

7.7. Results of a Series of pH Measurements On a Mature G. Sulfurreducens Biofilm. Black and Red Lines Represent pH Values Calculated From Ratiometric Measurements Using C-SNARF-4. The Glass Surface of the Electrode is At Z=0. Blue and Grey Lines Indicate the DAPI and Reflection Signals, Indications of Biomass Density. The Current Density of This Biofilm Was 4 A M-2 at the Time of Imaging.....134

Figure Page

7.8. Representative Images From C-SNARF-4 Calibration Curve With *Geobacter spp*. Biomass Grown With Fumarate as an Electron Acceptor. Panels A-C, E-G, I-K are Single Frames Used for pH Analysis and Have Been Adjusted for Contrast and Brightness Using the Contrast/Brightness and "Sharpen" Functions in Imagej. Yellow Boxes Represent Measurement Areas; Two With Biomass and Two Without. Panels D, H, and L are Maximum Projections of Both C-SNARF-4 Emission Regions From Z-Stacks Taken of the Slide Volume.....136

7.9. pH Values Measured With C-SNARF-4 in the Presence of *Geobacter Spp*. Biomass and Without Biomass. Measurements Were Conducted In 30 Mm Phosphate Buffer at pH Values of 5.11 (N=8), 6.12 (N=6), 6.8 (N=6), 7.3 (N=6), and 7.8 (N=6) With and Without Biomass. Biomass Was Prepared by Growing *Geobacter Spp.* Planktonically With Acetate and Fumarate and Electron Donor and Acceptor, Pelleting 1 mL of Culture in a Centrifuge, and Resuspending In 0.1ml Of Buffer With 20 µm C-SNARF-4 Before Being Imaged On Slides With a Leica SP8 CLSM. Error Due to Biomass is the Difference Between Measurement Without Biomass and Measurements With Biomass.....137

7.10. Estimated Effect of Measured pH Error Due to Biomass Presence. Black Line Represents Initially Measured pH Gradient Based Upon C-SNARF-4 Signal. The Blue Line Represents the Relative Biomass Concentration as Measured By DAPI. The Dashed Line is the Modeled Error, Assuming the Bulk pH is Accurate and the pH Error (Figure 7.9) Scales With Biomass Concentration..... 139

Figure Page

7.11. Time Course of the Fluorescence Ratio Near the Anode Surface of a *Geobacter Sulfurreducens* Anode Respiring Biofilm as Calculated From the Fluorescent pH Indicator HPTS. A) Top-Down Transmitted Light Micrograph of the Measured Biofilm/Etched Glass Region ~5μm From the Anode Surface. Nine Regions of Interest are Indicated, Three Without Biofilm, Three Near the Edge of the Biofilm, And Three Deeper Into the Biofilm. Medium Flow At the Time of Imaging is From Right to Left. B) Fluorescence Ratio and Current for Each Region of Interest Indicated in A.....141

S1 Individual VFA accumulation for all batch methanogenic digestions from chapter 4 as measured by HPLC. Red lines represent digestions without pretreatment; black lines represent digestions with thermally pretreated WAS. Error bars represent ± one standard error (n=3).....162

S2 Individual VFA accumulation for all batch methanogenic digestions with BES from chapter 4 as measured by HPLC. Red lines represent digestions without pretreatment; black lines represent digestions with thermally pretreated WAS. Error bars represent ± one standard error (n=3).....162

S3 Methane recovery rates in batch methanogenic digestions from chapter 4. Solid points represent measured values from digestions with pretreatment (black) and without (red). Dashed lines represent modeled recovery rates from fitted parameters (Table 4.1). Error bars and shaded regions represent ± one standard error.....163

Figure Page

S4 Individual current measured in each MEC reactor from chapter 6. The black line represents the average of three MECs, and the gray shaded area represents ± one standard error.....163

S5 Average accumulations of individual VFAs from methanogenic (top) and electrogenic (bottom) digestions in chapter 6. Error bars represent ± one standard error.....164

S6 Average recovery rate of methane or circuited electrons from methanogenic and electrogenic batch digestions in chapter 6. Error bars and light red lines represent ± one standard error.....165

S7 Protein concentrations in methanogenic and electrogenic digestions in chapter 6. Solid lines represent digestions with PS and WAS substrate and ADS inoculum; dashed lines represent control digestions with only ADS inoculum. Error bars represent ± one standard error.....166

S8 Carbohydrate concentrations in methanogenic and electrogenic digestions in chapter 6. Solid lines represent digestions with PS and WAS substrate and ADS inoculum; dashed lines represent control digestions with only ADS inoculum. Error bars represent ± one standard error.....166

Figure Page

S9 Calibration curve of HPTS in 30mM phosphate buffers at various pH values without biomass. Calibration was conducted in the MEFC with an ITO coverslip in place, but without any biomass. Points represent the average ratio from the bulk region of a z-stack. Dashed line represents the calibration curve fitted by the least squares technique.....167

# PREFACE

In this dissertation I describe how accurate kinetic parameters of anaerobic digestion may be obtained from batch tests of model substrates, individual and mixed municipal sludges, and pretreated municipal wastewater sludges. Though previously reported results of batch tests to determine these parameters have yielded inconsistent results, here I show how incorporating measurements of intermediate products, especially semi-soluble chemical oxygen demand, yields accurate values. I describe how relatively simple and complex wastes are each able to generate complex recovery patterns that consist of multiple kinetic events.

In chapter 1 I outline the historical necessity of wastewater treatment before discussing modern practices and regulations in the United States. I describe the composition of municipal wastewater along with the specific components that require treatment before discharge into the environment. I discuss the general processes of wastewater treatment and solids stabilization by anaerobic digestion. I give an overview of the biochemical reactions that comprise the anaerobic digestion process. The strengths and limitations of experimental procedures used to quantify the rates of these reactions are discussed, with emphasis on biochemical methane potential tests. I conclude by describing an alternative experimental platform, the microbial electrochemical cell.

In chapter 2 I review the biochemical reactions of the anaerobic digestion process, the experimental procedures utilized to calculate process rates, and common assumptions which are made in these calculations. The variation of reported rates of hydrolysis and

methane production are discussed. The use of biochemical methane potential (BMP) tests for determining ultimate methane potential and methane production rates are discussed in detail. Previous anaerobic digestion studies conducted in microbial electrochemical cells are analyzed and this platform is compared to traditional analytical approaches.

In chapters 3 and 4 I examine the effects of waste activated sludge pretreatment on the rate and extent of methane recovery in batch digestion tests. Previous studies have reported wide variations in parameters after pretreatment, some claiming increases in the degradability of solids after pretreatment or increased recovery of methane. The studies I present here address this uncertainty by performing rate calculations that incorporate concentrations of intermediate products throughout digestion. In chapter 3 I present kinetics for the digestion of waste activated sludge without pretreatment and with alkaline or thermal pretreatment. In chapter 4 I see if the effects of thermal pretreatment carry over when pretreated waste activated sludge is mixed with primary sludge, a common configuration at operating wastewater treatment plants.

Though a single rate-limiting step is most commonly assumed to govern the overall rate of anaerobic digestion, multiple kinetic events are commonly observed. In chapters 4 and 5 I identify the sources for these multiple kinetic events when model substrates are used and when complex mixed sludges are digested. In these two chapters, I perform parallel digestions in methanogenic digesters and microbial electrochemical cells, a platform technology that couples the metabolism of anode respiring bacteria to the same

hydrolytic and fermentative community found in traditional anaerobic digestion. The rate of anode respiration is equivalent to the rate of methane generation if an upstream process is rate limiting. I use microbial electrochemical cells to collect much more highly resolved rate data in conjunction with measurements of intermediate products. In chapter 5, I examine the complex recovery patterns of the model proteinaceous substrate casein and the carbohydrate cellulose when digested separately or combined. One of the goals of this study is to determine if commonly observed multiple events are due to different classes of substrates being utilized. In chapter 6 I perform comparative digestions of mixed municipal sludges in methanogenic and electrogenic reactors to determine the source of multiple kinetic recovery events resulting from complex waste streams.

The results of digestions conducted in microbial electrochemical cells for chapters 5 and 6 indicate that anode respiring biofilms exhibit unique kinetic limitations distinct from planktonic methanogens. Previously, it has been reported that pH gradients formed due to anode respiration are an important kinetic limitation of these systems. Identifying the structure and dynamics of these gradients under different conditions in microbial electrochemical cells is essential to the use of these systems as sensors or in larger-scale treatment processes. In chapter 7, I examine the previously reported measurements of pH gradients in anode biofilms. I present a newly developed flow cell designed to facilitate rapid measurement of pH gradients within anode biofilms. I critically examine the only previously reported optical pH measurement of anode biofilms and identify fundamental problems with this method.

# 1 INTRODUCTION

## 1.1 Urbanization and the Built Environment

Seven percent of all humans that have ever lived are alive today. These 7.8 billion people represent the largest population of humans alive at a single time in history. Most of this population increasingly resides in urban environments, with 55% of global and 82% of U.S. population living in cities (United Nations, 2018). The population density of these urban areas is much greater than that of rural areas. Historically, the benefit of this has been increased security, shared resources, and the specialization of labor into non-agricultural niches. Every city, historical and modern, has had to balance these benefits with a dramatically increased incidence of disease and the potential degradation of local ecosystems from concentrated waste produced by human society.

Of the wastes produced in cities (municipal solid waste, industrial solid waste, air pollution, municipal and industrial wastewater), municipal wastewater is the greatest potential contributor to human disease and environmental degradation. For this reason, historically and in modern times, municipal sewer systems have been utilized to collect and separate human waste from residences and public areas (De Feo et al., 2014). Wastewater that contains human feces and urine is referred to as sewage. Treatment of collected sewage has evolved over time and still varies depending on the specific needs, resources, and regulatory requirements of each community.

## 1.2 Constituents of Municipal Wastewater and Sewage

Municipal wastewater consists of solid and liquid waste produced from domestic, commercial, and industrial sources that is collected in a municipal sewer network.

Wastewater from domestic and commercial sources consists of human urine and feces, kitchen waste, and graywater from washing machines, showers, and baths. The composition of industrial wastewaters is heavily process dependent, but can contain high concentrations of metals, organic chemicals, and BOD-rich compounds. Because of this, many industrial sites are required to perform pretreatment before discharging their wastewaters to the municipal sewer system (*40 C.F.R. § 403 - General Pretreatment Regulations for Existing and New Sources of Pollution*, 1978). The primary goal of municipal wastewater treatment is to remove organic material, human pathogens, and inorganic compounds that would contaminate potable water sources. This protects the local population as well as any population centers downstream in the same watershed.

Putrescible material, if released into water sources, will stimulate rapid growth of aerobic heterotrophic microorganisms. The respiration of these organisms will lower the oxygen concentration in the surrounding area, resulting in the death of animal life from hypoxia. Long term anoxic conditions create “dead zones” in which the most animal life is not supported. Anoxic water with putrefying organic material is difficult to adequately treat for human consumption.

Nutrient release in discharged wastewater pose a similar environmental risk. The release of inorganic nutrients such as phosphorus and nitrogen can also induce anoxic conditions through the stimulation of autotrophic growth of algae or cyanobacteria. When this biomass begins to decay it also stimulates aerobic heterotrophic bacterial growth and subsequent oxygen consumption. This process is called eutrophication. In

either case, the material that leads to the stimulation of aerobic heterotrophs and oxygen consumption is referred to as biochemical oxygen demand, or BOD. Before a voluntary ban in 1994, laundry detergent contained phosphate, a major source of phosphorus. Today, dishwashing detergent remains a source of phosphorus in greywater.

Human pathogens, when released into watersheds, can persist and come into contact with local populations. This could occur directly, when individuals swim in or utilize the contaminated water as a drinking source or indirectly, if the pathogens are able to persist through typical drinking water treatment. Removal or inactivation of pathogens in both drinking water and wastewater is accomplished through disinfection processes.

## 1.3 Wastewater Treatment in the United States

Americans produce more than 33.7 billion gallons of wastewater each day (North East Biosolids and Residuals Association, 2007). Wastewater collected in municipal sewers undergoes treatment in centralized facilities before being discharged back into the environment. Figure 1.1 illustrates a typical treatment train carried out in an advanced municipal wastewater treatment plant.

The Federal Water Pollution Control Act passed in 1972 made it unlawful for any pollutant to be discharged from a point source to any "navigable waterway" in the United States without a permit (U.S. Federal Government, 2011). Additionally, this act requires that municipal wastewater treatment plants conduct at least primary and secondary treatment to remove approximately 90% of the BOD found in typical municipal wastewaters. Many larger communities will utilize advanced wastewater treatment techniques to remove nutrients and pathogens as well. Due to these regulations, dramatic

increases in environmental water quality have been observed (U.S. Environmental Protection Agency, 2004).

## 1.4 Wastewater Treatment

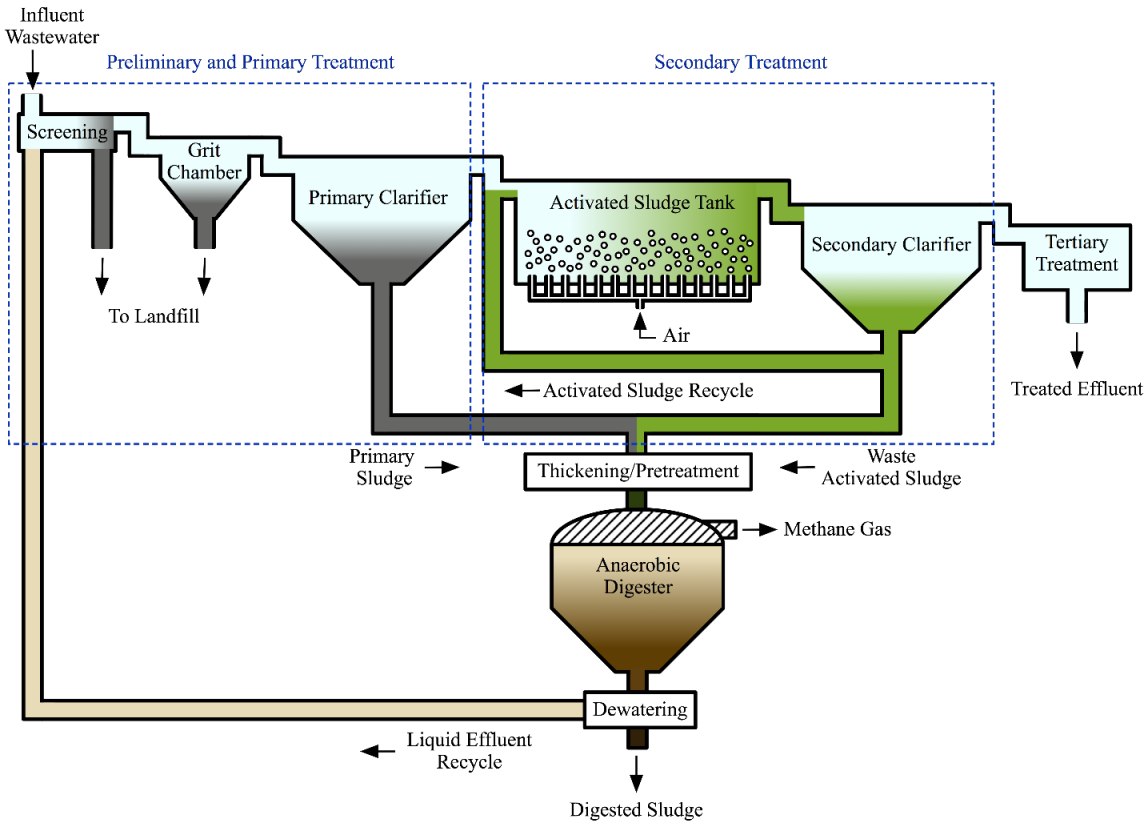


Figure 1.1 Process flow diagram for a typical municipal wastewater treatment system with anaerobic digestion of primary and secondary sludges.

All wastewater treatment facilities separate solids from the waste stream. This is referred to as primary treatment. This begins with coarse screening of debris such as tree branches or large rags, followed by the removal through settling of inorganic solids such as sand and grit. Were they not removed, these components could clog and impair the functionality of subsequent processes. Screened material and grit are almost always

disposed of in a landfill. Primary treatment culminates with the use of a clarifier to allow organic solids to settle out of the waste stream. These initial biological solids comprise around 66% of the total BOD present in typical municipal wastewater (Shizas and Bagley, 2004). Once separated, these solids are referred to as primary sludge. Primary sludge is readily biodegradable and very diverse in composition (Parkin and Owen, 1987).

Eighty four percent of facilities also perform secondary or advanced wastewater treatment to remove dissolved and colloidal BOD as well as the biological nutrients, nitrogen and phosphorus (U.S. Environmental Protection Agency, 2015). The most commonly used form of secondary treatment, in terms of volume of waste treated, is the activated sludge process. Aerobic heterotrophic bacteria are utilized to consume the dissolved and colloidal BOD. This consumed BOD is either assimilated and used for biomass growth, or it's oxidized to $CO_2$ through the respiratory process. In both cases, this BOD is removed from the liquid fraction of the wastewater. The biomass generated is then allowed to settle out in a secondary clarifier. A portion of these solids are transferred back into the aeration tank to maintain high concentrations of appropriate organisms and to select for the desired strains. In this way, the aeration tank is "activated" through the continuous recycle of concentrated heterotrophic biomass. The portion of settled biomass which is not recycled is referred to as waste activated sludge. The activated sludge separated in the secondary clarifier represents approximately 42% of the remaining BOD and 14% of the total influent BOD (Shizas and Bagley, 2004).

Waste activated sludge is less biodegradable, and less readily concentrated through settling. It is composed of complex heterotrophic biomass (Nagler et al., 2016).

Finally, many facilities also filter and disinfect effluents to reduce the concentration of human pathogens in a process referred to as tertiary treatment. Different techniques are used to accomplish this, such as chlorination, UV disinfection, advanced oxidation, or membrane filtration. Often the degree to which effluents are "polished" depends on the intended fate of the treated effluent. Effluents utilized for irrigation of public parks or agriculture are typically treated to a much higher degree than those simply discharged into a stream.

## 1.5 Sludge Stabilization and Treatment

Primary and secondary treatment each generate large quantities of waste sludges. In 2004, approximately 7.1 million dry tons of wastewater solids were used and disposed of from treatment plants in the United States (North East Biosolids and Residuals Association, 2007). About half of these solids were put to beneficial use through land application in agricultural settings. Of the remaining half, about a third were incinerated while the rest were disposed of in landfills. Treatment and handling of solids is often responsible for a third of the operating budget of a wastewater treatment plant.

The ability to land apply solids depends on their quality level as defined by the EPA (*40 C.F.R. § 508 - Standards For the Use or Disposal of Sewage Sludge*). Higher quality sludges have low concentrations of pathogens and reduced vector attraction, such as flies and mosquitos. Vector attraction reduction is accomplished by removing or degrading the easily biodegradable material from sludges. Class A biosolids, the

category with the most possible uses, requires at least 38% volatile solids reduction or the use of a documented successful technique for vector attraction reduction. This process is referred to as sludge stabilization. Pathogen reduction is often accomplished through sludge heating. High quality sludges are a potential revenue source for wastewater treatment plants.

A variety of techniques have been used to stabilize sludges (North East Biosolids and Residuals Association, 2007). The following list is ranked in order of prevalence of use.

- Aerobic digestion – Utilizes aerobic heterotrophs to respire degradable solids to $CO_2$. One of the most commonly utilized techniques.
- Anaerobic digestion – Utilizes anaerobic organisms to hydrolyze and ferment solids to $CO_2$ and methane gas. Methane can be recovered and utilized as an energy source. Though fewer facilities report utilizing this method than aerobic digestion, this technique is used to treat much larger volumes of sludge.
- Lime/Alkaline – The addition of alkali to sludges has been used to raise their pH above 12. This inhibits vector attraction and kills most pathogens. This can also be an exothermic reaction, generating heat sufficient to further reduce pathogens.
- Long-term Storage and Treatment – Utilizes a combination of aerobic and anaerobic digestion, and drying through evaporation and/or transpiration via associated plants.

- Composting – Sludges are mixed with plant material and aerobically co-digested. This process generates enough heat to significantly reduce the number of pathogens.
- Thermal (non incineration) – Heating helps to dry the sludges and reduce the number of pathogens through a form of pasteurization.

## 1.6 Anaerobic Digestion

### 1.6.1 Economic Benefits of Anaerobic Digestion

Anaerobic digestion is the most commonly used form of sludge stabilization in terms of volume of sludge treated. One reason for its widespread use is that, in addition to stabilizing sludges, anaerobic digestion also generates methane gas as a valuable byproduct. This collected methane, the primary component to natural gas, is a readily combustible fuel source which can be used to heat the digesters themselves or for electricity generation in conjunction with an internal or external combustion engine (Cano et al., 2015). This energy recovery can help to offset the high costs of secondary and tertiary treatment, particularly the cost of aeration. Produced methane gas can also be collected and sold, either through shipping to a centralized repository or direct injection into natural gas pipelines. The reduction of sludge volume reduces tipping fees associated with biosolids disposal in landfills. In some cases, increased sludge quality and grade facilitates the sale and utilization of biosolids in agricultural settings, further offsetting upstream treatment costs. When implemented at the appropriate scale, anaerobic digestion offers multiple avenues of revenue or cost offsets. For these reasons,

anaerobic digestion is utilized for approximately 30% of all treated wastewater in the United States (U.S. Environmental Protection Agency, 2015). The purity of the gas collected is also a major challenge to successful methane co-generation. Impurities such as siloxanes can damage most generators, while toxic gasses such as hydrogen sulfide, or it's combustion product sulfur dioxide, can be dangerous to local populations (Appels et al., 2008).

### 1.6.2 The Biochemical Process of Anaerobic Digestion

Primary and Waste Activated Sludges are typically mixed and thickened before undergoing anaerobic digestion, increasing the total suspended solids entering the digester (Tchobanoglous et al., 2014). During anaerobic digestion, this complex particulate biomass undergoes a series of biotransformations before finally being converted to methane and carbon dioxide. A schematic of this process is shown in figure 1.2. Each of the biochemical steps is catalyzed by a unique consortium of microorganisms.

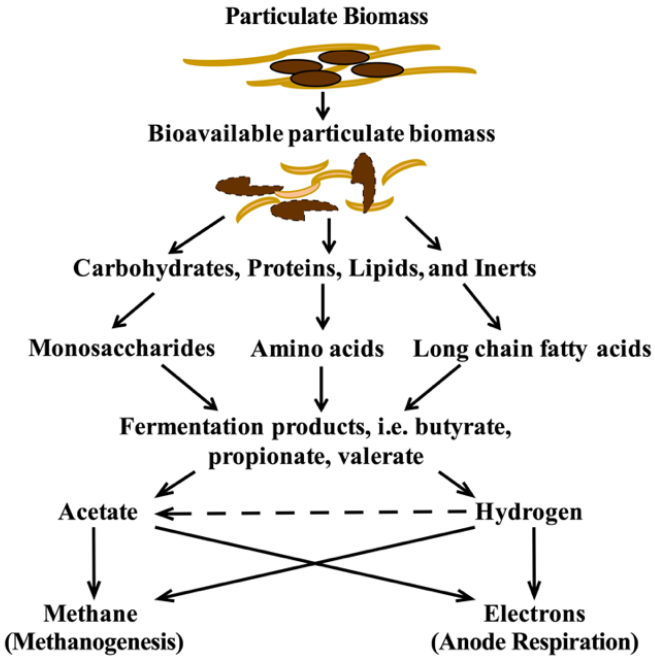


Figure 1.2 Schematic diagram of the parallel and sequential biochemical conversions during anaerobic digestion.

First, complex particulate biomass is hydrolyzed to smaller molecular weight, more bioavailable, compounds. Subsequent additional hydrolysis steps break these compounds into individual proteins, carbohydrates, and lipids. A final series of hydrolysis reactions results in reduction of these components to amino acids, monosaccharides, and fatty acids. These hydrolysis reactions are generally considered to be the rate-limiting steps for anaerobic digestion. Sometimes hydrolysis rates are accelerated through pre-treatment of primary and waste activated sludges. Commonly utilized pre-treatments expose the sludge to high temperatures or pressures, alkaline environments, or pulsed electric fields to catalyze rapid disintegration and hydrolysis of particulate biomass.

Monomers and small molecules generated through hydrolysis are fermented into volatile fatty acids in a process called acidification. Sequential fermentations occur until all degradable organic matter is converted to acetate, carbon dioxide, and hydrogen, the sole substrates for acetoclastic and hydrogenotrophic methanogenesis. Acetate or carbon dioxide and hydrogen are respired through this process to methane gas.

Methanogens and fermenters are syntrophically linked. Together, they perform acetogenesis and methanogenesis to convert volatile fatty acids to methane, but neither consortium can carry out their metabolic functions without the action of the other. Ethanol fermenters, for example, are only able to gain energy for growth when hydrogen, one of the products of their metabolism, is kept at a very low concentration due to the respiration of hydrogenotrophic methanogens (Thauer et al., 2008).

This close association of community members in different niches is a common feature of anaerobic digesting microbial communities. Often, small changes in the conditions of a reactor can have large implications for the function of the community. Methanogens, in particular, are inhibited at pH values lower than 6.4, a condition which can readily occur if methanogenic rates and alkalinity are unable to counter the effects of acidogenesis. Managing anaerobic digesters to prevent acidification or "souring" necessitates careful control of loading rates and operational conditions.

### 1.6.3 Quantifying Anaerobic Digestion Rates

The design and optimization of anaerobic digesters is performed using empirically-measured kinetic parameters. These measurements have been conducted in continuously stirred tank reactors as well as batch digestion systems. In each case, the most common

parameters measured are the rate of methane production and the ultimate methane yield per mass of feedstock. Rate measurements are accomplished through volumetric gas production measurements in conjunction with gas chromatography to quantify methane abundance. Because hydrolysis is considered to be rate-limiting in normal digester performance, the rate of methane production is often assumed to be representative of the combined rates of particulate hydrolysis. In this way, methane production rates are used to calculate concentration-independent rate constants. Batch anaerobic digestions exhibit a saturation curve with respect to cumulative methane production, so first order kinetic models are most commonly used to generate $k_{hyd}$ rate constants. These reported constants are utilized by industry to calculate the necessary size and appropriate loading of large-scale anaerobic digesters.

A wide variety of rate constants for municipal wastewater sludges have been reported. Some of this variation is due to variations in the composition of municipal sludges. As sludges are composites of substances with different digestion rates, the relative abundance of these different fractions could cause variation in the observed composite methane production rate. However, sludges of similar composition digested under analogous conditions are also reported to have different hydrolysis rates. Previous studies have shown that small variations of experimental conditions can result in different measured rates. Furthermore, variation in rates has been attributed to differences in the structure and abundance of the complex microbial community in anaerobic digesters and inoculum collected from them. Previous studies have also indicated that hydrolysis is not

rate limiting under all conditions. Kinetic studies of anaerobic digestion that measure different rate-limiting steps are not directly comparable. In essence, not all reported rates are true "hydrolysis rates".

In this work, I propose modifications to the most commonly used analytical tool for studying anaerobic digestion, the Biochemical Methane Potential test. This is a batch test in which a specific amount of substrate is loaded with inoculum from an active anaerobic digestion community. The total amount of methane produced is then quantified over time. I will describe a series of modifications to this protocol which allow the tracking of hydrolysis, acidogenesis, acetogenesis, and methanogenesis independently. These techniques will allow interrogation of anaerobic digestion rates when methanogenesis is rate limiting and when it is not, allowing for more precise rate constant approximations within a useful contextual framework.

### 1.6.4 Anaerobic Digestion in Microbial Electrochemical Cells

Microbial electrochemical cells (MXCs) are a platform technology based upon the catalytic activity of microorganisms on anodes or cathodes. These organisms are able to catalyze oxidation (anode) or reduction (cathode) reactions from a wide range of donors and acceptors. When introduced to the system under the right conditions, electrode-utilizing bacteria commonly form biofilms on the conductive surfaces of electrodes, maximizing the number of cells in close association with the electroactive surface, and generating relatively high current densities. In the case of anodic biofilms, electrons from soluble donors in the bulk liquid are respired to the anode through a conductive biofilm matrix, direct contact, or indirectly by utilizing soluble redox mediators.

Organisms that are able to catalyze these anodic reactions are referred to as anode respiring bacteria, or ARB. Some ARB, notably those of the genus *Geobacter*, form thick biofilms with many layers of cells actively respiring through a highly conductive matrix. These ARB utilize acetate as their primary electron donor and compete with methanogens for substrate during anaerobic digestion. Some applications of MXCs focus on optimizing power output, while others target the production of valuable chemical products. Some studies have also shown increased sludge stabilization when anodes are added to the anaerobic digestion chamber. Combined methanogenic and electrogenic systems have also been shown to have enhanced pH buffering capacities.

In this work, it will be shown that, in addition to being an alternative anaerobic digestion technology, MXCs are also a potentially valuable diagnostic tool. Observed current is the real-time respiration rate of the ARB, and may be recorded as arbitrarily frequently as is required. Batch BMP tests may be replicated in MXCs by using a methanogenic inhibitor to suppress methanogens and shuttle all electrons to current via ARB. With sufficient active surface area, ARB-catalyzed acetate oxidation will not be rate limiting, and the rates of up-stream processes like hydrolysis and acidification can be measured through current production. In this way, highly resolved kinetic measurements of the rate limiting steps of anaerobic digestion may be conducted. Current measurements can be taken on the order of seconds to minutes, whereas the most highly resolved methane production measurements are on the order of hours.

MXCs are still a maturing technology, and some fundamental knowledge gaps remain with respect to transport processes within ARB biofilms. In addition to uncertainty about the mechanisms of extracellular electron transport, the formation of limiting pH gradients within respiring biofilms is not well understood. Direct observation of these pH gradients is necessary to the optimization of MXC systems for large scale utilization and as diagnostic tools.

# 2 TESTS TO MEASURE ANAEROBIC DIGESTION KINETICS

## 2.1 Processes in Anaerobic Digestion

During anaerobic digestion, settleable (>~10μm) solids combined from primary sludge (PS) and waste-activated sludge (WAS) undergo a series of sequential biochemical conversions. These solids consist of particles of fecal, kitchen, or industrial origin (PS) and of heterotrophic biomass generated from BOD conversion during secondary treatment (WAS) (Tchobanoglous et al., 2014). PS solids are typically more rapidly biodegraded than WAS flocs, which have intact cell membranes resilient to initial disintegration and hydrolysis (Parkin and Owen, 1987). Each sludge contains biopolymers of carbohydrates and proteins, as well as hydrophobic fats (Rittmann and McCarty, 2001). These result in an important property of sludges (especially mixed sludges): they always contain particulates with a wide variety of inherent degradability. Modeling and predicting digester performance in light of this becomes extremely difficult to generalize and simplifying assumptions must be made. The common simplifying assumptions that are employed are discussed in section 2.2.

Figure 2.1 illustrates the sequential bioconversions that occur to particulate biomass during anaerobic digestion. Diverse particulates first undergo disintegration through mechanical separation and primary hydrolysis. This is an essential, and possibly rate-limiting, step as most of the solids initially present are not bioavailable to hydrolytic enzymes or microorganisms due to their enclosure within larger flocs or cell walls. Disintegration and primary hydrolysis increases the surface area available for subsequent biological hydrolysis of particulates to their most prominent components: carbohydrates,

proteins, and lipids. Similarly, these large biomolecules are further hydrolyzed to their component parts of monosaccharides, amino acids, and long chain fatty acids. Each of the steps to this point fall under the broad category of hydrolysis. Hydrolysis is facilitated through excreted exo-enzymes or through microbial membrane-bound enzymes and direct microbial attachment (Morgenroth et al., 2002).

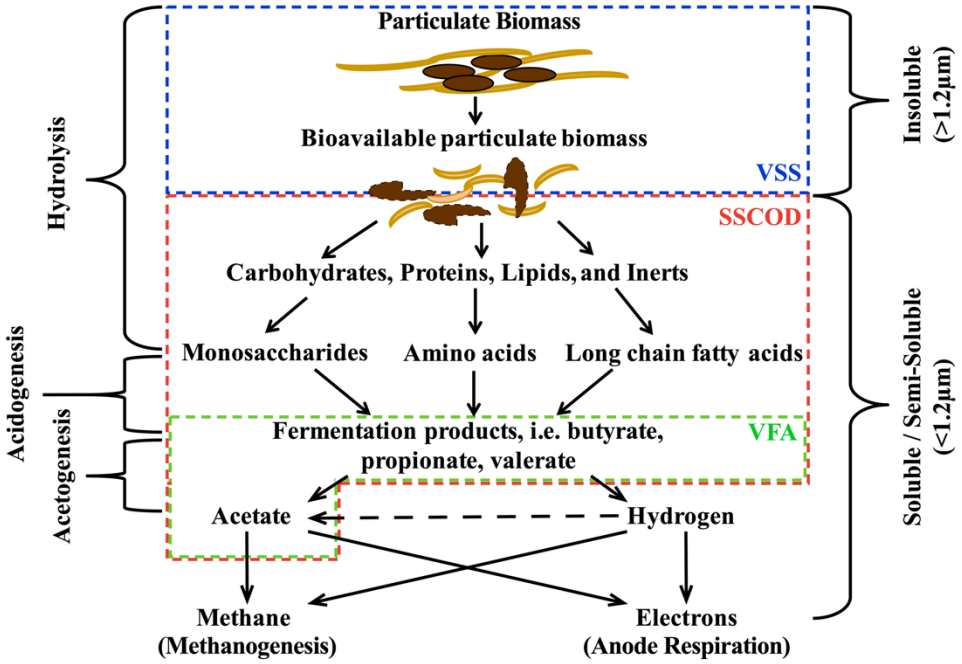


Figure 2.1 Schematic diagram of the sequential and parallel reactions occurring during anaerobic digestion. Boxes indicate the commonly measured quantities volatile suspended solids (blue), semi-soluble chemical oxygen demand (red), and volatile fatty acids (green).

Carbohydrate, protein, and lipid monomers are bioavailable to be fermented to short-chain fatty acids, and eventually acetate and hydrogen in processes called acidogenesis and acetogenesis, respectively as shown in Figure 2.1 (Eastman and Ferguson, 1981). Hydrogen may be converted to additional acetate through the activity

of homo-acetogens (Figure 2.1, dashed line), although this is unlikely to occur in the presence of hydrogenotrophic methanogens (Parameswaran et al., 2009; Parameswaran et al., 2010). If this does not occur, accumulation of hydrogen may thermodynamically inhibit further VFA production through fermentation. The final step in traditional anaerobic digestion is methanogenesis by methanogenic archaea. There are two general categories of methanogens, acetoclastic and hydrogenotrophic. Acetoclastic methanogens disproportionate acetate to carbon dioxide and methane, while hydrogenotrophic methanogens use hydrogen to reduce carbon dioxide to methane (Madigan et al., 2015). Typical anaerobic digestion processes utilize planktonic methanogens and an HRT/SRT of 15-25 days (Tchobanoglous et al., 2014).

## 2.2 Anaerobic Digestion in Microbial Electrochemical Cells

Anode respiring bacteria (ARB) fill a similar ecological niche as methanogens, using acetate and hydrogen as electron donors and a conductive anode as an electron acceptor (Torres et al., 2010). One distinction, however, is that ARB in microbial electrochemical cells (MXC) are almost always grown as biofilms on the electrode surface as opposed to planktonic cells (Marcus et al., 2010). A microbial biofilm consists of a community of organisms that adhere to one another, often in association with a solid surface (Rittmann and McCarty, 2001). Microbial biofilms are ubiquitous in natural environments. It has been estimated that most microbial biomass resides within biofilms (Andrews et al., 2010; Rittmann and McCarty, 2001). For a microorganism, biofilms can offer several specific benefits such as protection from predators, localized beneficial

microenvironments, proximity to electron acceptors or donors, or close association with syntrophic partners (Chosterton et al., 1978; Donlan, 2002; Stanley and Lazazzera, 2004).

Figure 2.2 shows a schematic diagram of a microbial electrolysis cell (MEC), a specific configuration of MXC. A potentiostat is used to set the anode potential to promote colonization and respiration by ARB. Anaerobic digestion tests are performed by adding substrate and hydrolytic and fermentative inoculum to the anode chamber where an anode respiring biofilm has been pre-grown. A three-electrode system is used to poise the anode potential via a Ag/AgCl reference electrode and a potentiostat. In the configuration shown, an anion exchange membrane separates the anode and cathode chambers. Current may be continuously monitored for the duration of the batch digeston tests.

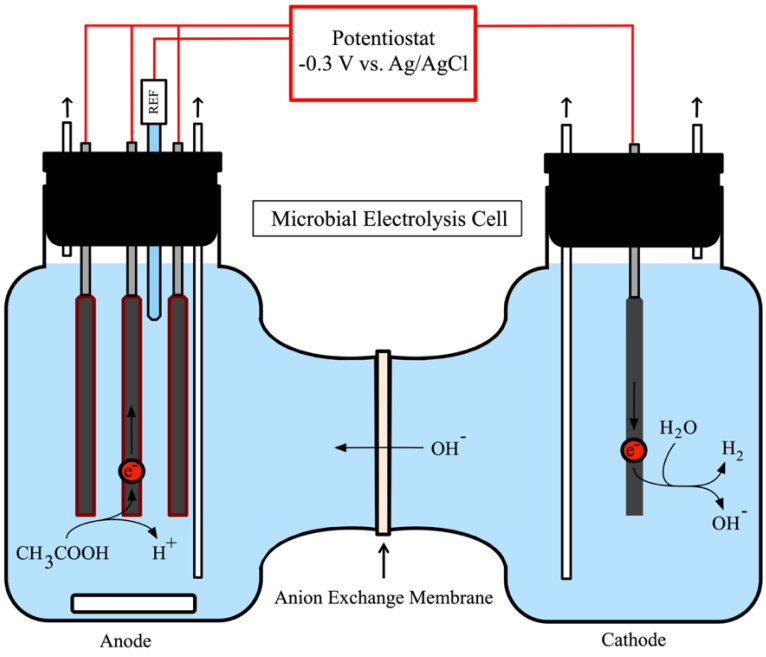


Figure 2.2 Schematic diagram of a microbial electrolysis cell (MEC).

## 2.3 Batch Tests Used to Quantify Anaerobic Digestion Kinetics

Biochemical methane potential (BMP) batch tests are the most commonly used batch test to assay methane production during anaerobic digestion. Though batch assays had been described before, Owen et al. described the first formal protocol for determining the amount of methane that can be produced per mass of substrate (Owen et al., 1979). These tests consist of anaerobically combining sludge and/or other particulate substrates with inoculum, typically from an anaerobic digester, in a serum bottle that is sealed with a butyl rubber stopper to facilitate continued anaerobic conditions and gas sampling (Owen et al., 1979). Over time, the methane produced is measured until minimal additional gas production is observed. This original protocol notes that sufficient inoculum (as gVSS $L^{-1}$) should be added relative to the substrate (gCOD $L^{-1}$) to avoid nutrient limitation or excessive gas. The primary benefit to this technique over more rigorous respirometry tests is that it may be conducted relatively quickly with inexpensive materials. Chynoweth et al. acknowledge the wide-spread use of this test by 1993, but describe several sources of variability, such as the inoculum source, the inoculum-to-feed ratio, and the particle size of the substrate (Chynoweth et al., 1993). They suggest a minimum inoculum-to-feed ratio of 2 (on a VSS to VSS ratio) be used to avoid inhibition due to product accumulation. Chynoweth et al. also sieve their sludge and only use solids with a particle size of >1mm. The stated purpose is to avoid irreproducible initial rates from unknown quantities of small, easily degradable, particulates. Chenoweth et al. also describe wide variation in results from certain kinds of lignocellulosic biomass grown and harvested under different conditions. This, with the

reticence to use small particulates, suggests that substrate characteristics other than VSS contribute to the hydrolysis rate in ways the authors did not quantify.

The BMP protocol was further amended in 2004 by Hansen et al. to include corrections to measured gas produced based upon the temperature and pressure at which the digestions were conducted (Hansen et al., 2004). Hansen et al. also suggest that a minimum of triplicate digestions be conducted for at least 50 days due to the known variability of the test. One of the most cited revisions to the BMP protocol is from Angelidaki et al., 2009. Here, the authors emphasize the necessity of preliminary substrate characterization and preparation to obtaining reproducible BMP results (Angelidaki et al., 2009). The authors suggest that activity tests using acetate and cellulose be performed on inoculum prior to use in BMP tests. They also reiterate the importance of considering particle size and ensuring no nutrient limitation occurs. These recommendations are a response to the wide variety of methane potential values that are being reported for similar feedstocks from BMP tests. Angelidaki et al. also acknowledge that, when conducted in a reproducible way, BMPs may also allow us to measure anaerobic digestion kinetics in addition to methane recovery. They suggest a first-order approach.

Trzinski et al. elaborate on kinetic calculations from BMP tests, describing a protocol for calculating first-order kinetic rate-constants and lag-phases using a modified Gompertz equation (Trzcinski and Stuckey, 2012). The authors also suggest that hydrolysis kinetics may be calculated from SCOD accumulation in instances when

methane is rate-limiting. This incorporation of intermediates into rate calculations could further reduce variability observed between labs and experiments with similar substrates. Koch et al. also present a detailed description of calculating hydrolysis kinetics from BMP tests, but instead suggest a Monod-like equation for fitting (Koch and Drewes, 2014). The authors present a way to predict hydrolysis constants from the duration of the test until the 1% criterion is met (Ingenieure, 2006).

Recently, two additional reviews have been published which focus on standardizing BMP tests to reduce the continued variability of reported results (Holliger et al., 2016; Stromberg et al., 2014). Holliger et al. is the product of a workshop with many members of the field, and essentially reiterates guidelines described in Angelidaki et al., 2009. Stromberg et al. focus on common error associated with the measurement of produced methane, such as correcting for the temperature and pressure of the room the tests are performed in, and the presence of water vapor in measured samples. The authors also discuss the potential importance of accounting for dissolved methane in certain circumstances. Perhaps most importantly, they describe how accounting of headspace methane when using sealed digestion vessels is essential (Stromberg et al., 2014). This is a very important factor that is often not adequately mentioned in BMP studies and may result in the underestimation of methane production. Many papers only quantify excess gas produced (Aldin et al., 2011; Sosa-Hernández et al., 2016; Vavilin and Angelidaki, 2004), while some add headspace methane to this value (Angelidaki et al., 2009; Girault et al., 2012; Trzcinski and Stuckey, 2012), and many are unclear about their specific

protocol, simply referencing Owen et al. 1979, which states that you may or may not need to account for headspace methane.

A few studies have performed anaerobic digestion studies in electrogenic reactors instead of methanogenic (Lee et al., 2008; Parameswaran et al., 2010; Parameswaran et al., 2009; Torres et al., 2007; Velasquez-Orta et al., 2011; Sun et al., 2019). These tests essentially swap out the methanogens with anode respiring bacteria (ARB), as indicated in Figure 2.2. The advantage of this is that current production is the actual respiration rate of the ARB and may be measured arbitrarily frequently, allowing much finer resolution of individual kinetic events that occur in anaerobic digestion. As ARB compete with methanogens for substrate, a methanogenic inhibitor 2-bromoethanesulfonate (BES) has been used to selectively shuttle electrons through the ARB (Parameswaran et al., 2010; Parameswaran et al., 2009). A potential complicating factor is that biofilms have different kinetic limitations than planktonic methanogens typically found in BMP tests. The kinetics of biofilm processes are defined by the gradients formed within the biomass (Popat et al., 2014). This may be the concentration of a substrate as it diffuses into, and is utilized by, a biofilm; this results in a decreasing concentration as a function of depth into the biofilm. If a biofilm is sufficiently deep, substrate concentration within portions of the biofilm may be zero (Rittmann and McCarty, 2001). In this case, the metabolism of the innermost cells will be dominated by decay processes. This could ultimately result in detachment of the biofilm if these inner layers are the primary connection of the biofilm to the surface. Metabolic products of the

cells within a biofilm must also diffuse out, often resulting in a concentration gradient. Diffusive transport into and out of biofilms is the limiting factor for the ultimate depth of a biofilm in a given environment (Rittmann and McCarty, 2001). How the underlying properties of biofilms will affect kinetic measurements of anaerobic digestion via ARB remains to be shown.

## 2.4 Kinetic Expressions Used to Model Hydrolysis

The anaerobic digestion process is commonly modeled with relatively simple kinetic expressions, considering the number of processes and distinct microbial communities that are involved. This is because: 1) a comprehensive mechanistic model would be very complex and difficult to effectively utilize and 2) the rate and extent of methane accumulation in batch tests is approximated reasonably well by simple kinetic expressions (Aldin et al., 2011; Morgenroth et al., 2002; Pavlostathis and Gomez, 1991; Vavilin et al., 1996). One explanation for this is the rate-limiting step model, which states that the kinetics of a multistep process are defined by the slowest step in the process (Parkin and Owen, 1987; Pavlostathis and Gomez, 1991). Most researchers consider hydrolysis to be rate-limiting at conditions typically found in anaerobic digestors (Eastman and Ferguson, 1981; Parkin and Owen, 1987; Pavlostathis and Gossett, 1988; Sanders et al., 2000; Vavilin et al., 1996; Veeken and Hamelers, 1999). Thus, by modeling hydrolysis, the rate limiting step, the entire anaerobic digestion process may be approximated. A further implication of the rate-limiting step model is that reactions that occur after the rate-limiting step proceed at the same rate as the rate-limiting step. This means that, if only hydrolysis is limiting, then measuring methane

accumulation should allow indirect determination of the hydrolysis rate. Batch digestions in which the rate and extent of methane production from a substrate are commonly performed for this purpose. These tests are described in section 2.3. The following sections describe the three most commonly used kinetic expressions to model hydrolysis in anaerobic digestion: first-order, Monod, and Gompertz. Table 2.1 lists studies using each of these modeling approaches. Surface-based kinetics have also been described, but are less commonly adopted in BMP studies, possible due to the difficulty in measuring particle sizes or the relatively homogenous solids present in municipal sludges (Aldin et al., 2011; Sanders et al., 2000; Vavilin et al., 1996).

Table 2.1 Kinetics used in selected batch anaerobic digestion studies.

| Study | First-Order | Monod | Gompertz |
|---|---|---|---|
| (Eastman and Ferguson, 1981) | X | X | |
| (Llabrés-Luengo and Mata-Alvarez, 1987) | X | X | |
| (Pavlostathis and Gossett, 1988) | X | X | |
| (Tong et al., 1990) | X | | |
| (Pavlostathis and Gomez, 1991) | X | X | |
| (J.-J. Lay et al., 1996) | | | X |
| (Veeken and Hamelers, 1999) | X | | |
| (Miron et al., 2000) | X | | |
| (Veeken et al., 2000) | X | | |
| (Batstone et al., 2002) | X | | |
| (Vlyssides, 2004) | X | | |
| (Cai et al., 2004) | | | X |
| (Bolzonella et al., 2005) | X | | |
| (Eskicioglu et al., 2006) | X | | |
| (Yasui et al., 2008) | X | X | |
| (Vavilin et al., 2008) | X | X | |
| (Angelidaki et al., 2009) | X | | |
| (Rincón et al., 2010) | X | | |
| (Velasquez-Orta et al., 2011) | X | | |
| (Aldin et al., 2011) | X | X | X |
| (Lay et al., 2011) | | | X |
| (Trzcinski and Stuckey, 2012) | X | | X |
| (Girault et al., 2012) | X | | |
| (Parameswaran and Rittmann, 2012) | X | | X |
| (Chen et al., 2012) | | | X |
| (Rivera-Cancel et al., 2012) | | X | |
| (Trzcinski and Stuckey, 2012) | | | X |
| (Young et al., 2013) | X | | |
| (Stromberg et al., 2014) | X | | |
| (Koch and Drewes, 2014) | | X | |
| (Koch et al., 2015a) | | X | |
| (Li et al., 2016) | | X | X |
| (Sosa-Hernández et al., 2016) | | | X |
| (Nazari et al., 2017) | X | | |
| (Hobbs et al., 2017) | | | X |
| (Dandikas et al., 2018) | X | | |
| (Donoso-Bravo et al., 2019) | | | X |
| (Pečar et al., 2020) | X | | X |
| (Peces et al., 2020) | X | | |
| (Xu et al., 2020) | X | | |

### 2.4.1 First-Order Kinetics

First-order kinetics are the most commonly used approximation for hydrolysis rates, as exemplified in Table 2.1. Eastman and Ferguson first described a first-order approach to kinetics from BMPs as an acceptable simplification based upon the rate-limiting step assumption (Eastman and Ferguson, 1981). First-order kinetics depend upon two parameters: 1) the maximum possible methane that may be produced and 2) a first-order rate constant. First-order kinetics are valid only when the overall rate of a process is determined by a single rate-limiting step. Veeken and Hamlers presented an example of a first-order kinetic expression for cumulative methane production:

$$M = M_{max} [1 - \exp ( -k_{hyd} t )] \quad \text{Equation 2.1}$$

where M is the cumulative methane [gCOD $L^{-1}$] at time t [d], $M_{max}$ is the ultimate methane produced [gCOD $L^{-1}$], and $k_{hyd}$ is the first-order hydrolysis rate constant [$d^{-1}$] (Veeken and Hamlers, 1999). While first-order kinetics require a single rate-limiting step, that step may shift from one process to another throughout a digestion. This is the approach taken in the widely-used ADM1 (Batstone et al., 2002). The rate-limiting process is calculated at each timepoint and those first-order kinetics are used for the overall process. Similarly, Rincón et al. describe fast and slowly-hydrolyzing material with distinct rate constants, with the overall process being the sum of these two (Rincón et al., 2010).

### 2.4.2 Monod Kinetics

The second most common kinetic expression used to describe anaerobic digestion uses Monod kinetics to model biomass growth. Monod kinetics were developed by

Jacques Monod, and relate the specific growth rate of bacteria to a limiting substrate concentration (Monod, 1949; Rittmann and McCarty, 2001). Eastman and Ferguson first applied this approach to approximate hydrolysis rates from BMPs (Eastman and Ferguson, 1981). Since then, many studies have used a version of Monod kinetics (Table 2.1). Koch and Drewes formulated the following Monod-type kinetic expression to fit cumulative methane production:

$$B = (B_{max} \cdot k_h \cdot t) / (1 + k_h \cdot t) \quad \text{Equation 2.2}$$

where B is the cumulative methane [gCOD $L^{-1}$] produce at time t [d], $B_{max}$ is the ultimate methane produced [gCOD $L^{-1}$], and $k_h$ is the hydrolysis rate constant [$d^{-1}$] and is equivalent to the reciprocal of the time when ½ of the ultimate methane is recovered (Koch and Drewes, 2014).

### 2.4.3 Gompertz Kinetics

Originally created to describe human mortality to determine the value of annuities, the Gompertz equation describes a sigmoidal curve consisting of a lag phase, an exponential growth phase, and a stationary phase (Gompertz, 1825; Zwietering et al., 1990). The key parameters are the duration of the lag phase, the maximum rate during the exponential phase, and the ultimate value at which carrying capacity or substrate limitation occur. Lay et al. describe the derivation of the equation to represent methane accumulation:

$$M = P \cdot \exp\{-\exp[((R_m \cdot e)/P) \cdot (\lambda - t) + 1]\} \quad \text{Equation 2.3}$$

where M is the cumulative methane [gCOD $L^{-1}$] at time, t [d], P is the ultimate methane production potential [gOD $L^{-1}$], $R_m$ is the maximum rate of methane production [gCOD

$L^{-1}d^{-1}$], e is the exponent of 1, and λ is the lag phase [d] (Lay et al., 1996). This expression is widely used because of its ability to fit delays in methane recovery. This delay can represent growth kinetics if biomass is limiting, inhibition due to toxic compounds, or the transition from a preferred substrate to a less favorable one. Table 2.1 shows that many researchers continue to use Gompertz kinetic expressions to fit data. Interestingly, Gompertz fits are often use in conjunction with first-order kinetic expressions. Hydrolysis rate constants are commonly calculated from first-order rate equations, while lag times are calculated from the Gompertz equation. Indirectly, this means that biomass growth (or another form of inhibition) is often used to account for delays in methane formation, but is not incorporated into kinetic rate constants. Gompertz fits are typically performed by minimizing the sum squares of error in an iterative approach to parameter estimation.

Figure 2.3 shows an example of fittings performed with first-order, Monod, and Gompertz kinetic models. The BMP fitted in Figure 2.3 exhibits a lag phase before appreciable methane accumulation and multiple methane recovery events, features commonly observed in BMPs of complex substrates such as during the co-digestion of kitchen waste or after pretreatment. While cumulative methane production is approximated well for all models, the methane production rate is not.

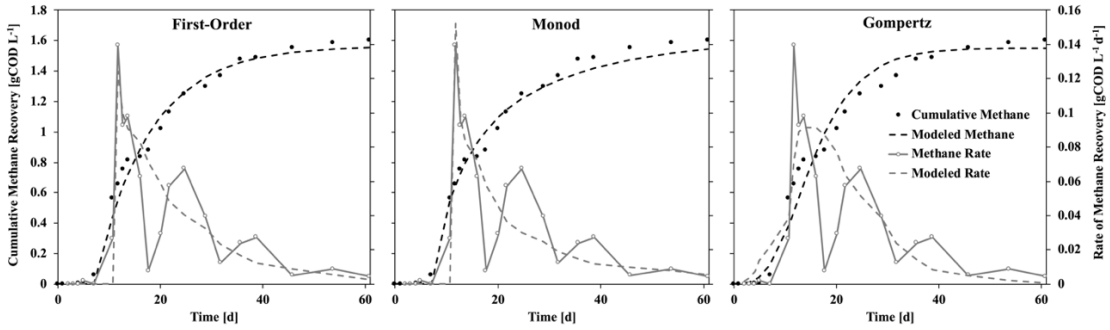


Figure 2.3 Example model fittings from first-order, Monod, and Gompertz kinetics for methane accumulation in a BMP test. Solid black points indicate cumulative methane produced from a BMP tests. Dashed black lines represent modeled cumulative methane. Gray lines represent the rate of methane accumulation. Dashed gray lines represent modeled methane recovery rates.

## 2.5 Limitations to Simple Kinetic Approaches

Simplified kinetic expressions such as those shown here are very useful for approximating methane recovery from many BMP tests, but complex recovery patterns are often observed that do not match first-order or simple Monod kinetics. Clear non-first order behavior is regularly observed. In his original paper, Monod discussed that growth with complex substrates could result in multiple exponential phases when the utilization of one substrate inhibits the utilization of the other (Monod, 1949). This is the same phenomenon that is often observed during the batch anaerobic digestion of complex wastes, commonly during co-digestion or after pretreatment. Yasui et al. observed at least three distinct degradable organic fractions in primary sludge, each with distinct kinetics that resulted in individual methane recovery events (Yasui et al., 2008). During respirometry experiments of the aerobic digestion of thermally pretreated WAS, Burger et al. showed a similar pattern of multiple recovery events (Burger and Parker, 2013). BMP tests conducted for the co-digestion of food waste with municipal sludge similarly

observed 2-3 methane recovery peaks, instead of the expected single event as first-order or Monod kinetics would suggest (Koch et al., 2015; Li et al., 2016).

While cumulative recovery may be reasonably fitted with simple expressions, rates of methane or electron recovery are much harder to fit and are almost always non first-order, as is apparent in Figure 2.3. A recent study of thermally pretreated WAS also exhibited multiple methane recovery peaks (Toutian et al., 2020). While cumulative recovery may be roughly approximated by first-order kinetics in each of these cases, the methane production rate is clearly not fit by these kinetics. This represents a significant gap in our ability to model and predict digester performance during co-digestion or after sludge pretreatment. Through approaches like that taken by Trzcinski et al. to incorporate intermediate products, better kinetic measurements might be able to be performed (Trzcinski et al., 2012). Similarly, the increased resolution by MXCs provide an opportunity to identify the specific cause of the individual recovery events that are commonly observed.

# 3 THE EFFECTS OF PRE-TREATMENT ON THE KINETICS OF WASTE-ACTIVATED SLUDGE DIGESTION


## Abstract

Anaerobic digestion is a widely implemented technique for stabilizing municipal sludges and recovering energy as methane gas. Hydrolysis of complex particulate biomass into simple soluble molecules is generally considered the rate-limiting step for anaerobic digestion. To maximize sludge stabilization and methane recovery, municipal sludges may be pretreated to pre-solubilize and increase the ultimate biodegradability of particulate COD. The traditional test for anaerobic digestion efficiency is the biochemical methane potential (BMP) test, in which the rate and total amount of methane produced from a given substrate is measured with the addition of an inoculum of anaerobic digested sludge (ADS). One limitation of traditional BMPs is that intermediate products are not measured. In this study, BMP tests were performed to analyze the degradation rates and ultimate methane recovery from waste activated sludge (WAS) without pretreatment, with alkaline pretreatment, and with thermal pretreatment. Intermediate samples were collected and analyzed for volatile suspended solids, semi-soluble chemical oxygen demand, volatile fatty acids, and pH. Both pretreatments resulted in significantly decreased initial and final VSS concentrations, as well as more ultimate methane generation. Methane generation was a good proxy for solids hydrolysis of untreated WAS, but not of pretreated WAS. This is because much of the methane produced was from pre-solubilized SSCOD and not biological hydrolysis, resulting in overestimation of hydrolysis rates. Incorporating SSCOD resulted in the computation of

slower hydrolysis rate constants, similar to those measured by VSS destruction directly. These indicate that solids remaining after pretreatment are hydrolyzed at a slower rate than the original WAS solids.

Acknowledgements

Michelle N. Young, Prathap Parameswaran, Bruce E. Rittmann, and César I Torres contributed to the experimental design, data collection, and analysis of the results presented in this chapter. This chapter is currently being submitted for peer-reviewed publication with the above-mentioned as authors.

## 3.1 Introduction

Anaerobic digestion (AD) is commonly used for sludge stabilization and energy recovery through the conversion of waste biomass to methane ($CH_4$) gas. The rate-limiting step for anaerobic digestion often is the hydrolysis of particulate biomass to soluble, biologically available components (Rittmann et al., 2008; Velasquez-Orta et al., 2011; Wang et al., 2009). Solids pre-treatment to disintegrate and partially solubilize particulate biomass could increase the rate and $CH_4$ recovery efficiency of AD processes (Carlsson et al., 2012). Several pretreatment techniques have been the focus of research and commercialization over the last decade. They include alkaline lysis, mechanical lysis, thermal hydrolysis, microwave treatment, ultrasonic treatment, and pulsed electric field treatment (Carlsson et al., 2012; Carrère et al., 2010; Rittmann et al., 2008). Thermal pretreatment processes like CAMBI™ and EXELYS™ have been implemented around the world to treat side-streams of waste-activated sludge (WAS) to improve $CH_4$ recovery and sludge stabilization during AD (Burger and Parker, 2013; Carrère et al., 2010; Gonzalez et al., 2018). Thermal pretreatment, which increases WAS temperatures to 90-190ºC and pressure of (200 – 600 KPa), results in increased cell lysis and chemical oxygen demand (COD) solubilization (Gonzalez et al., 2018; Kim et al., 2003). While not commercially implemented, alkaline pretreatment has been widely explored in the laboratory due to its easy implementation and significant cell lysis and COD solubilization (Chang et al., 1997; Stuckey and McCarty, 1984).

Immediate markers of the effects of any pretreatment on waste activated sludge (WAS) are the disintegration and size reduction of particulate COD and the solubilization

of biomass to semi-soluble COD (SSCOD), which is the COD associated with the permeate fraction after filtration through a 1.2-µm glass-fiber filter (versus 0.45-µm for traditional soluble COD (SCOD)) (Lee et al., 2010; Salerno et al., 2009; Zhang et al., 2009). For alkaline, thermal, and pulsed electric field pretreatments, the initial SSCOD increased 10- to 30-fold after pretreatment (Burger and Parker, 2013; Carlsson et al., 2012; Kim et al., 2003; Lee et al., 2010; Rittmann et al., 2008).

The rate of gas production in a BMP is commonly approximated through a first-order rate expression and exhibits a saturation curve: a high rate of $CH_4$ production in the first 10 days, followed by slow $CH_4$ production for the final 30-60 days (Trzcinski and Stuckey, 2012). Since the BMP assay includes an active methanogenic inoculum, such as sludge from an anaerobic digester, fermentation and methanogenesis generally occur at faster rates than hydrolysis when the substrate is particulate; thus, the $CH_4$ production rate usually is a direct measurement of the hydrolysis rate for a biomass substrate (Eastman and Ferguson, 1981). BMP results also have been reported for substrates and loadings in which methanogenesis was not limiting (Li et al., 2016; Neves et al., 2006; L. Zhang et al., 2016); however, it can be difficult to determine which AD process was rate-limiting, especially because intermediate products are typically not measured.

The specific case of sludge pretreatment presents a challenge to calculate hydrolysis rates using BMP assays. First, pretreatment can increase the rate of solids hydrolysis prior to biological digestion, leading to it no longer being the rate-limiting step. Second, pretreatment can directly hydrolyze solids to soluble products that are

available for methane production but are not associated to biologically based hydrolysis. Thus, estimating the overall solids hydrolysis from methane production data after pretreatment can under-estimate hydrolysis kinetics in the first case or over-estimate hydrolysis kinetics for the second condition.

To effectively determine accurate kinetics of batch digestions after pretreatment, it is essential to measure the rate of production and extent of accumulation of intermediate products, not only $CH_4$. A few studies have shown that the SCOD concentration increased before $CH_4$ production reached its maximum rate in batch BMP assays with an anaerobic inoculum (Neves et al., 2006; Trzcinski and Stuckey, 2012), but the dynamics of hydrolysis, SSCOD and SCOD production and consumption, and $CH_4$ production have not been explored systematically in batch anaerobic digestion studies. Tracking SSCOD and soluble liquid-phase components (such as proteins, carbohydrates, and volatile fatty acids (VFAs)) during a BMP assay will illuminate the mechanisms by which pre-treatment increases the rate and extent of VSS conversion to $CH_4$, making it possible to identify which step is rate-limiting at any time during digestion and methanogenesis (Veeken et al., 2000; Neves et al., 2006; Jimenez et al., 2016).

We conducted batch methanogenic digestion largely following the established BMP protocol (Angelidaki et al., 2009; Owen et al., 1979), but with an important modification: We collected liquid samples at regular timepoints and analyzed them for intermediate products. The modified BMPs were conducted with unpretreated, alkaline pretreated, and thermally pretreated WAS. First-order rate constants were calculated for

each condition in four ways: based on cumulative $CH_4$ production; particulate COD hydrolysis (cumulative $CH_4$ + SSCOD and VSS solubilization); and SSCOD hydrolysis (cumulative $CH_4$ + VFAs). By combining these more-detailed analyses, we were able to distinguish rate limitation based on hydrolysis of particulate COD, hydrolysis of semi-soluble COD, or methanogenesis.

## 3.2 Materials and Methods

### 3.2.1 Municipal Wastewater Sludge and Pretreatment Techniques

WAS was obtained from the secondary clarifier underflow and ADS from the Mesa (AZ) Northwest Wastewater Reclamation Plant (NWWRP), which employs the Anoxic-Oxic (A/O) process. For thermal pretreatment, WAS was autoclaved at 121°C and for 30 min. and allowed to cool at 23°C overnight (Carrère et al., 2010). For alkaline pretreatment, we followed the procedure described by (Cai et al., 2004): slowly adding 10 M NaOH to WAS until a stable pH of 12 was maintained. Once the pH was stable, the mixture was stirred at 500 rpm for 30 min and allowed to sit for 24 hours at pH 12 before adjusting the pH using 2M HCl to a stable pH 7. Control and pretreated WASs were stored for a maximum of 4 days at 4°C prior to the setup of BMP assays. Inoculation with ADS ensured that significant hydrolytic, fermentative, and methanogenic capacities were present at the start of the assay.

### 3.2.2 Modified BMP Assays

Except for the regular sampling of the mixed liquor, the BMP protocol developed by Owen et al., as modified by Angelidaki et al., was followed (Owen et al., 1979; Angelidaki et al., 2009). Prior to inoculation, ADS was degassed of excess $CH_4$ by

stirring capped serum bottles in a shaker table at 150 rpm and 37°C for 5-7 days and degassing daily. The inoculum-to-sample volume ratio was 3:7 (i.e., 54 mL anaerobic digested sludge (ADS) with 126 mL sample). Additional buffer or trace elements, as suggested by Angelidaki et al., were not necessary due to adequate availability of these components in the WAS itself. For a negative control, 54 mL of ADS was added to 126 mL of basal media (detailed in Parameswaran et al. 2012) that included 100 mM of PBS buffer. The mixtures were added to 200-mL serum bottles. Each sample was set up in quadruplicate, allowing multiple samples to be taken during the duration of the test and facilitating the full suite of measurements described below.

To initiate the batch experiments, the serum bottles were inoculated and sparged with 100% UHP $N_2$ gas for 15 minutes and sealed with butyl-rubber stoppers (Bellco Glass, NJ) and aluminum caps. The bottles were incubated on a shaker table at 150 rpm and 37°C. Periodically, the volume of gas produced was measured with a frictionless gas syringe (Popper and Sons, NY) and assayed for $CH_4$ and $H_2$ composition by gas chromatography (GC-2010, Shimadzu, MD), although $H_2$ was not detected. The portion of $CH_4$ remaining in the headspace of each bottle was also accounted for when calculating $CH_4$ production, as it can represent a significant fraction of the ultimate $CH_4$ produced. The headspace $CH_4$ volume for each timepoint was calculated by multiplying the $CH_4$ gas fraction determined by gas chromatography by the headspace volume at the time of sampling. Gas produced in the ADS negative control was subtracted from the inoculated batch digestions.

The modified BMP process featured periodic removal of 9 mL of slurry sample from a bottle for pH, SSCOD, VSS, and VFA analyses. To prevent the liquid volume of any serum bottle from becoming too depleted, the sampled bottles were rotated: i.e., the first sample was taken from bottle one, the second from bottle two, etc. This allowed samples to be taken at many intermediate time points without depleting the volume of any single bottle, and the decrease in volume was accounted for in all calculations. At day 62, when gas production had tapered off and no additional VSS destruction was observed, final gas production was measured and bulk samples were taken for final analyses.

### 3.2.3 Chemical Analyses

Total COD (TCOD), total suspended solids (TSS), and volatile suspended solids (VSS) were measured prior to filtering. SSCOD, total alkalinity, and VFAs were measured after filtering the sample through a 1.2-µm glass-fiber filter (Whatman GF-C, UK). For VFA analysis, the samples were further filtered through a 0.2-µm Acrodisc® PVDF membrane filters (Pall Life Sciences). A Thermo Scientific, Inc. Orion 2 Star bench-top pH meter was used to measure pH in the mixed liquor and filtrate.

COD was quantified using HACH HR COD kits (range 10-1,500 mg/L), and total alkalinity was determined using HACH TNT 870 kits (range 35-400 mg$CaCO_3$/L). Values were measured using a HACH DR 2800 spectrophotometer (Genesys 20, Thermo Spectronic, MA). TSS and VSS were determined according to *Standard Methods* (Clesceri et al., 1998).

Biogas $CH_4$, $H_2$, and $CO_2$ composition samples were taken with a gas-tight syringe (SGE 500 µL, Switzerland) and analyzed using a gas chromatograph (GC 2010, Shimadzu) equipped with a thermal conductivity detector and a Carboxen™ 1010 PLOT column (Supelco, Bellefonte, PA). Gas analyses was carried out in duplicate.

High-performance liquid chromatography (HPLC; Model LC-2 0AT, Shimadzu, Columbia, MD) was used for VFA quantification, which included acetate, lactate, propionate, butyrate, valerate, isovalerate, and isobutyrate. The HPLC was equipped with an Aminex HPX-87H (Bio-Rad Laboratories, Hercules, CA, 1997) column to separate simple acids and alcohols. A 2.5-mM sulfuric acid eluent was fed at a flow rate of 0.6 mL/min, and chromatographic peaks were detected using photo-diode array at 210 nm and refractive index detectors. The oven temperature was held at 50°C, and the total elution time was 90 min.

### 3.2.4 Calculations

$CH_4$ produced in the batch experiments is reported in terms of its equivalent COD concentration (gCOD $L^{-1}$):

$$1\ \text{mL}\ CH_4 = \frac{1\ \text{mmol}\ CH_4}{22.4\ \text{mL}}\ \frac{273.15\ \text{K}}{310.15\ \text{K}}\ \frac{8\ \text{meq}\ e^-}{\text{mmol}\ CH_4}\ \frac{8\ \text{mg COD}}{\text{meq}\ e^-} = 2.52\ \text{mg COD} \qquad \text{Equation 3.1}$$

The COD mass equivalent of $CH_4$ was then normalized to the corresponding liquid volumes in the batch serum bottles to obtain equivalent $CH_4$-COD concentrations.

First-order kinetic constants for hydrolysis were calculated three ways: based on cumulative $CH_4$, cumulative $CH_4$ + intermediate SSCOD concentration (PCOD hydrolysis), and cumulative $CH_4$ + intermediate VFA accumulation (SSCOD hydrolysis).

$CH_4$ production was used to estimate first-order hydrolysis kinetics as described previously (Bolzonella et al., 2005; Koch and Drewes, 2014; Pavlostathis and Gomez, 1991). The first-order rate equation in terms of ultimate COD recovery is:

$$P = P_{max} [1 - \exp (-k_{hyd} t)] \quad \text{Equation 3.2}$$

where P is the cumulative COD of the products (SSCOD, VFA, $CH_4$) of batch digestion at time t (gCOD $L^{-1}$), $P_{max}$ is the ultimate product recovery from the batch digestion at the end of the incubation time (gCOD $L^{-1}$), and $k_{hyd}$ is the first-order rate constant ($day^{-1}$).

This first-order equation is not able to accurately represent hydrolysis when a significant portion of the substrate has been pre-hydrolyzed by pretreatment. Without adjustment, the presence of pre-hydrolyzed material results in artificially large apparent $k_{hyd}$ value, because methane is being produced from material that has already been hydrolyzed, and hydrolysis is no longer rate-limiting. The addition of SSCOD and VFA values into cumulative methane rate calculations accounts for portions of COD already hydrolyzed, but not yet converted to $CH_4$, which is an important substrate source in the case of pretreatment. Cumulative methane + SSCOD was used to show the rate of particulate COD (PCOD) hydrolysis to the semi-soluble form. Similarly, cumulative $CH_4$ + VFA was used to show the rate of SSCOD hydrolysis or the rate of complete solubilization. To account for pre-hydrolyzed material already present, we included an additional term, $P_{start}$, which represents the initial amount of hydrolysis products present at the start of the batch tests in the form of pre-solubilized fractions. As no methane was initially present for any digestion, $P_{start}$ for PCOD hydrolysis was the initial SSCOD

concentration, while, for SSCOD hydrolysis, $P_{start}$ was the initial VFA concentration. The modified equation is:

$$P = (P_{max} - P_{start}) [1 - \exp (-k_{hyd} t)] + P_{start} \quad \text{Equation 3.3}$$

If $P_{start}$ approaches $P_{max}$, the amount of material released due to hydrolysis during the BMP test decreases to zero. For digestions with small initial concentrations of SSCOD or VFAs, such as those without pretreatment, Equation 3 approaches Equation 2.

In the case of Net VSS destruction (Net VSS = sample VSS – VSS of the ADS control), Equation 3 was modified for solids removal instead of product accumulation:

$$P = (P_{max})[\exp (-k_{hyd}t)] + VSS_{NBD} \quad \text{Equation 3.4}$$

where $VSS_{NBD}$ is the non-biodegradable fraction of VSS left after Pmax, the ultimate solids removal in this case, has been reached. The parameter $P_{start}$ is not needed int his case, as fitting begins from the starting VSS value, already reduced in the case of pretreatment.

The parameters $P_{max}$, $k_{hyd}$, and $VSS_{NBD}$ were estimated using the least-squares method with Solver in Excel. $P_{start}$ is a measured value in each case, corresponding to the products initially present at the start of digestion. In the case of $CH_4$ accumulation, parameters were estimated for each of the four replicates of each condition individually. The compound parameters of PCOD hydrolysis and SSCOD hydrolysis were analyzed with all data for each condition combined due to the alternating sampling protocol that was used.

For statistical significance, we used an unpaired student's t-Test assuming unequal variance. A p-value of $\leq 0.05$ is the threshold for significance.

## 3.3 Results and Discussion

### 3.3.1 Alkaline Pretreatment Converted the Greatest Proportion of PCOD to SSCOD

Figure 3.1 shows that pretreatment reduced the initial WAS VSS concentrations, 4.8 ± 0.3 g COD $L^{-1}$, by an average of 21% and with minimal differences between alkaline and thermal treatments. These reductions are similar to results obtained by Kim et al. (2003): 15 - 40% initial PCOD solubilization from alkaline pretreatment, 18% PCOD solubilization by thermal pretreatment, and 41% initial PCOD solubilization with thermal pretreatment (Burger and Parker, 2013). Our lower solubilization percentage likely was due to lower temperature and pressure of thermal pretreatment (120°C and 15 psig versus 150°C and 44psig for Burger and Parker (2013)).

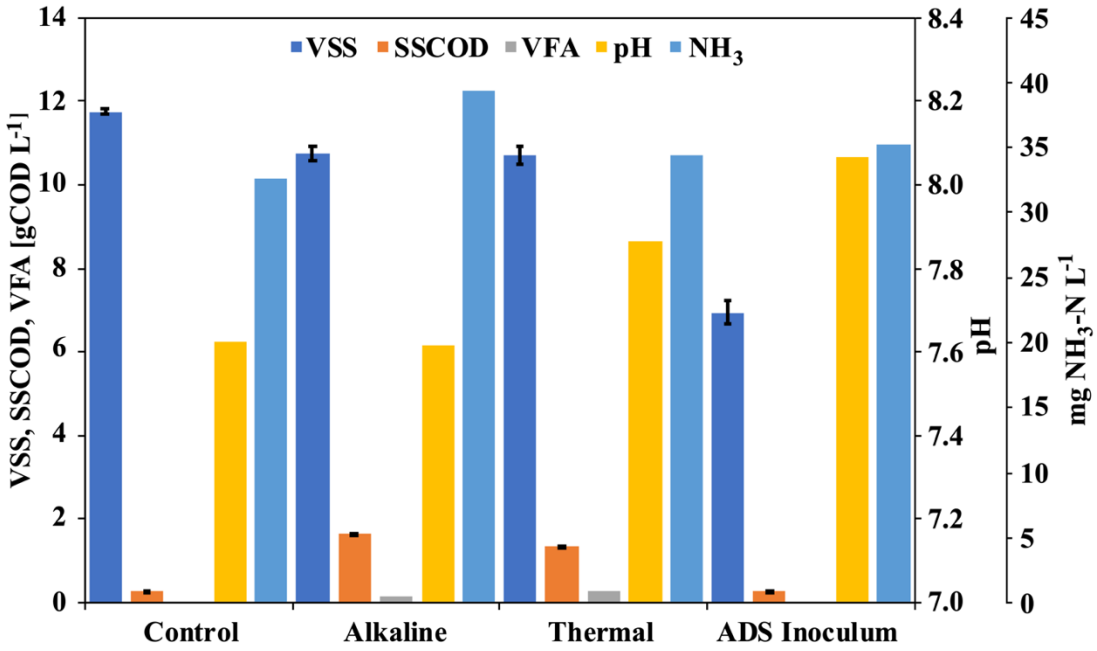


Figure 3.1 Initial conditions for inoculated batch digestions fed with pretreated and unpretreated WAS. Shown are VSS, SSCOD, and VFA concentrations, along with pH at the start of each experiment. Error bars represent ± one standard error.

Thermal and alkaline pretreatments increased SSCOD concentrations, although alkaline pretreatment resulted in ~20% more SSCOD than thermal pretreatment. Defined as the COD of the material passing through 1.2-μm glass-fiber filters, SSCOD includes truly soluble and colloidal fractions. Thus, SSCOD is a combined measure of all material following disintegration and initial hydrolysis, with VFAs comprising only a small fraction of SSCOD solubilized from pretreatment in all cases.

Thermally pretreated batch digestions had slightly higher initial pH values compared to control or alkaline pretreatment. Alkaline pretreatment was completed by adjusting the pH back to 7, while thermal pretreatment had no adjustment. Ammonium release during pretreatment, also shown in Figure 3.1, contributed to increases in pH. Thermal pretreatment also generated VFAs, up to 286 mg COD/L.

### 3.3.2 Thermal Pretreatment Resulted in the Greatest Ultimate Methane Recovery and the Greatest Risk of Inhibition

Figure 3.2, which shows cumulative methane recovery, intermediate concentrations of SSCOD and VSS, and pH values at timepoints throughout the batch duration, demonstrates that alkaline and thermal pretreatment significantly increased the ultimate $CH_4$ yield in batch digestions (alkaline $p = 0.004$, thermal $p = 0.001$). Without pretreatment, digestions recovered 50% of the initial substrate COD (starting SSCOD + VSS – VSS from ADS) as $CH_4$. This is similar to typical mesophilic AD processes (Tchobanoglous et al., 2014). Alkaline pretreatment resulted in 54% COD recovery, while thermal pretreatment led to 65% recovery, even though alkaline pretreatment converted more particulate COD to SSCOD. Small decreases in cumulative methane are

due to subtraction of control BMPs or decreases in the headspace methane percentage from one day to the next.

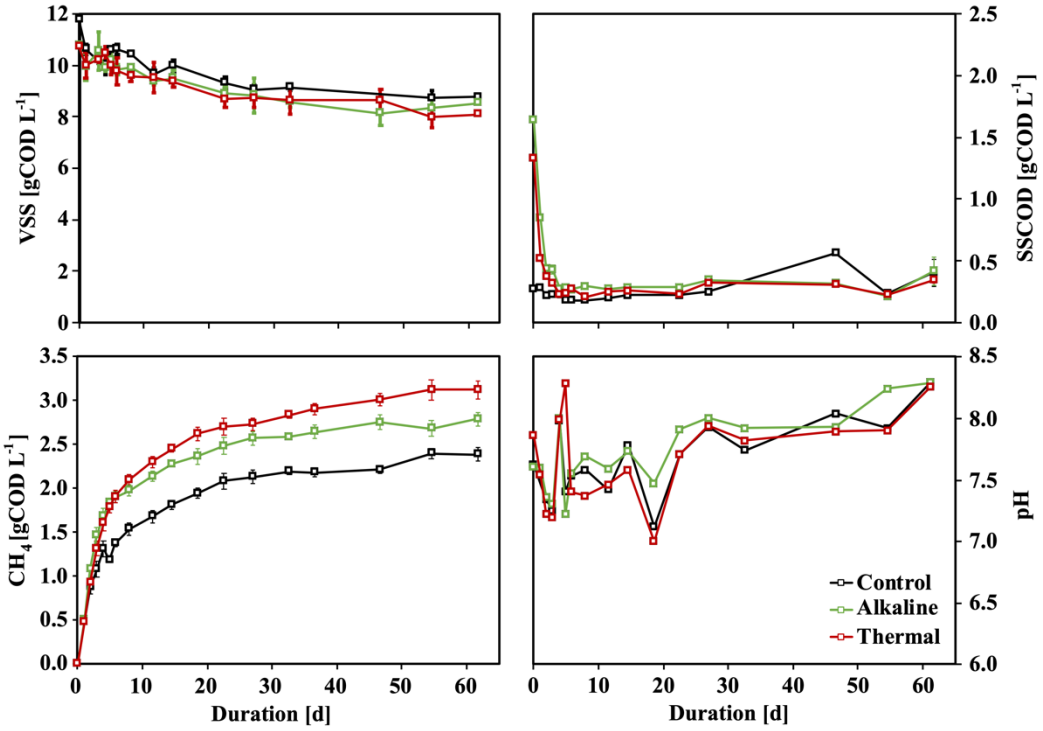


Figure 3.2 Volatile suspended solids, SSCOD, cumulative $CH_4$ production, and pH for BMPS of control, alkaline pretreated, or thermally pretreated WAS. VSS, SSCOD, and pH show all measurements from four biological replicates of each condition and error bars represent ± one standard error of the technical replicates of each sample. Cumulative $CH_4$ shows the average of four biological replicates; error bars represent ± one standard deviation.

Figure 3.2 shows that the initial SSCOD represented less than 3% of the COD ultimately recovered as $CH_4$ with no pretreatment. For thermally pretreated batch digestions, however, the starting SSCOD accounted for 33% of the $CH_4$ ultimately produced, and alkaline pretreatment released the greatest proportion (65%) of SSCOD that was ultimately recovered as $CH_4$. Thus, pretreatment significantly reduced the

amount of biologically based hydrolysis necessary to make WAS COD available for fermentation. Furthermore, pretreatment resulted in significantly less final VSS, decreasing from 8.75 ± 0.08 gCOD $L^{-1}$ for control to 8.51 ± 0.06 gCOD $L^{-1}$ ($p = 0.03$, n = 3,3, two-sample t test) for alkaline and 8.07 ± 0.04 g COD $L^{-1}$ ($p < 0.001$, n = 3,3, two-sample t test) for thermal.

Total VFA results in Figure 3.3 demonstrate that VFAs were negligible in all batch digestions after the first day. Formate and acetate were the only VFAs present immediately after pretreatment.

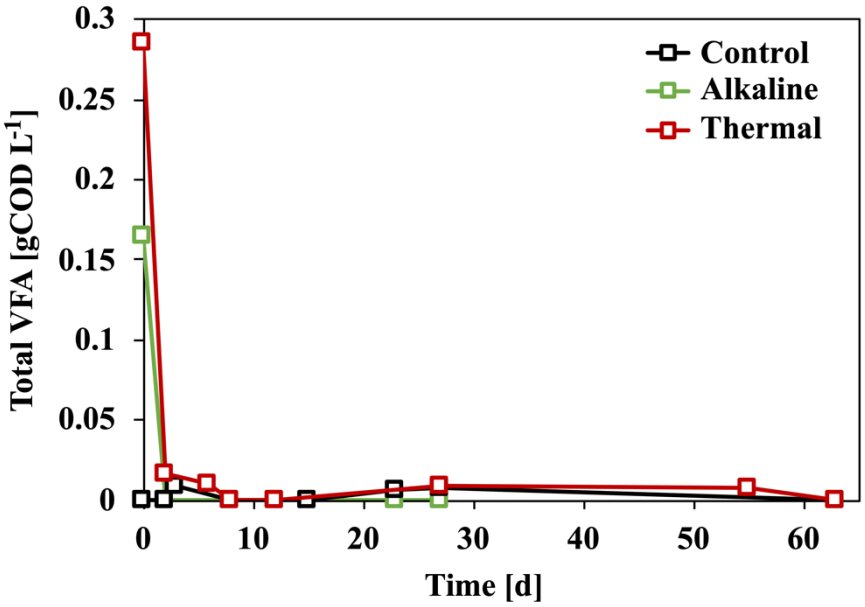


Figure 3.3 The combined total volatile fatty acid concentration as determined by HPLC analysis of samples taken from all biological replicates.

### 3.3.3 Hydrolysis Rate Constants Derived from Methane Alone are Overestimated After Pretreatment

Hydrolysis rate constants ($k_{hyd}$) were calculated four ways using first-order kinetics for hydrolysis based on product formation (Equation 3) or solids destruction (Equation 4). In terms of product formation, three methods were used: (1) $CH_4$ accumulation, which assumes that hydrolysis is the rate-limiting step in digestion and no intermediate accumulation of products; (2) $CH_4$ accumulation + SSCOD (PCOD hydrolysis); and (3) $CH_4$ accumulation + VFAs (SSCOD hydrolysis). The fourth method, VSS removal, is a direct measure of PCOD hydrolysis, but has limited precision due to variability inherent to VSS measurements of sludge slurries. All model parameters are reported in Table 3.1, and the fitted data are shown in Figure 3.4. The parameters $k_{hyd}$, $P_{max}$, and $VSS_{NBD}$ are fitted parameters, while $P_{start}$ is measured.

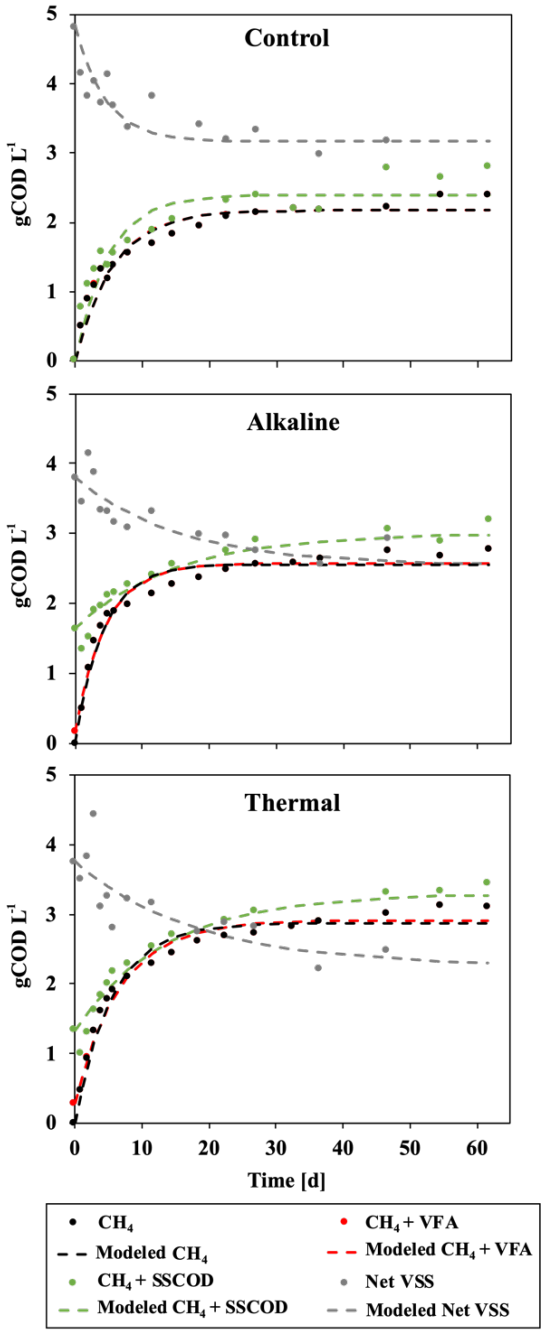


Figure 3.4 Modeled product formation and VSS solubilization with first-order approximations for BMPs with no pretreatment, alkaline pretreatment and thermal pretreatment of WAS. Points are measured quantities; dashed lines are modeled data using Equation 3 ($CH_4$, $CH_4$+SSCOD, $CH_4$+VFA) and Equation 4 (Net VSS).

Table 3.1 Ultimate COD recoveries ($P_{max}$) and hydrolysis constants ($k_{hyd}$) calculated Equation 3 and Equation 4. $P_{start}$ values used are shown for modeled product accumulation. Fitted non-biodegradable solids fractions, $VSS_{NBD}$, are shown for modeled VSS destruction. $R^2$ values are shown for the measured and modeled data.

| Sludge Pretreatment | Analysis | Data Fitted | $P_{max}$ [gCOD $L^{-1}$] | $k_{hyd}$ [$d^{-1}$] | $P_{start}$ [gCOD $L^{-1}$] | $VSS_{NBD}$ [gCOD $L^{-1}$] | $R^2$ |
|---|---|---|---|---|---|---|---|
| Control | PCOD hydrolysis | VSS | 1.64 | 0.22 | - | 3.17 | 0.78 |
| | PCOD hydrolysis | Methane + SSCOD | 2.40 | 0.20 | 0.00 | - | 0.90 |
| | SSCOD hydrolysis | Methane + VFA | 2.17 | 0.18 | 0.00 | - | 0.96 |
| | $CH_4$ production | Methane | 2.17 | 0.18 | 0.00 | - | 0.96 |
| Alkaline | PCOD hydrolysis | VSS | 1.26 | 0.06 | - | 2.54 | 0.72 |
| | PCOD hydrolysis | Methane + SSCOD | 3.01 | 0.07 | 1.64 | - | 0.91 |
| | SSCOD hydrolysis | Methane + VFA | 2.57 | 0.22 | 0.17 | - | 0.97 |
| | $CH_4$ production | Methane | 2.56 | 0.24 | 0.00 | - | 0.97 |
| Thermal | PCOD hydrolysis | VSS | 1.50 | 0.06 | - | 2.25 | 0.66 |
| | PCOD hydrolysis | Methane + SSCOD | 3.30 | 0.07 | 1.33 | - | 0.94 |
| | SSCOD hydrolysis | Methane + VFA | 2.91 | 0.15 | 0.29 | - | 0.98 |
| | $CH_4$ production | Methane | 2.87 | 0.18 | 0.00 | - | 0.98 |

As expected from a typical BMP test, control experiments had a methane production rate constant ($k_{hyd}$ = 0.18 $d^{-1}$) similar to PCOD hydrolysis ($k_{hyd}$ = 0.22 $d^{-1}$ from VSS and $k_{hyd}$ = 0.20 $d^{-1}$ from methane + SSCOD) and SSCOD hydrolysis ($k_{hyd}$ = 0.18 $d^{-1}$ based on methane + VFAs). Since all $k_{hyd}$ values were almost the same, the rate of methane production was limited by PCOD hydrolysis and, thus, had a similar rate constant. Consistent with limitation by hydrolysis is that accumulations of SSCOD and VFAs were negligible. The hydrolysis rate constants obtained fell within the range of those previously reported for WAS: 0.06 – 0.25 $d^{-1}$ (Girault et al., 2012; Pavlostathis and Gossett, 1988; Veeken et al., 2000).

When thermal or alkaline pretreatment was employed, a significant amount of SSCOD was present at the start of the experiment for both pretreatments ($P_{start}$), leading

to a smaller PCOD fraction to be hydrolyzed during digestion. This PCOD fraction was hydrolyzed at a slower rate than the total fraction present in the control experiment, showing a $k_{hyd}$ = 0.06 - 0.07 $d^{-1}$ for both pretreatments when methane + SSCOD or methane + VFA was the basis for the hydrolysis rate constant. The slower hydrolysis rates suggest the pretreatments solubilized the most easily degradable solids into SSCOD, leaving a more recalcitrant fraction to be hydrolyzed.

In pretreatment batch digestions, the first-order rate constants obtained from methane production rates were much higher than the hydrolysis constants that include methane + SSCOD or VSS. This over-estimation of hydrolysis kinetics occurred because a significant fraction of the methane produced in these experiments came from the initial SSCOD fraction obtained from the pretreatment itself, not from hydrolysis during the BMP test. Values for hydrolysis rate constants for methane + VFAs also were artificially high, although not as high as for methane alone. These over-estimations mean that VFAs were not the main components of the SSCOD.

## 3.4 Conclusions

The extent and rate $CH_4$ recovery from WAS were significantly increased in BMP tests by alkaline or thermal pretreatment. Both pretreatments pre-hydrolyzed a significant portion of the PCOD and VSS, resulting in increases in initial SSCOD. With both pretreatments, using the rate of methane production as a proxy for the solids hydrolysis rate over-estimated the hydrolysis rate constant, although methane generation was a good proxy for untreated WAS. The reason for the over-estimation is that much of the methane produced came from SSCOD generated by pre-treatment, not from

hydrolysis of solids. The hydrolysis rates computed by taking into account the SSCOD concentration were lower and in line with hydrolysis rates based directly on VSS. The accurate hydrolysis rates indicate that the WAS solids remaining after pretreatment were more slowly hydrolyzed than the original WAS solids.

The benefits of pretreatment of sludges often are described as twofold: an increase in the rate of methane production and an increase in the total methane produced. The increase in rates are often assumed to stem from a faster hydrolysis rate as solids are more easily degradable after treatment. Our results suggest that the increase in methane production rates is not associated to faster hydrolysis of biological solids, but to the high fraction of solid of hydrolyzed during pretreatment. Our results also point out the hydrolysis kinetics are accurately estimated by simultaneous measurement of $CH_4$ and SSCOD when pre-treatment generated significant SSCOD.

# 4 CALCULATING KINETIC PARAMETERS FROM BATCH ANAEROBIC DIGESTION OF MIXED MUNICIPAL SLUDGES WITH THERMALLY PRE-TREATED WAS


## Abstract

Anaerobic digestion (AD) is commonly used to stabilize municipal sludges and recover energy in the form of combustible methane gas. This process has been modeled and optimized using batch methanogenic digestion tests to analyze the methane production rate and total methane recovery efficiency of specific wastes. These batch tests are also used to test the effectiveness of sludge pretreatments to increase the rate of digestion and the biodegradability of sludges. Thermal pretreatment is one of the most common techniques used to pretreat sludges before digestion. Thermal processes are designed to rapidly hydrolyze complex biomass into more soluble and bioavailable fractions. In this study we present results from a series of batch methanogenic digestions that tested the effect of pretreating only the more recalcitrant sludge, waste activated sludge (WAS). Thermal pretreatment, performed at 121°C and 15 psi, converted 13% of the WAS volatile suspended solids to semi-soluble chemical oxygen demand (SSCOD). Batch digestions were loaded in a manner representative of typical AD processes in municipal wastewater treatment, with a 1:1 v/v primary sludge (PS) and WAS. In addition to measuring methane production, volatile suspended solids (VSS), SSCOD, and volatile fatty acids (VFA) were measured for each batch digestion at discrete time points to precisely measure the rates of each step of the AD process. On average, pretreatment resulted in increased methane accumulation at all time points ($p=7E^{-11}$, n=22, one sample

t test), but the ultimate methane at the final time point was not significantly different (p=0.13, n=3,3, two sample t test). First order methane accumulation constants were 0.12 ± 0.01 $d^{-1}$ without pretreatment and 0.14 ± 0.01 $d^{-1}$ with pretreatment. Due to the smaller relative COD content by volume of the WAS as compared to PS, the potential benefits of WAS pretreatment were minimized. Under these conditions, pretreating WAS alone before performing mixed sludge digestion did not result in increased methane production rates or increased total methane recovery.

Acknowledgements

Collette Wilson and Sarah Brown contributed to the data collection and Prathap Parameswaran, and César I Torres contributed to the experimental design and analysis of the results presented in this chapter. This chapter is prepared and will be submitted for peer-reviewed publication with the above-mentioned as authors.

## 4.1 Introduction

The process of anaerobic digestion (AD) is commonly used to stabilize and recover energy from sludges produced during municipal wastewater treatment. Energy is recovered in the form of combustible methane gas. Typically, primary sludge (PS) and waste activated sludge (WAS) are mixed and concentrated before being fed to the anaerobic digester (U.S. Environmental Protection Agency, 1999). These solids are retained in the anaerobic environment of the digester for 15-30 days, during which time between 40-60% of the solids are converted to methane gas under typical operation (Tchobanoglous et al., 2014) and sludge stabilization is achieved for beneficial biosolids end-use. This process occurs in several distinct steps: disintegration, hydrolysis, acidification, acetification, and methanogenesis (Parkin and Owen, 1987). Typically, disintegration and hydrolysis are assumed to be the rate-limiting steps of anaerobic digestion (Eastman and Ferguson, 1981; Trzcinski and Stuckey, 2012; Vavilin et al., 2008).

The AD process has been modeled and optimized using biochemical methane potential (BMP) tests, batch assays used to evaluate the total amount of recoverable methane as well as the rates of methane evolution from given substrates (Angelidaki et al., 2009; Owen et al., 1979). These batch tests may also be used to test the effectiveness of sludge pretreatments to increase the rate of digestion and the biodegradability of sludges. Often, methane accumulation in BMPs is used to calculate first-order rate constants to predict process rates and recoveries for a given substrate (Koch and Drewes, 2014; Trzcinski and Stuckey, 2012). The reported values for these parameters can vary

widely, even for similar substrates (Holliger et al., 2016; Stromberg et al., 2014). It has been suggested that incorporating measurements of intermediates would help to standardize this process and eliminate variability due to loading and inoculum activity (Trzcinski and Stuckey, 2012).

Sludge pretreatments are intended to 1) increase the rate of anaerobic digestion and 2) increase the biodegradability of sludges, resulting in increased stabilization and methane production (Cano et al., 2015; Carrère et al., 2010; Donoso-Bravo et al., 2019). There are many different techniques used for sludge pretreatment including focused pulse technologies, alkaline incubation, and thermal processes (Cai et al., 2004; Cano et al., 2015; Zhang et al., 2009). Thermal pretreatment is one of the most commonly used techniques to pretreat sludges before digestion (Carlsson et al., 2012). Thermal processes are designed to rapidly hydrolyze complex biomass into more soluble and bioavailable fractions by subjecting the sludge to increased temperature (70-190 °C) and pressure (4-6 atm) (Appels et al., 2010; Carlsson et al., 2012). While thermal pretreatment is at times applied to a combination of WAS and PS, it is also proposed to treat the WAS fraction alone as it is typically more difficult to digest (Bougrier et al., 2008; Burger and Parker, 2013; Gonzalez et al., 2018).

In this study, we present results from a series of batch methanogenic digestions with and without thermally pretreated WAS and unpretreated primary sludge as substrates. Our goal was to determine the overall benefits of thermal pretreatment of WAS in terms of rates and extent of methane production. In addition to monitoring

cumulative methane production, intermediate sludge samples were also taken to evaluate semi-soluble chemical oxygen demand (SSCOD), pH, and volatile suspended solids (VSS). Digestions were also carried out with the methanogenic inhibitor bromoethane sulfonate (BES) to more precisely measure the individual rates of the AD process upstream of methanogenesis. First-order hydrolysis rate constants and maximum hydrolysis rates were calculated for sludge digestions with and without pretreatment.

## 4.2 Materials and Methods

### 4.2.1 Sludge Sampling and Pretreatment

Primary sludge, waste activated sludge, and anaerobic digested sludge were all collected from the Greenfield Water Reclamation Plant (GWRP) in Mesa, Arizona. Primary sludge (PS) was sampled from an active recirculation line associated with the primary settler. Waste activated sludge (WAS) was sampled from the recycle flow of the secondary settler to the aeration basin. Anaerobic digested sludge (ADS) was sampled directly from the anaerobic digester. All sludge samples were immediately analyzed for total suspended solids (TSS), volatile suspended solids (VSS), total chemical oxygen demand (TCOD), and semi-soluble oxygen demand (SSCOD), as described in the following methods. A portion of the waste activated sludge was set aside for pretreatment. The PS and untreated WAS were stored at 4°C to preserve the substrate integrity until use. WAS was thermally pretreated by autoclaving at 121°C and 15 psi for 30 minutes before being allowed to cool overnight as previously described (Carrère et al.,

2010). ADS was incubated at 30°C and stirred for two days to degas and remove residual substrate as previously described (Angelidaki et al., 2009).

### 4.2.2 Batch Methanogenic Digestion Loading

Batch methanogenic digestions were conducted by modifying the standard protocol (Owen et al., 1979; Angelidaki et al., 2009). Batch digestions were performed in 1-liter bottles (500 mL liquid volume) with rubber stoppers fitted with 4mm ID PTFE gas and liquid sampling lines (Mcmaster-Carr). PS collected from the GWRP was diluted to 30 g TSS/L to represent typical solids concentrations fed to a digester and mixed at a 1:1 volume/volume ratio with the WAS, either pretreated or non-pretreated, to form the blended substrate solution. Batch methanogenic digestions were loaded according to a food to microorganism (F/M) ratio of 1.5. that is, 1.5 g substrate COD / 1 g ADS VSS. Digestions were conducted in triplicate. Two control digestions were conducted with ADS inoculum alone, diluted with water to the concentration used in the experimental digestions. Methane and intermediate product production from these digestions were subtracted from all experimental data. All digestions were replicated with 10 mM bromoethane sulfonate (BES) to inhibit methanogenesis and allow accumulation of intermediate products.

### 4.2.3 Gas Measurements

Volumetric gas production was measured by connecting a gas-tight frictionless glass syringe (Perfektum, New Hyde Park, NY) to the headspace and allowing it to equilibrate to atmospheric pressure. Methane remaining in the headspace after excess gas removal was added to the calculated cumulative methane production by multiplying the

headspace volume at the time of measurement by the measured methane concentration, as shown in equation 4.1:

$$CH_{4,t} = (mL_{produced,t} \times CH_4\,\%) + (mL_{headspace,t} \times CH_4\,\%) \quad \text{Equation 4.1}$$

where $CH_{4,t}$ is the methane that was produced by time, t, $mL_{produced,t}$ is the total gas that was produced by time, t, $CH_4$ % is the fraction of the total gas that is $CH_4$, and $mL_{headspace,t}$ is the volume of the headspace at time, t. The headspace volume is increased each time a liquid sample is taken. Methane composition of the headspace was measured by gas chromatography (GC 2010, Shimadzu) using a gas-tight syringe (SGE 500 µL, Switzerland). GC measurements were taken each time volumetric gas production was measured. For GC measurements, a Carboxen™ 1010 PLOT column (Supelco, Bellefonte, PA) was utilized for separating sample gases with argon carrier gas at a constant pressure of 42.3 kPa and a constant flow rate of 10 mL/min and temperatures of 150ºC for the injector and 220ºC for the detector was used. The volume of methane produced by each BMP was converted to units of g COD using equation 4.2:

$$1\ mL\ CH_4 = \frac{1\ mmol\ CH_4}{22.4\ mL}\ \frac{273.15\ K}{310.15\ K}\ \frac{8\ meq\ e^-}{mmol\ CH_4}\ \frac{8\ mg\ COD}{meq\ e^-} = 2.52\ mg\ COD \quad \text{Equation 4.2}$$

### 4.2.4 Analytical Methods

Chemical oxygen demand (COD) was measured with HACH HR COD kits. Values were measured using a HACH DR 2800 spectrophotometer (Genesys 20, Thermo Spectronic, MA). Semi-soluble chemical oxygen demand (SSCOD) measured by passing samples through 1.2 micron glass fiber filters (Whatman, GF/C) before COD analysis as described in (Lee et al., 2010). TSS and VSS were determined according to Standard

Methods (Clesceri et al., 1998). VSS measurements were converted to g COD by using the conversion 1.42 g COD/g ADS VSS, as described in (Rittmann and McCarty, 2001).

Samples for VFA analysis were filtered through a 0.22 μm PVDF membrane filters before being analyzed by high-performance liquid chromatography (LC-20AT, Shimadzu, Columbia, MD). An Aminex HPX-87H column (Bio-Rad Laboratories, Hercules, CA) was used to separate organic acids. The column was operated at 65°C at a flow rate of 0.6 mL/min. Analytes were detected using a Diode Array Detector (SPD-M20A, Shimadzu, Columbia, MD) and a Refractive Index Detector (RID-10A, Shimadzu, Columbia, MD).

### 4.2.5 Modeling First-order Hydrolysis Constants and Maximum Rates of Recovery

When modeling first-order kinetics, it is typically assumed that no products are initially present. This is not the case in many batch digestions, especially when the substrate has undergone pretreatment to pre-hydrolyze or pre-ferment material. Not accounting for this material will result in over-estimation (if methane is initially produced from pre-solubilized and fermented material) of kinetic parameters. It is for this reason that we introduced the parameter $P_{start}$. Similarly, incorporating concentrations of intermediate products prevents under-estimation of kinetic parameters by accounting for material that undergoes hydrolysis but is not immediately converted to methane. In the case of SSCOD + $CH_4$, for example, the products, P, at time, t, are defined as:

$$P = CH_{4,t} + SSCOD_t - P_{start} \quad \text{Equation 4.3}$$

where $CH_{4,t}$ is the cumulative methane at time t, $SSCOD_t$ is the SSCOD concentration at time t, and $P_{start}$ is the initial product concentration present at the start of the batch digestion, in this case the initial SSCOD concentration.

First-order rate constants were calculated four ways: from cumulative $CH_4$ production, VSS destruction, cumulative $CH_4$ production + SSCOD concentration, and cumulative $CH_4$ production + VFA concentration. In every case except for VSS, the first-order rate equation in terms of ultimate COD recovery, after incorporation of Equation 4.3, was expressed as:

$$P = (P_{max} - P_{start}) [1\text{-}exp (-k_{hyd}t)] + P_{start} \quad \text{Equation 4.4}$$

where P is the cumulative products recovered at time t in g COD $L^{-1}$, $P_{max}$ is the ultimate COD potential [g COD $L^{-1}$], $P_{start}$ represents products present at the beginning of the digestion in g COD $L^{-1}$, and $k_{hyd}$ is the first-order rate constant [$d^{-1}$]. This is a modified version of the first-order rate equation described previously (Angelidaki et al., 2009; Parameswaran and Rittmann, 2012; Trzcinski and Stuckey, 2012). In the case of VSS, the equation was modified to represent solids removal instead of product accumulation with the following equation:

$$P = (P_{max})[1+ exp (-k_{hyd}t)] + VSS_{NBD} \quad \text{Equation 4.5}$$

where $PCOD_t$ is the VSS [g COD $L^{-1}$] concentration at time, t, $PCOD_{max}$ is the ultimate VSS destruction [g COD $L^{-1}$], and $PCOD_{NBD}$ is the non-biodegradable fraction of the VSS [g COD $L^{-1}$]. In both cases parameters were estimated by minimizing sum relative error of measured and predicted values with Solver in Excel as described in (Koch and Drewes, 2014). Parameters were estimated for each replicate digestion (n=3). Maximum

product recovery rates were calculated from the slope of the initial linear regions of cumulative recovery, d0-d5 for methanogenic digestions, and d0-d3 for digestions with BES.

## 4.3 Results and Discussion

### 4.3.1 Effects of Pretreatment

Thermal pretreatment was performed on WAS to assess its ability to increase the rate or extent of methane recovery from this sludge fraction after combination with PS. Figure 4.1 shows the COD contributions of PS and WAS to each digestion after mixing and the addition of ADS inoculum. Only 1 ± 1% of the WAS COD was found in semi-soluble form without pretreatment (Figure 4.1). After thermal pretreatment, this fraction was increased to 24 ± 1% of the total WAS COD, indicating pre-hydrolysis of solids was achieved (Figure 4.1). We observed similar results of thermal pretreatment to those reported in previous studies for this temperature and duration (Carrère et al., 2010). The semi-soluble fraction increased by 0.66 ± 0.01 g COD $L^{-1}$, equivalent to 27 ± 1% of the initial WAS VSS.

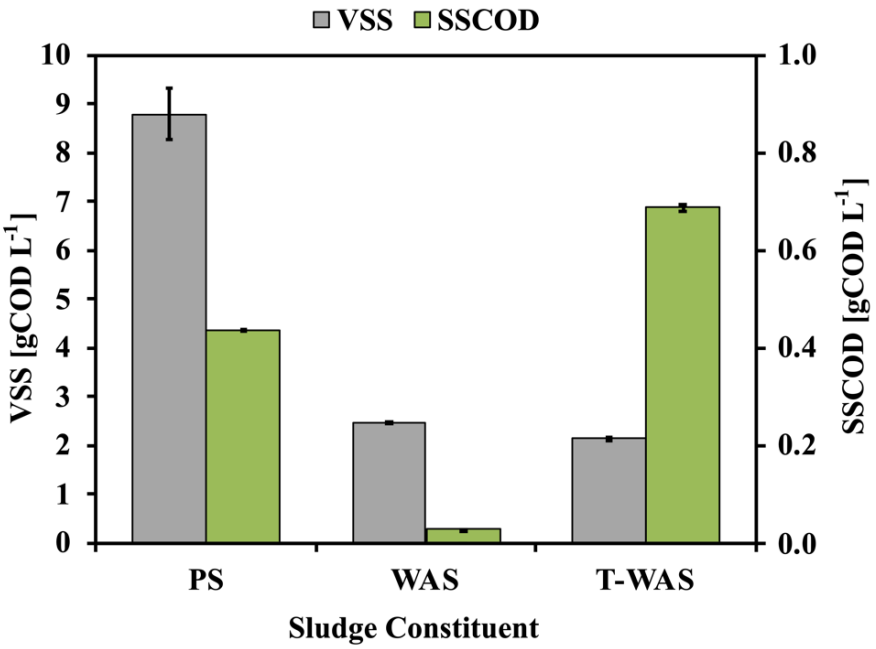


Figure 4.1 Distribution of loaded substrate between the solid and liquid fractions of primary sludge (PS), waste activated sludge (WAS), and thermally pretreated waste activated sludge (T-WAS). Error bars represent ± one standard error (n=3).

WAS solubilization has the potential to increase the ultimate methane recovery if the solubilized or partially solubilized portion corresponds to a fraction that would otherwise not be degraded under the timescale of anaerobic treatment. However, because the concentration of raw WAS was 10 ± 0.1 g COD $L^{-1}$ as compared to the concentration of raw PS of 38 ± 2 g COD $L^{-1}$, the fraction of thermally pretreated WAS present as SSCOD only represented 6 ± 0.04% of the total loaded substrate COD, when combined 1:1 on a volumetric basis. If pre-solubilization of bioavailable solids is the only benefit of this form of thermal pretreatment, then only a marginal increase in ultimate methane recovery should have been expected. If, however, this form of thermal pretreatment

results in increased biodegradability of the remaining pre-treated solids, a greater ultimate methane recovery as well as a faster methane production rate could be expected.

### 4.3.2 Methane Recovery and Intermediate Hydrolysis Product Accumulation

Methane accumulated at a rapid rate until day 8, when production decreased for both sets of digestions (Figure 4.2, panel D). The rate of methane production during this initial period was 0.82 ± 0.20 g COD $L^{-1}D^{-1}$ without pretreatment and 0.96 ± 0.08 g COD $L^{-1}D^{-1}$ with pretreatment, a non-significant increase (p=0.29, n=3,3, two sample t test) (Table 4.1). The congruency of this initial, highest rate of methane production indicates that the limiting process for anaerobic digestion was the same in both cases and was not affected by thermal pretreatment. It is notable that the increase in initial SSCOD in batch digestions with thermally pretreated WAS during days 0-5 did not result in immediately increased methane production rates. This could indicate that hydrolysis and solubilization of WAS solids was not immediately limiting in these batch digestions, but possibly methanogenesis itself was rate-limiting in this phase. On average pretreatment resulted in increased methane accumulation at all time points ($p=7E^{-11}$, n=22, one sample t test), but the ultimate methane at the final time point, 8.2 ± 1.3 g COD $L^{-1}$ without pretreatment vs. 10.2 ± 0.7 g COD $L^{-1}$ with pretreatment, was not significantly different (p=0.13, n=3,3, two sample t test).

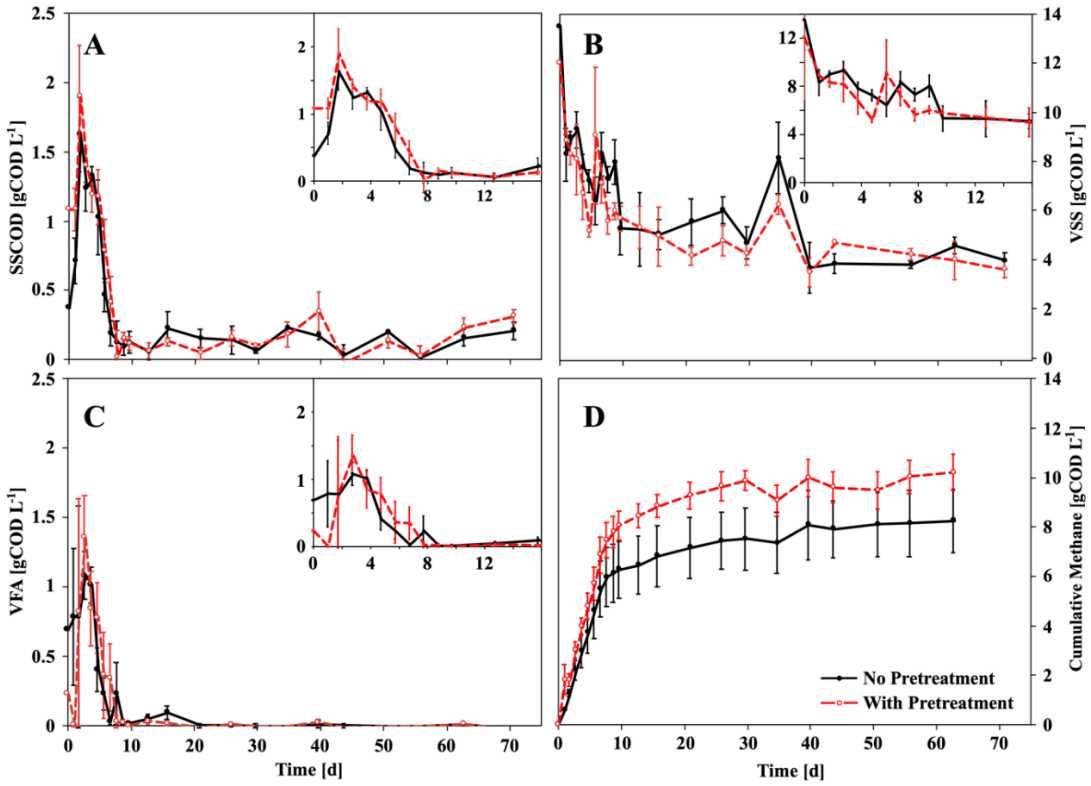


Figure 4.2 SSCOD, VSS, total VFA, and cumulative methane for batch methanogenic digestions with and without pretreatment. The insets show the first 16 days of the respective data. Red lines represent batch methanogenic digestions with thermally pretreated WAS. Black lines represent batch methanogenic digestions with no pretreatment. Error bars represent ± one standard error (n=3).

The first eight days of maximum methane production corresponded a period of SSCOD accumulation (Figure 4.2, panel A). Accumulations of intermediate products have been associated with highly degradable fractions of substrate. If pretreatment increased the degradability of the WAS solids, a greater accumulation of intermediate products would be expected with the same inoculum, as was used here. Thermal pretreatment resulted in significantly more SSCOD for the first day, 0.37 ± 0.01 g COD

$L^{-1}$ without pretreatment vs. 1.08 ± 0.03 g COD $L^{-1}$ with pretreatment (p=0.02, n=3,3, two sample t test). However, by day 2 there was no significant difference (p=0.19, n=3,3, two sample t test) in the maximum accumulation of SSCOD of 1.63 ± 0.27 g COD $L^{-1}$ without pretreatment and 1.90 ± 0.37 g COD $L^{-1}$ with pretreatment. The majority of this SSCOD was in the form of VFAs (Figure 4.2, panel C). The accumulation of intermediate products in this initial period, along with the simultaneous reduction of the majority of VSS in the same period (Figure 4.2, panel B), suggests that hydrolysis of most of the COD occurred in this period. As no significant differences in either accumulated SSCOD or VFAs occurred, no increased biodegradability can be inferred due to the thermal pretreatment.

The accumulation of VFAs indicates that the rate limiting process was acetogenesis or methanogenesis during this initial eight-day period. If this were not the case, no accumulation would be expected to be observed as all hydrolyzed COD would be fermented and subsequently converted to methane gas before intermediate products could accumulate. After day 10, VFA intermediates were below the detectable limits in batch methanogenic digestions, indicating that a process other than methanogenesis was limiting. While both sets of batch digestions show a similar trend in VFA accumulation, there was a delay in VFA accumulation in the digestions containing thermally pretreated WAS (Figure 4.2, panel C).

Figure 4.3 shows product accumulation in batch digestions that were conducted with the methanogenic inhibitor BES to observe the rates of intermediate accumulation in

the absence of consumption and eventual conversion to $CH_4$. With BES, PCOD was semi-solubilized by hydrolysis to SSCOD before being further hydrolyzed and fermented to VFAs. In the absence of methanogenesis, VFAs accumulated until product inhibition prevented further fermentation. There was significantly more SSCOD in the pretreated batch digestion with BES only for the first day, $1.40 \pm 0.10$ g COD $L^{-1}$ without pretreatment vs. $1.98 \pm 0.11$ g COD $L^{-1}$ with pretreatment ($p=0.02$, $n=3,3$, two sample t test) after which there was no significant increase in SSCOD accumulation due to thermal pretreatment (Figure 4.3, panel A). This mirrors the results seen in the uninhibited digestions. Similar trends of VSS removal were also observed for pretreated and unpretreated digestions with BES as those without, and no significant decrease in VSS concentration was observed past the first day for pretreated samples (Figure 4.3, panel B). Methanogenesis inhibition resulted in the accumulation of a greater concentration of intermediates; more than double the magnitude of SSCOD and VFA concentrations were present. No further increase in VFA or SSCOD accumulation was observed after day 8 (figure 4.3), when less than half of the COD recovered as methane in methanogenic digestions was present as intermediates, indicating product inhibition.

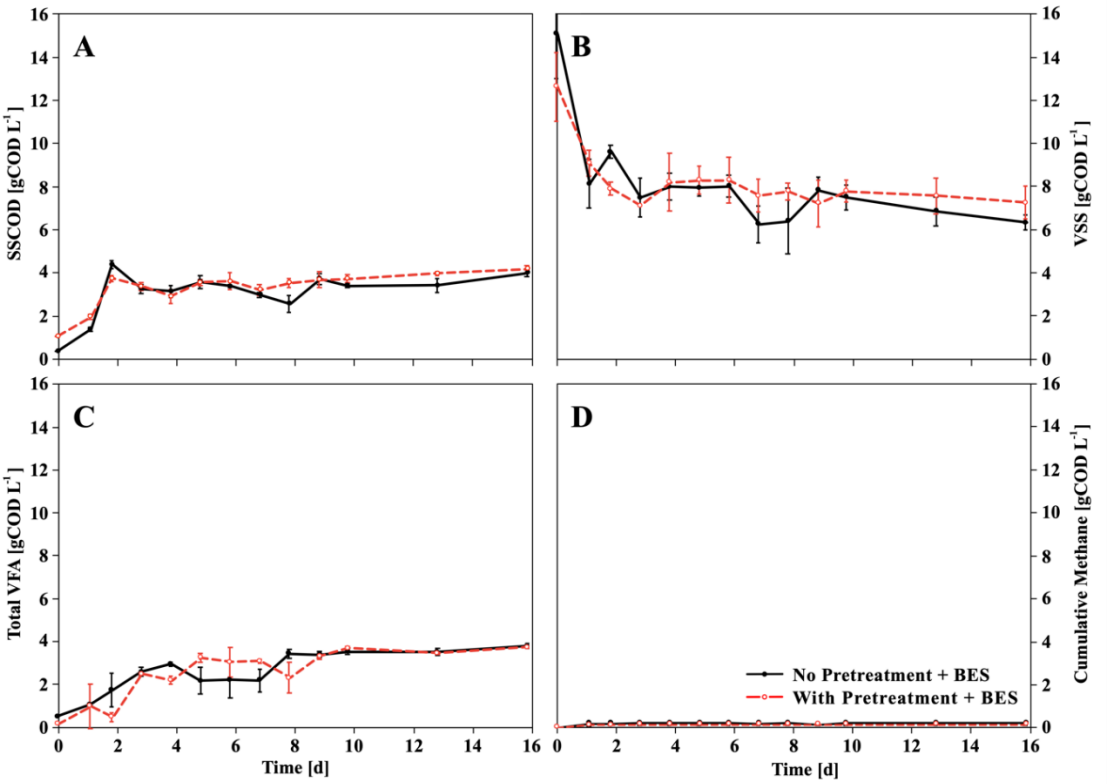


Figure 4.3. SSCOD, VSS, total VFA, and cumulative methane for batch methanogenic digestions with and without pretreatment with BES added to inhibit methanogenesis. Red lines represent batch methanogenic digestions with thermally pretreated WAS. Black lines represent batch methanogenic digestions with no pretreatment. Error bars represent ± one standard error (n=3).

The individual constituents of the transient VFA accumulation are shown in supplementary Figures 10.1 and 10.2. The initial peak VFA accumulation was primarily composed of acetic acid and propionic acid, with smaller components consisting of isovaleric acid, isobutyric acid, butyric acid, and caproic or isocaproic acid. VFA accumulation in BMPs with BES was dominated by acetic acid and propionic acid, with smaller fractions of butyric acid, isobutyric acid, valeric acid, and isovaleric acid. The

trends of VFA accumulation in both sets of BMPs was similar, with no apparent differences induced by this mode of thermal pretreatment.

### 4.3.3 Calculation of First-order Rate Constants

Hydrolysis rate constants are commonly approximated by fitting methane accumulation in batch methanogenic digestions with a first-order rate equation. Using Equation 4.4 and Equation 4.5, the ultimate methane potential and hydrolysis constant were fitted simultaneously by minimizing the sum relative error between predicted and measured product concentrations. Hydrolysis constants may be accurately estimated from cumulative methane alone only when hydrolysis is rate-limiting. By combining cumulative methane with transient SSCOD, hydrolysis resulting in semi-solubilized material that is not immediately converted to methane is accounted for in the rate approximation. This is indicative of particulate COD (PCOD) hydrolysis, the first steps of anaerobic digestion after disintegration. Similarly, combining cumulative methane with transient VFAs indicates the cumulative rate of SSCOD hydrolysis. Finally, parameters were also estimated directly from VSS reduction. This is a more direct measurement of hydrolysis, but these measurements are more prone to variability and are less precise.

Hydrolysis constants of $0.12 \pm 0.01$ $d^{-1}$ without pretreatment and $0.14 \pm 0.01$ $d^{-1}$ with pretreatment were estimated from methane alone (Figure 4.4, Table 4.1). While the pretreated value was slightly higher, the values were not significantly different from each other ($p=0.086$, $n=3,3$, two sample t test). For digestions without pretreated WAS,

incorporating SSCOD generated a significantly larger ($p=0.031$, $n=3,3$, two sample t test) hydrolysis constant with a value of $0.16 \pm 0.01$ $d^{-1}$. This indicates that without pretreatment, the earlier stages of PCOD hydrolysis proceeded faster than subsequent SSCOD hydrolysis. After thermal pretreatment the PCOD hydrolysis constant of $0.17 \pm 0.01$ $d^{-1}$ was not significantly different ($p=0.09$, $n=3,3$, two sample t test) than the value calculated from methane alone, $0.14 \pm 0.01$ $d^{-1}$. For batch digestions producing methane, thermal pretreatment did not result in significantly different hydrolysis constants for any calculation method (Figure 4.4, Table 4.1).

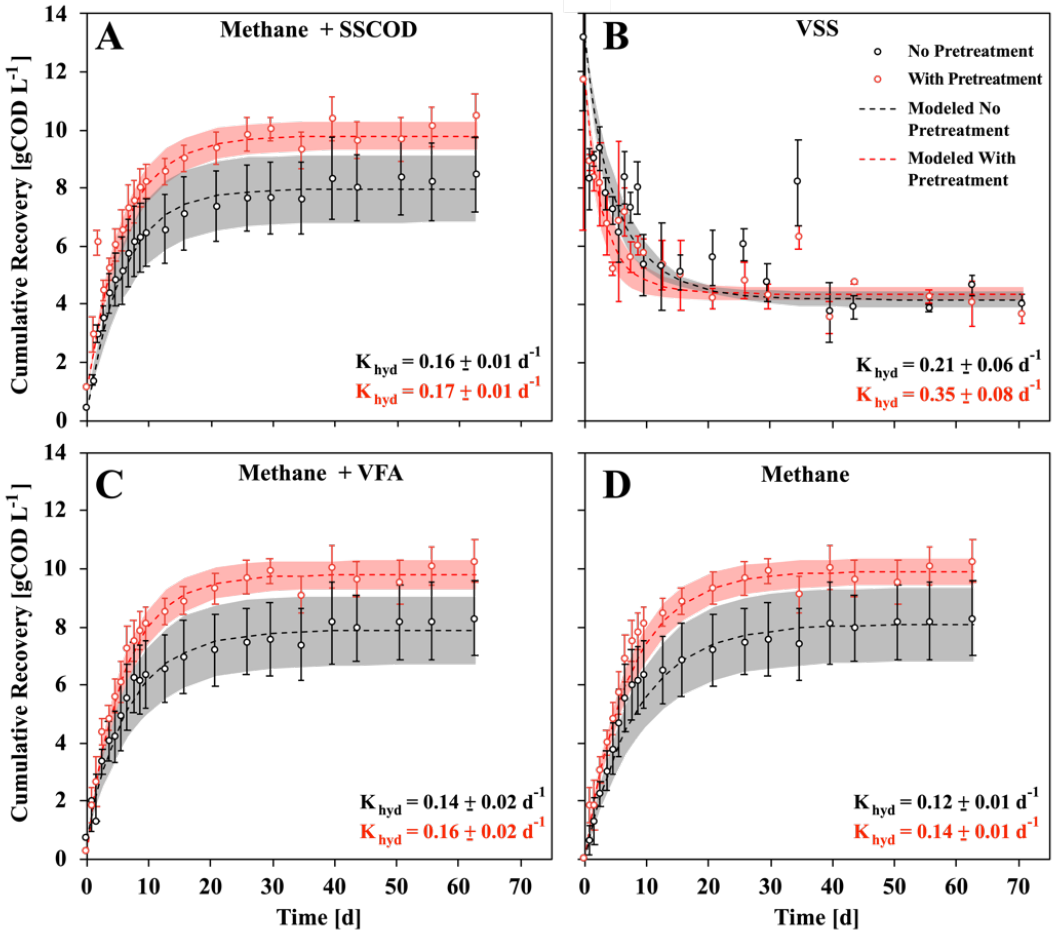


Figure 4.4 Modeled product formation with first-order approximations for batch methanogenic digestions. Rates are shown for VSS destruction, methane accumulation, methane + SSCOD, and methane + VFAs. Circles represent measured quantities; error bars indicate ± one standard error (n=3). Dashed lines represent modeled first order reactions fitted to the measured data; shaded areas represent ± one standard error of modeled data (n=3).

Table 4.1 First-order kinetic parameters for batch methanogenic digestions with and without pretreatment and BES. Details about the modeled and measured parameters may be found in section 2.5 of the methods. R-squared values are reported for the fit between modeled and measured data.

| Experiment | Measurement | Max Rate [gCOD $L^{-1}D^{-1}$] | $P_{start}$ [gCOD $L^{-1}$] | $VSS_{NBD}$ [gCOD $L^{-1}$] | $P_{max}$ [gCOD $L^{-1}$] | $k_{hyd}$ [$d^{-1}$] | $R^2$ |
|---|---|---|---|---|---|---|---|
| No Pretreatment | Methane | 0.82 ± 0.20 | 0.00 ± 0.00 | - | 8.09 ± 1.26 | 0.12 ± 0.01 | 0.97 |
| | Methane + SSCOD | 0.95 ± 0.16 | 0.37 ± 0.01 | - | 7.98 ± 1.16 | 0.16 ± 0.01 | 0.98 |
| | Methane + VFA | 0.80 ± 0.14 | 0.69 ± 0.01 | - | 7.89 ± 1.17 | 0.14 ± 0.02 | 0.98 |
| | VSS | 0.94 ± 0.01 | - | 4.18 ± 0.29 | 8.97 ± 0.29 | 0.21 ± 0.06 | 0.72 |
| Pretreatment | Methane | 0.96 ± 0.07 | 0.00 ± 0.00 | - | 9.91 ± 0.45 | 0.14 ± 0.01 | 0.98 |
| | Methane + SSCOD | 0.88 ± 0.05 | 1.08 ± 0.03 | - | 9.80 ± 0.48 | 0.17 ± 0.01 | 0.95 |
| | Methane + VFA | 1.13 ± 0.08 | 0.23 ± 0.00 | - | 10.56 ± 0.66 | 0.16 ± 0.02 | 0.99 |
| | VSS | 1.19 ± 0.10 | - | 4.38 ± 0.23 | 7.35 ± 0.66 | 0.35 ± 0.08 | 0.85 |
| No Pretreatment + BES | SSCOD | 1.10 ± 0.06 | 0.37 ± 0.00 | - | 3.99 ± 0.17 | - | - |
| | VFA | 0.81 ± 0.12 | 0.50 ± 0.00 | - | 3.79 ± 0.12 | - | - |
| | VSS | 1.17 ± 0.05 | - | 7.14 ± 0.18 | 8.76 ± 2.09 | - | - |
| Pretreatment + BES | SSCOD | 0.79 ± 0.06 | 1.08 ± 0.00 | - | 4.19 ± 0.16 | - | - |
| | VFA | 0.70 ± 0.07 | 0.17 ± 0.00 | - | 3.74 ± 0.06 | - | - |
| | VSS | 0.67 ± 0.16 | - | 7.61 ± 0.37 | 5.38 ± 1.76 | - | - |

First-order hydrolysis constants were not calculated from digestions with BES due to the clear presence of product inhibition, as evidenced by the much lower accumulation of products (Figure 4.3) when compared to methanogenic digestions (Figure 4.2). This indicates that the presence of accumulated SSCOD and VFAs thermodynamically slowed upstream hydrolysis processes, preventing the use of the first-order rate model, designed to emulate product accumulation that is limited only by substrate concentration. However, we were able to compare the maximum rates of product accumulation in digestions with BES to those of methanogenic digestions, as the initial accumulation occurs before product inhibition takes place. These maximum rates were calculated as the slope of the initial linear region of product accumulation, d0-d5 for methanogenic and d0-d3 for digestions with BES, and are reported in Table 4.1. In methanogenic batch

digestions, pretreatment significantly increased (p=0.05, 3,3, two sample t test) the rate of SSCOD hydrolysis from 0.80 ± 0.14 gCOD $L^{-1}d^{-1}$ to 1.13 ± 0.08 gCOD $L^{-1}d^{-1}$. In general, maximum product recovery rates from methanogenic digestions with pretreatment were higher or no different than methanogenic digestions without pretreatment. In methanogenically inhibited batch digestions, however, pretreated digestions tended to exhibit the same or lower product recovery rates. This could indicate that increased degradability resulted in increased product inhibition, even in the initial stages of digestion. This suggests that batch digestions using VFA accumulation as a proxy for hydrolysis are at risk of underestimating rate parameters at high loadings.

## 4.4 Conclusions

Due to the smaller relative COD content by volume of the WAS as compared to PS, the potential benefits of WAS pretreatment are minimized under typical loading conditions encountered at a wastewater reclamation facility. Pretreating WAS alone before performing mixed sludge digestion did not result in significantly increased methane production rates or increased total methane recovery. These results do not support the suggestion that thermal pretreatment of this kind results in increased biodegradability of the remaining solids. While thermal pretreatment was found to increase initial PCOD hydrolysis to SSCOD, subsequent SSCOD hydrolysis occurred at similar rates and remained a possible rate-limiting step. As other thermal pretreatment processes do show increased methane recovery, it would be valuable to determine at what

point thermal pretreatment at higher temperatures could result in a benefit to treating WAS alone, rather than the entire waste stream.

# 5 MODEL SUBSTRATES YIELD COMPLEX RECOVERY PATTERNS DURING METHANOGENIC AND ELECTROGENIC BATCH ANAEROBIC DIGESTION


## Abstract

Anaerobic digestion (AD) is commonly used to recover energy contained within municipal sewage as combustible methane gas. Kinetic parameters for specific substrates are often measured using biochemical methane potential (BMP) tests that analyze the methane production rate and total methane recovery efficiency. These parameters are used to design municipal-scale plants, but there is a large degree of variability associated with reported parameters. This is partially due to the complex nature of the biochemical transformations occurring during AD. Particulate material is first hydrolyzed until soluble before being stepwise fermented to acetate and hydrogen, the substrates for methanogenesis. While hydrolysis is often considered rate-limiting and parameters for this process are calculated based upon downstream processes, this may often not be the case, resulting in inaccurate measurements. Some models assume independent hydrolysis and digestion of different classes of organic polymers, such as protein and carbohydrates. Results presented here test this assumption, and several others about the calculation of kinetic parameters of AD. BMP tests were conducted with casein and cellulose as model substrates.

In addition to traditional BMP tests, a new technique for monitoring digestion kinetics was utilized, a microbial electrolysis cell. This system utilizes the unique activity of anode respiring bacteria to replace gas production from methanogenesis with current production, a value that can be measured in real-time to provide high-resolution rate data.

The model substrates casein and cellulose were found to yield a complex pattern of multiple concurrent methane and current recovery events. Most of these recovery events were found to be associated with the consumption of volatile fatty acid (VFA) intermediates, and not independent hydrolysis events. It was also found that using methane or current alone greatly underestimates the rates of particulate hydrolysis in these batch tests. Incorporating VFAs and methane or current into rate calculations yielded much more accurate results.

Acknowledgements

Michael Waddington, Sharad Kumar Vellore Suresh, Jimmy Xu, Prathap Parameswaran, and César I Torres contributed to the experimental design, data collection, and analysis of the results presented in this chapter. This chapter will be prepared for submission for peer-reviewed publication with the above-mentioned as authors.

## 5.1 Introduction

Anaerobic digestion is a widely-used technology for the stabilization of municipal wastewater sludges and the recovery of energy in the form of methane gas (McCarty et al., 2011; Rittmann, 2008). In this process, primary and secondary sludge particulates are hydrolyzed to semi-soluble and soluble fractions of chemical oxygen demand (COD) before being fermented to produce volatile fatty acids, carbon dioxide, and hydrogen (Parkin and Owen, 1987). The final stabilization step is for acetate and hydrogen to be converted to methane gas via methanogenesis. These two substrates are utilized by distinct archaeal groups, acetoclastic and hydrogenotrophic methanogens (Thauer et al., 2008). Hydrogenotrophic methanogens are syntrophically linked with acidogenic fermenters, and are important hydrogen consumers in the anaerobic community (Parameswaran et al., 2009). Excess hydrogen may be converted to acetate through the activity of homoacetogens, shuttling electrons to acetoclastic methanogens (Parameswaran et al., 2010).

The maximum rate of solids destruction or methane production during anaerobic digestion depends upon the recalcitrance of the substrate. Recalcitrant substrates comprised of high molecular weight polymers typically undergo hydrolysis at a slower rate, and thus the subsequent processes of fermentation and methanogenesis are delayed due to substrate limitation (Sanders et al., 2000). Due to the relative heterogeneity of municipal sludges and the presence of recalcitrant components, hydrolysis is generally assumed to be rate-limiting (Parkin and Owen, 1987). Kinetic parameters of AD rates are used in the design process for municipal-scale digesters (Batstone et al., 2015). These

parameters are most commonly derived from simplified kinetic models utilizing first-order degradation kinetics (Vavilin et al., 2008). These parameters are typically measured with biochemical methane potential (BMP) tests that use the production rate of methane as an indirect measure of the rate-limiting anaerobic digestion step (Angelidaki et al., 2009; Hansen et al., 2004; Owen et al., 1979). Cumulative methane produced over the course of a BMP test most commonly show a saturation-like accumulation curve. This is often the justification for the use of first-order kinetic models (Koch and Drewes, 2014). BMP curves rarely show a perfect first order relationship, however (Burger and Parker, 2013; Yasui et al., 2008); some BMPs show periods of rapid methane recovery separated by periods of reduced recovery, clearly exhibiting non first-order kinetics. Limitations on the frequency at which gas data may be collected could be obscuring a higher order kinetic process or processes that would otherwise be observed.

While BMP tests can be effective for estimating the final stabilization efficiency of a given substrate, the limitations on the frequency with which kinetic data may be recorded hamper accurate parameter estimation (Stromberg et al., 2014). Microbial Electrolysis Cells (MEC) are an alternative platform for kinetic measurements that utilize the current produced by anode respiring bacteria (ARB), instead of methane gas production, as indicators of the cumulative rate of anaerobic digestion (Lusk et al., 2017). MECs allow real-time monitoring of respiration rates of ARB (Torres et al., 2007). Figure 5.1 shows results of batch AD experiments conducted in MECs using cellulose and casein as substrates. The rate of COD recovery was measured every two minutes in

the form of current. Multiple distinct kinetic events were observed in both conditions despite the relatively simple substrates used. Also, more events were observed as the substrate loading was decreased. These results demonstrate the ability of the MEC platform to collect rate data at high temporal resolution. However, the rate data alone do not provide an explanation of what the multiple kinetic events represent. Previous studies have observed similar kinetic events in batch methanogenic experiments, suggesting that the events could be from multiple hydrolysis events of different components of the waste or due to the accumulation of VFA intermediates (Yasui et al., 2008; Trzcinski and Stuckey, 2012).

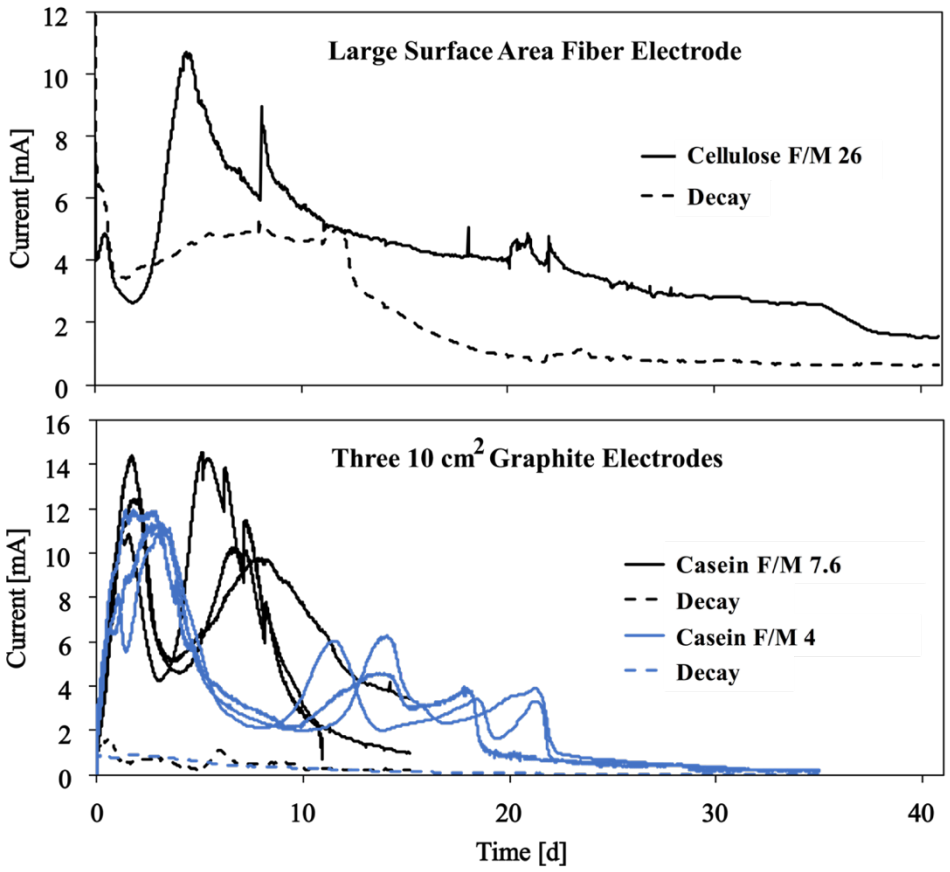


Figure 5.1 Examples of batch anaerobic digestion experiments carried out in MECs. The top panel shows results from cellulose digestion in an MEC with a high surface area carbon fiber anode and a high substrate loading. The bottom panel shows the results of casein digestion in MECs at higher (black) and lower (blue) loadings. In both panels, dashed lines indicate MECs that were run without substrate to measure endogenous biofilm decay.

Co-digestion of food waste or FOG in traditional AD systems is becoming more common (Koch et al., 2014). In these operations, high loadings of COD-dense solids are added to digesters with the intent to increase methane production rates. Methane increases due to these additional substrates rarely meet the theoretically predicted values

(Tandukar and Pavlostathis, 2015). This could be an indication that, at high loadings of these more labile substrates, the AD process is less approximated by first order kinetics and BMP tests are not able to predict digester performance. It has been shown that co-digestion can increase VFA concentrations, sometimes resulting in the souring of AD reactors (Koch et al., 2015). Some AD models assume independent hydrolysis of proteins, carbohydrates, and lipids (Girault et al., 2012; Young et al., 2013). The experiments presented here were designed to test the independence of hydrolysis of carbohydrate and protein fractions of a waste stream, as well as identify the nature of the multiple kinetic events observed in MEC and BMP batch anaerobic digestions. Here experiments are presented using cellulose and casein as model substrates in BMP and MEC batch tests inoculated with anaerobic digested sludge (ADS). Methane and current production were monitored for combined and individual substrates and samples were taken regularly for volatile fatty acid (VFA) analysis.

## 5.2 Materials and Methods

### 5.2.1 Inoculum

Anaerobic digested sludge (ADS) was obtained from the Mesa Northwest Wastewater Reclamation plant in Mesa, AZ for use in BMP and MEC experiments. The Mesa plant has an 18 MGD-capacity and utilizes an activated sludge process with anoxic-oxic zones for biological nutrient removal. Sampled ADS was incubated at 30°C and stirred for 5 days to degas and remove residual digestible material, as recommended by (Angelidaki et al., 2009). The volatile suspended solids (VSS) of the ADS were measured according to standard methods immediately before loading into the MECs and BMPs.

### 5.2.2 Mineral Medium

A mineral solution of 100 mM phosphate buffer (15 mM $Na_2HPO_4$, 85 mM $KH_2PO_4$), 10 mM ammonium chloride, and a trace mineral solution containing 0.5 g/L EDTA, 0.114 g/L $CoCl_2 \cdot 2H_2O$, 0.01g/L $H_3BO_3$, 0.02g $Na_2MoO_4 \cdot 2H_2O$, 0.001g/L $Na_2SeO_3$, 0.01 g/L $Na_2WO_4 \cdot 2H_2O$, 0.02 g/L $NiCl_2 \cdot 6H_2O$, 1.16 g/L $MgCl_2$, 0.05 g/L $MnCl_2 \cdot 4H_2O$, 0.05 g/L $ZnCl_2$, 0.01 g/L $CuSO_4 \cdot 5H_2O$, 0.01 g/L $AlK(SO_4)_2$, and 0.114 g/L $CaCl_2 \cdot 2H_2O$ was prepared in 18 MΩ $DiH_2O$. This solution was autoclaved and sparged with $N_2$ gas until anaerobic. This medium was used for both BMP and MEC experiments.

### 5.2.3 Batch Methanogenic Digestion Tests

Batch methanogenic digestion tests were conducted similarly to the protocol for BMPs previously outlined except that all experiments were conducted in vessels that allowed intermittent sampling of the liquid fraction in addition to the headspace gas volume and composition (Angelidaki et al., 2009; Owen et al., 1979). Hereafter, the batch digestions are referred to as "BMPs" though they have been modified significantly to be able to sample intermediate liquid fractions. Degassed inoculum was added to minimal mineral media and supplemented with particulate substrates. Casein, cellulose or both were added to methanogenic and electrogenic batches to achieve food to microorganism (F/M) ratios (gCOD/gVSS) shown in Table 5.1. The total volume of inoculum, media, and substrate was 350 mL for all experiments. All BMP experiments were conducted in air-tight one-liter bottles fitted with gas and liquid sampling locations. Headspace gas production volume was periodically measured with a glass syringe (SGE 500 μL,

Switzerland). $CH_4$ and $CO_2$ composition within the headspace was measured by gas chromatography (GC 2010, Shimadzu Corporation, Columbia, MD) utilizing a thermal conductivity detector in conjunction with a packed bed column (Shin Carbon ST 100/120 mesh, Restek Corp., Bellefonte , PA), and nitrogen as the carrier gas.

Table 5.1 Initial loadings of all BMP and MEC experiments. F/M loadings are based upon the ratio of the initial substrate concentration in g COD/L to the ADS inoculum mass in g VSS/L. MEC and BMP experiments were conducted sequentially. The overall loadings vary due to slight differences in the solids content of the ADS used in each case. BMPs and MECs loaded with casein and cellulose contained equal concentrations of each substrate on a COD basis.

| Type of Reactor | Substrate | Loading [gCOD/L] | F/M [gCOD/gVSS] |
|---|---|---|---|
| MEC | Nothing | 0.0 | 0 |
| MEC | Casein | 15.7 | 4 |
| MEC | Cellulose | 7.8 | 2 |
| MEC | Casein and Cellulose | 11.7 | 3 |
| BMP | Nothing | 0.0 | 0 |
| BMP | Casein | 15.1 | 4 |
| BMP | Cellulose | 7.5 | 2 |
| BMP | Casein and Cellulose | 11.3 | 3 |

### 5.2.4 Microbial Electrolysis Cell Tests

H-type MECs were constructed with an anode area of approximately 30 $cm^2$ as previously described (Parameswaran et al., 2009). Graphite electrodes were used for the anodes and cathode. Cathode chambers were initially filled with a 100 mM NaCl solution to provide sufficient electrolytes. An anode-respiring biofilm was pre-grown using inoculum from a previously grown microbial electrochemical cell. Biofilms were grown using acetate in minimal mineral medium with an anode potential set at -0.3 V vs.

Ag/AgCl (-0.1 V vs SHE) with a potentiostat (Bio-logic). When the anode respiring biofilms reached current densities greater than 5 $A/m^2$, the acetate medium was removed, the inoculum, medium, and particulate substrates were added and the experiment was started. Current production was continuously measured and logged using a potentiostat (bio-logic). 10 mM bromoethane sulfonate (BES) was added as a methanogenic inhibitor to MEC reactors. BES has been shown to have a measurable COD, though it is biologically unavailable.

### 5.2.5 Volatile Fatty Acid Analysis

Liquid samples for analysis were periodically taken from MEC and BMP experiments. Samples were filtered through 0.22 μm PVDF membrane filters before being analyzed by high-performance liquid chromatography (LC-20AT, Shimadzu, Columbia, MD). An Aminex HPX-87H column (Bio-Rad Laboratories, Hercules, CA) was used to separate organic acids. The column was operated at 50°C at a flow rate of 0.6 mL/min. Analytes were detected using a Diode Array Detector (SPD-M20A, Shimadzu, Columbia, MD) and a Refractive Index Detector (RID-10A, Shimadzu, Columbia, MD).

### 5.2.6 pH Measurements and Adjustments

Periodically, liquid samples were collected from MEC and BMP batch reactors to conduct pH measurements. When necessary, the bulk pH of either MEC or BMP reactors was adjusted to 7 by the addition of a small amount of concentrated sodium hydroxide solution.

### 5.2.7 Hydrolysis Modeling

Hydrolysis constants were calculated by fitting observed data with a first order rate expression. Fitted curves and constant values were calculated with a least-squares fitting technique in Microsoft Excel, using the solver function. Ultimate methane potential and the hydrolysis constants were both solved for. Parameters were fitted for cumulative methane, cumulative charge, cumulative methane + VFA, and cumulative charge + VFA.

## 5.3 Results and Discussion

### 5.3.1 Multiple Recovery Events are Observed From the Digestion of Casein and Cellulose

Experiments were set up in batch MECs and BMPs loaded with casein, cellulose, and a combination of both substrates. By observing the recovery kinetics of casein and cellulose separately in concurrent experiments, I define the pattern of recovery for each substrate individually. If these substrates were hydrolyzed independently of one another, then the experiments with both substrates should exhibit patterns of recovery analogous to the sum of the individual recoveries. Figure 5.2 shows the cumulative recovery as charge and methane for MECs and BMPs (converted to gCOD $L^{-1}$) as well as the rate of charge or methane recovery (in gCOD $L^{-1}d^{-1}$). Casein and cellulose produced recovery signals in similar timeframes, and it is not evident that one would be responsible for early recovery and another for delayed recovery. Each MEC and BMP showed at least three recovery events, more clearly indicated by the plots of recovery rate versus time. The MEC and BMP experiments fed with casein and cellulose also showed at least three

recovery events. The combined substrate experiments do not show more recovery events than experiments with only casein or cellulose. This indicates that the individual recovery events for single substrates occured at approximately the same time in each kind of reactor.

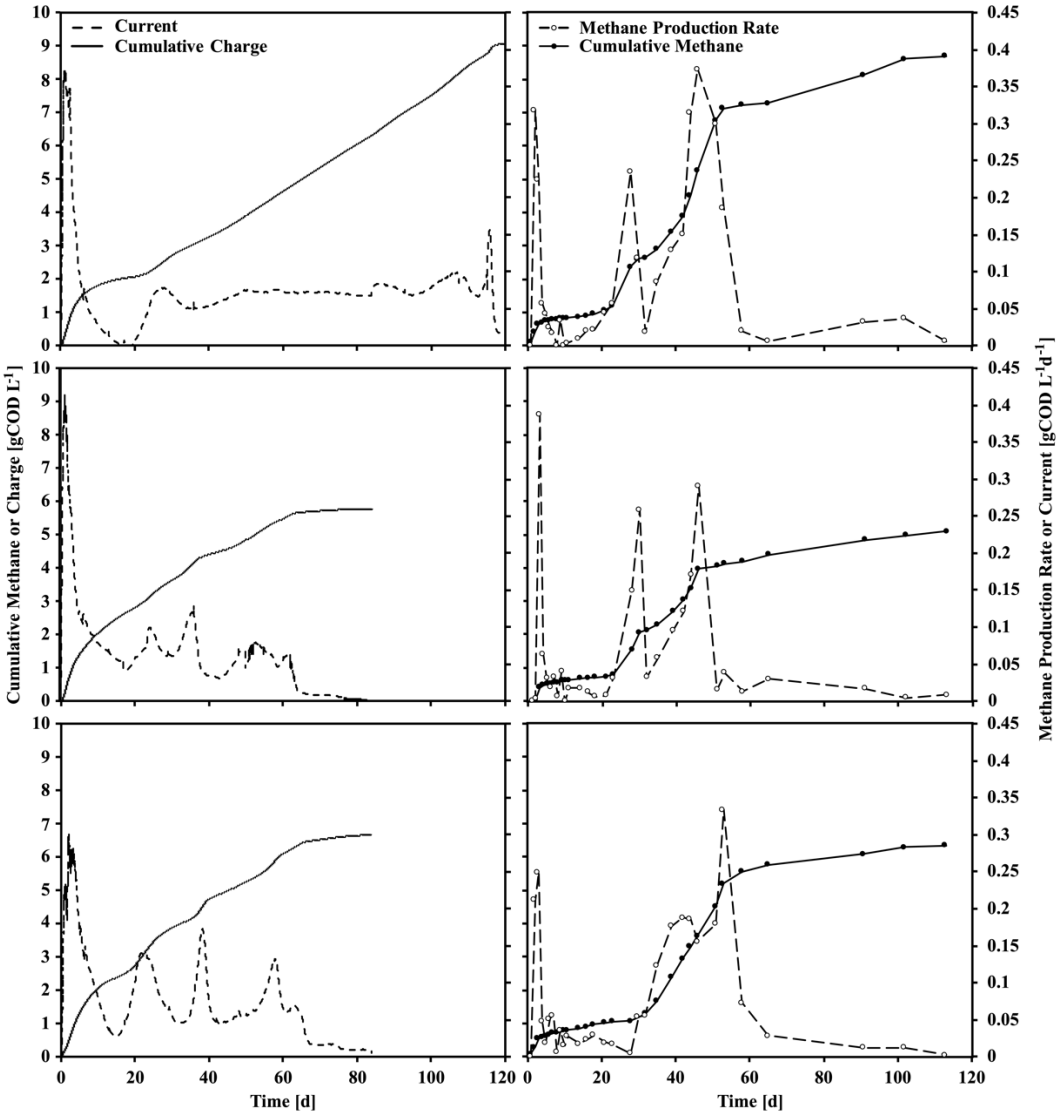


Figure 5.2 COD cumulative recovery and recovery rates for MEC and BMP experiments. Dashed lines represent current or methane production rates in gCOD $L^{-1}d^{-1}$ (right axis). Solid lines represent cumulative COD recovery in gCOD $L^{-1}$ (left axis). Values of control

MEC digestions and BMPs conducted with inoculum but without substrate have been subtracted from all datasets.

Multiple kinetic events were observed in both systems, in which the rate of recovery of methane or electrons increased for a period of time before decreasing again. When contrasting MEC and BMP experiments, it is apparent that MECs allowed more highly resolved recovery data. MEC curves were the product of direct measurements of ARB respiration rates in two-minute increments, while BMP curves were from daily (beginning) or weekly (end) measurements. BMP curves exhibited fewer total events while individual recoveries are defined by only three to five data points. This results in less precise fitting with modeled data, as is evident in the $r^2$ values in Figure 5.7.

### 5.3.2 Most Recovery Events Corresponded to VFA Consumption.

The typical rate measurement for hydrolysis in AD kinetic experiments are based on methane production. Similarly, the experiments in Figure 5.2 show the rates of methanogenesis and anode respiration. Both of these processes typically occur more quickly than upstream hydrolysis and fermentation steps and are thus used as indirect measurements for these processes. However, the rates of recovery in the MEC and BMP experiments all demonstrated three or more recovery events and not the typical first-order rate. In each case, one of these events took place primarily within the first five days and was concurrent with increasing VFA concentrations and some initial methane or current production, clearly shown in Figure 5.3. The production of VFAs resulted from the fermentation of solubilized substrates. As the only substrates added in these experiments are particulate, and there were negligible initial VFAs, this first event must be associated

with the hydrolysis of these added components. The accumulation of VFAs at this time indicates that either subsequent fermentation or utilization by methanogens or anode respiring bacteria was rate limiting during this period.

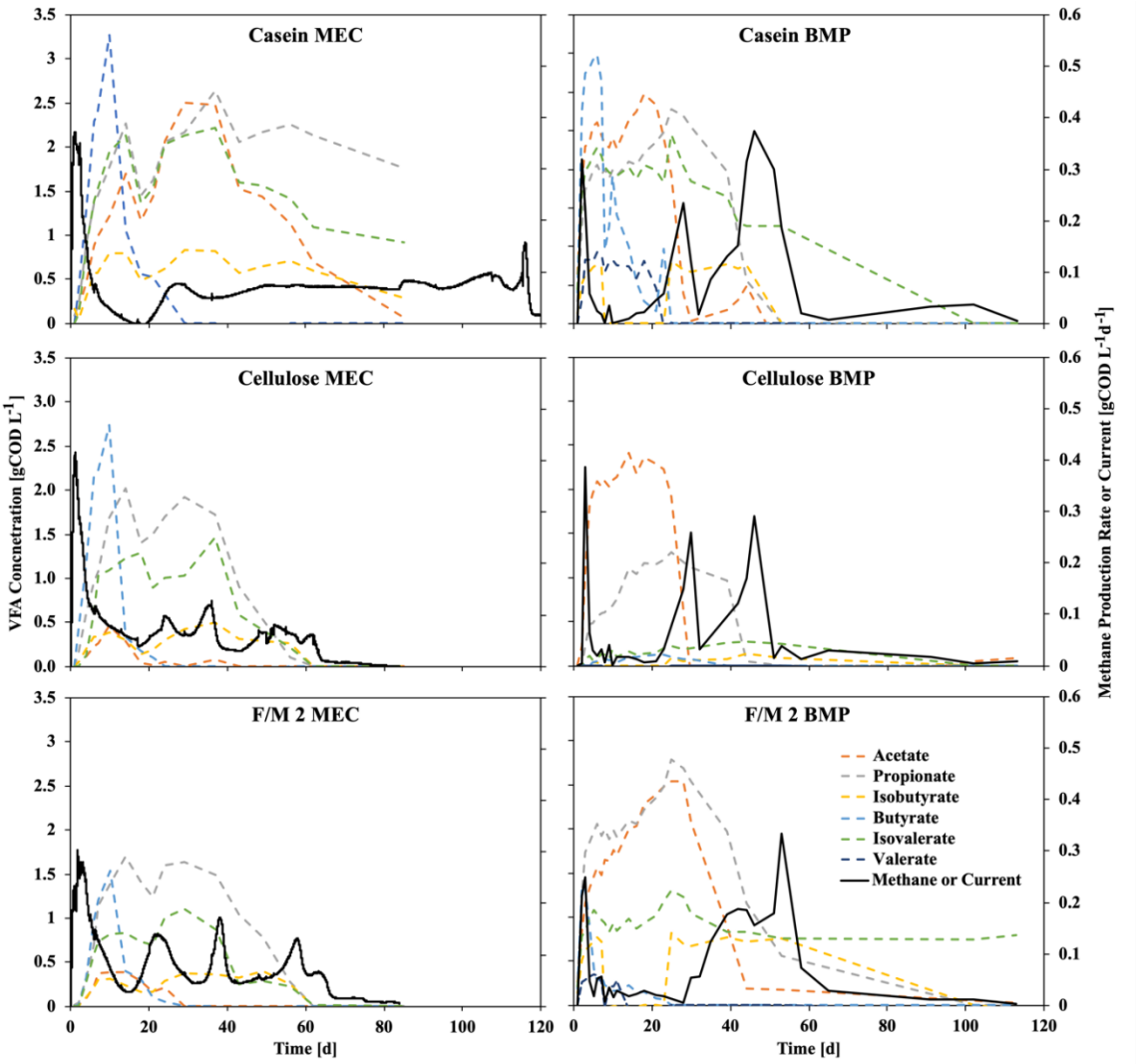


Figure 5.3 Individual VFA concentrations over time in MEC and BMP experiments. Dashed lines indicate acetate, propionate, isobutyrate, butyrate, isovalerate, and valerate concentrations over time as gCOD $L^{-1}$ (left axis). Solid black lines indicate current or methane recovery rates in gCOD $L^{-1}d^{-1}$ (right axis).

In all BMP experiments, the first event was followed by the accumulation of valerate, butyrate, propionate, and acetate. This was followed by a stall in methane generation and a fast acetate consumption (~ day 20). Acetoclastic methanogens were clearly limiting methane production until this second event, possibly due to inhibition or low concentrations. A third event was associated with propionate, now able to be fermented to acetate before being utilized for methanogenesis.

Current recovery in MECs after the first event was limited by stalled VFA fermentation and consumption. In each MEC experiment, accumulation of butyrate occurred immediately after the first current recovery event. This is a characteristic signal of high hydrogen concentrations leading to thermodynamic inhibition of butyrate fermentation. Subsequent VFAs produced were also consumed at a slower rate than in the parallel BMP experiments. This can be explained from the addition of BES, an inhibitor of hydrogenotrophic methanogens, a key hydrogen consumer whose presence allowed VFA fermentation to be thermodynamically favorable. The concentration of most VFAs persisted until approximately day forty, but acetate concentrations remained low, indicating that anode respiration was not limiting. This was not the case for the MEC loaded with casein. This experiment does show persistence of accumulated acetate, indicating that in this case anode respiration was a limiting rate.

VFA accumulation contributed to pH depression during the first thirty days for MEC and BMP experiments except the casein only fed BMP. These differences were due to varying rates at which planktonic methanogens and biofilm-bound ARB consumed and

produced acids. A greater degree of pH depression was observed in the MEC reactors than in the BMPs. The effect of this transient pH depression was minimized through the addition of 100 mM phosphate buffer to all conditions before the start of the experiment. This was specifically to prevent inhibition of methanogens and ARB. Periodic addition of a sodium hydroxide solution further prevented pH values from dropping below 6.3 for the duration of all the experiments.

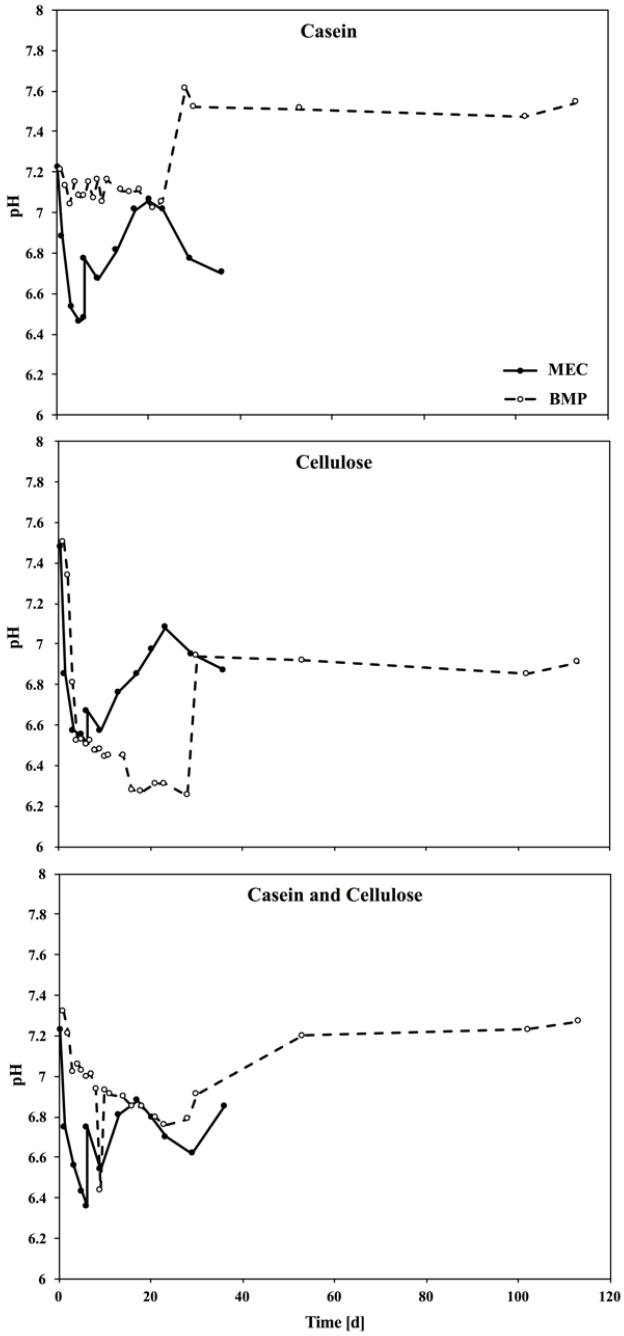


Figure 5.4 Bulk liquid pH measurements for MEC and BMP experiments. Solid points with solid lines indicate MEC pH values. Open points with dashed lines indicate BMP experiments.

### 5.3.3 Hydrolysis of Particulate Substrates Occurred Rapidly

I demonstrate that the first recovery event in each pattern was associated with particulate hydrolysis due to the accumulation of VFAs and methane or current. Figure 5.5 illustrates that, in all cases, the sum of all measured VFAs during these first recovery events and the current or methane produced in the same period accounted for virtually all the ultimate COD recovered. This is evidence that particulate hydrolysis occurred rapidly for casein and cellulose under these conditions and was not the rate limiting step.

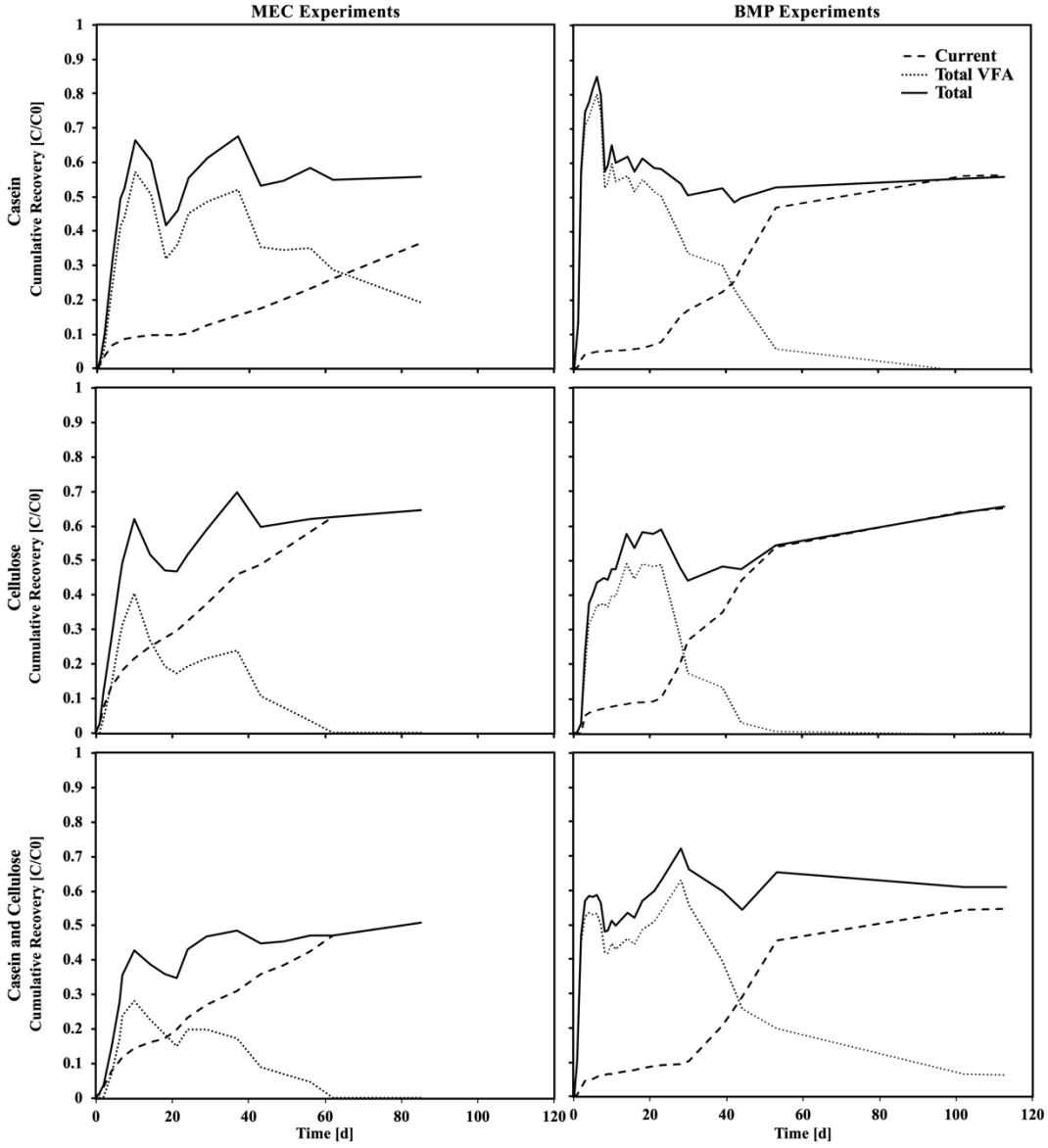


Figure 5.5 Recovery of current, methane, and VFAs as fractions of loaded COD. Dashed lines represent cumulative coulombs for MECs and cumulative methane for BMPs. Dotted lines indicate the sum of all VFAs measured by HPLC. Solid lines indicate the sum of Methane or Coulombs and VFAs.

Each MEC had a transient decrease in the total recovered COD around day twenty. This corresponded to the consumption of butyrate without proportional production of other VFAs or current. This could be the result of uptake and storage

processes in the microbial community. High concentrations of VFAs after the starvation conditions experienced by the AD inoculum and ARB could have triggered the production of storage materials that were re-released later, resulting in a temporary reduction in the observed total recovery, but no ultimate increase.

### 5.3.4 Methane or Current Alone Were Not Good Indicators of the Rate of Particulate Hydrolysis

COD recovery in Figure 5.2 was modeled using a first order rate function, and the results are shown in Figure 5.6 as dashed lines. This yielded hydrolysis rate constants between 0.010 $d^{-1}$ and 0.018 $d^{-1}$ for all experiments. In this case, using these values as a proxy for particulate hydrolysis greatly underestimates the true value. Methanogenesis, current production, or fermentation were all limiting at times in some experiments, not allowing for an accurate hydrolysis rate estimation. Even limiting the fitting to the first event did not yield realistic hydrolysis rates, as even though this recovery event was the result of hydrolysis, excess VFAs were accumulated that were unaccounted for. Methane or charge may only be used to approximate particulate hydrolysis when hydrolysis itself is the rate limiting process. This is not the case if intermediates are accumulating.

The total recovery from Figure 5.5 was also fitted with a first order rate function, visible as solid lines in Figure 5.6. This incorporated the accumulation of VFAs as well as methane and current production. Hydrolysis rate constants calculated from CH4 + VFA were 20 -100 times greater than those calculated with charge or methane alone. Interestingly, the constants were not consistent between BMP and MEC experiments of the same substrate. ARB have been shown to have a lower half-saturation constant, $K_s$,

for acetate than Methanogens (2.8mM for ARB vs 7mM for Methanogens)(Torres et al. 2007). While this would suggest that MECs would exhibit faster VFA utilization, the anode surface area can limit the utilization rate due to diffusion limitations. In all cases, however, the incorporation of intermediates into particulate hydrolysis calculations greatly improved the accuracy and meaningfulness of measured kinetic constants.

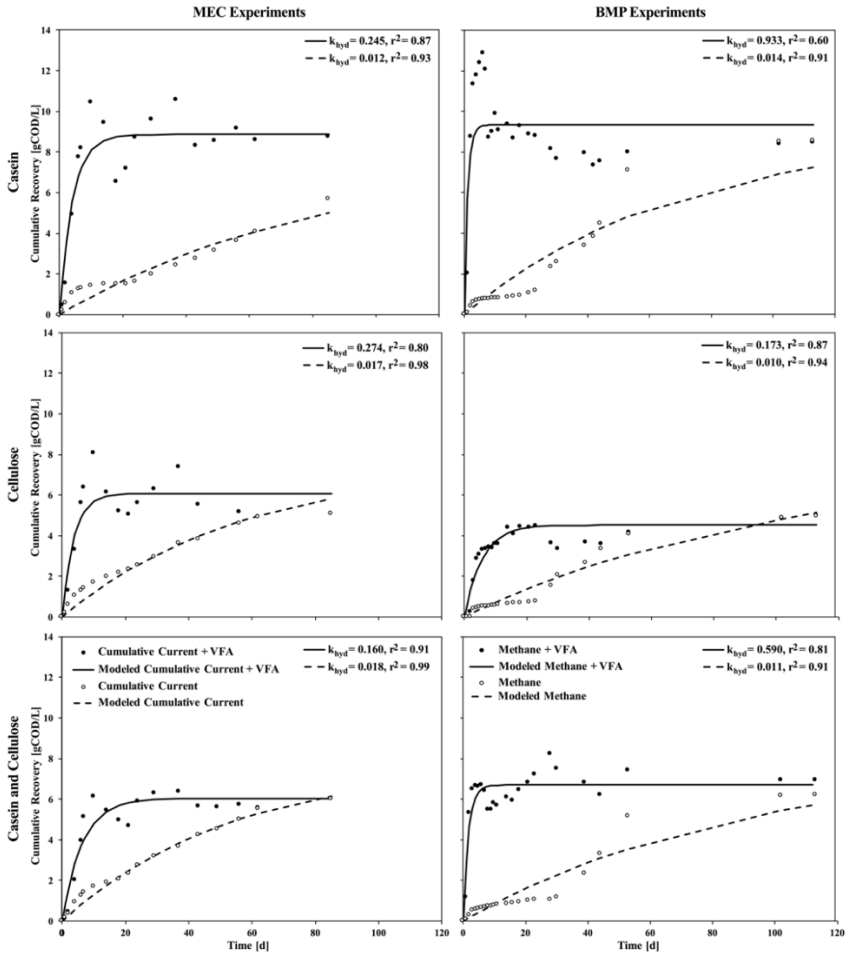


Figure 5.6 Modeled COD recovery assuming first order kinetics. Open circles indicate cumulative coulombs or methane. Dashed lines represent coulombs or methane modeled. Solids points are the sum of recovered methane or coulombs and the total measured VFAs. Solid lines illustrate the modeled coulombs/methane + VFAs.

## 5.4 Conclusions

Batch anaerobic digestion of the model substrates casein and cellulose resulted in a complex pattern of recovery events, whether using BMP tests or MEC batch digestions. Virtually all the ultimately recovered COD from the model particulate substrates casein and cellulose was hydrolyzed rapidly to VFAs in the first five to ten days of the batch digestion. Casein and cellulose were hydrolyzed and subsequently fermented concurrently, and there is no evidence that the multiple recovery events observed were due to multiple hydrolysis events. However, multiple events were the result of VFA accumulation, possibly inhibiting methane or current production before subsequent consumption. Because of this, methane or current production alone was not an accurate proxy for the rate of particulate hydrolysis. Hydrolysis kinetic measurements obtained using batch digestions should incorporate the accumulation of intermediate products to avoid underestimating actual rates.

# 6 KINETICS OF METHANOGENIC AND ELECTROGENIC BATCH ANAEROBIC DIGESTION OF MIXED MUNICIPAL SLUDGES


## Abstract

In the process of anaerobic digestion, acetoclastic and hydrogenotrophic methanogens, along with hydrolytic and fermentative bacteria, convert complex particulate biomass within municipal waste sludges into methane gas. To determine the kinetic rates of this process, methanogenic batch digestions are commonly used. Batch tests are performed by anaerobically digesting a specific substrate in a sealed vessel while measuring the rate of methane production and the total amount of methane produced. This requires frequent measurements of the volume and composition of the gas produced. Due to the necessity for produced gas to accumulate before measurement, a limited number of data points can be collected, typically no more than 1-3 per day. Electrogenic digestion tests take place in microbial electrochemical cells (MXC) and are an alternative anaerobic digestion technique that replaces methanogenic activity with an anode respiring biofilm that converts acetate and hydrogen to an electric current. By monitoring this current, we are able to measure the respiration rate of the anode respiring bacteria (ARB) directly in real-time. This direct measurement allows for more highly resolved characterization of the kinetics of anaerobic digestion of municipal sludges within electrogenic digesters. Parallel methanogenic and electrogenic batch experiments were conducted. Each digestion was loaded with primary sludge (PS), waste cultivated sludge (WAS) anaerobic digested sludge (ADS) to mimic conditions in digesters at municipal water reclamation facilities. The MEC biofilms were pre-grown using acetate medium so

that ARB would not be limiting and the intermediate products of hydrolysis and fermentation were monitored. The rate and extent of methane accumulation was faster than charge accumulation in electrogenic digestions. All digestions exhibited complex recovery patterns, and carbohydrates were found to be selectively digested before proteins in all cases.

Acknowledgements

Collette Wilson contributed to the data collection and Prathap Parameswaran, and César I Torres contributed to the experimental design and analysis of the results presented in this chapter. This chapter is prepared and will be submitted for peer-reviewed publication with the above-mentioned as authors.

## 6.1 Introduction

The process of anaerobic digestion is widely used to stabilize municipal sludges produced during the wastewater treatment process (U.S. Environmental Protection Agency, 1999). This stabilization process results in fewer solids to dispose of, higher quality solids, and it produces methane gas that may be used to offset the energy requirements of upstream treatment processes (Rittmann, 2008). Two types of sludges are produced and digested during typical activated sludge wastewater treatment, primary sludge (PS) and waste activated sludge (WAS) (Tchobanoglous et al., 2014).

Anaerobic digestion involves the disintegration, hydrolysis, and fermentation of solid sludges to produce methane gas, leading to 40-60% of solids converted into methane gas (Parkin and Owen, 1987). This multi-step process is most commonly modeled using simple first-order kinetics (Eastman and Ferguson, 1981; Pavlostathis and Gomez, 1991; Trzcinski and Stuckey, 2012). This is a simplification based upon the rate-limiting step assumption, that states that in a multistep process the overall rate is determined by a single rate-limiting step (Parkin and Owen, 1987; Pavlostathis and Gomez, 1991). Typically, hydrolysis is thought to be the rate limiting step in this process (Eastman and Ferguson, 1981; Parkin and Owen, 1987; Pavlostathis and Gossett, 1988; Sanders et al., 2000; Vavilin et al., 1996; Veeken et al., 2000). However, recovery patterns from batch anaerobic digestion tests often show multiple recovery events not consistent with first-order kinetics. At least three degradable fractions have been observed in primary sludge, each with distinct kinetics (Yasui et al., 2008). The authors

of this study propose these events correspond to multiple hydrolysis events. Similar complex patterns are commonly observed during the co-digestion of food-waste or after thermal pretreatment(Burger and Parker, 2013; Koch et al., 2015b; Li et al., 2016; Toutian et al., 2020). While cumulative recovery is often adequately represented by first-order kinetics even when multiple kinetic events are observed, the rate of methane or electron recovery are not.

Batch methanogenic tests are a commonly used technique for measuring the dynamics of batch anaerobic digestion of specific substrates (Angelidaki et al., 2009; Hansen et al., 2004; Owen et al., 1979; Stromberg et al., 2014). To conduct these assays, a small amount of the substrate is placed in a sealed bottle with a seed culture typically isolated from an active anaerobic digester. Gas production is then measured at regular intervals to show the cumulative methane production. Sometimes, batch methanogenic digestions are modified by adding buffer, or to allow intermediate liquid samples to be taken for analysis of digestion intermediates (Stromberg et al., 2014). These assays are also used to estimate hydrolysis constants for specific substrates based upon the rate and extent of methane recovery (Koch and Drewes, 2014; Sanders et al., 2000; Trzcinski and Stuckey, 2012; Vavilin et al., 2008).

An alternative potential sludge stabilization technology is to perform electrogenic digestion in a microbial electrochemical cell (MXC). An MXC is a technology that uses the activity of anode respiring bacteria (ARB) to oxidize an organic donor to produce an electric current (Debabov, 2008; Rabaey and Verstraete, 2005; Torres, 2012; Torres et

al., 2007). MXCs may also be used in fundamental studies to identify underlying rates of the multistep anaerobic digestion process (Parameswaran et al., 2009; Velasquez-Orta et al., 2011). Performing batch tests to measure kinetic parameters in MXCs has several advantages over traditional batch methane production tests. Current is analogous to the methane production rate in methanogenic digestions, and cumulative charge is equivalent to cumulative methane. Due to the necessity for gas to accumulate before measurement, methanogenic systems are limited in the frequency of measurements to hours or, more commonly, days. Current may be monitored continuously in and MXC, greatly increasing the resolution of collected kinetic data.

Our experiments were designed to test the utility of using current produced in MECs to track anaerobic digestion kinetics analogously to how methane production in batch methanogenic reactors is used as a proxy for hydrolysis rates. Chapter 5 examines this technique with the relatively simple substrates casein and cellulose. The results in Chapter 5 show that complex signals may arise from homogenous substrates, and that multiple "recovery events" were not necessarily the result of the hydrolysis of distinct fractions of particulate COD. Here this technique has been applied to the anaerobic digestion of real municipal sludges in proportions and concentrations relevant to wastewater treatment plants. PS and WAS solids are much more complex than casein or cellulose and could have fractions with distinct degradation kinetics. By analyzing methanogenic and electrogenic digestions and measuring intermediate products, it possible to determine whether hydrolysis is occurring simultaneously for all particulate

fractions and if distinct recovery events are the result of intermediate accumulation alone as was observed previously.

## 6.2 Methods

### 6.2.1 Sludge Sampling

Primary sludge (PS), waste activated sludge (WAS), and anaerobic digested sludge (ADS) were all collected from the Greenfield Water Reclamation Plant (GWRP) in Mesa, Arizona. PS was sampled from an active recirculation line associated with the primary settler. WAS was sampled from the recycle flow of the secondary settler to the aeration basin. ADS was sampled directly from the anaerobic digester. All sludge samples were immediately analyzed for total suspended solids (TSS), volatile suspended solids (VSS), total chemical oxygen demand (TCOD), and semi-soluble chemical oxygen demand (SSCOD) after sampling to calculate appropriate loadings for the digestions. ADS was allowed to degas for 48 hours prior to inoculation at 30 $^{o}$C with agitation.

### 6.2.2 MEC Biofilm Growth

Six MEC reactors were constructed as described previously (Torres et al., 2009). Briefly, glass anode and cathode chambers with a volume of ~ 350 mL were separated by an anion exchange membrane (AMI-7001, Membranes International, Glen Rock, NJ, USA). Anodes were constructed from three 10 $cm^2$ graphite rectangular prisms, while cathodes utilized a single 10 $cm^2$ graphite rectangular prism. An Ag-Ag/Cl reference electrode was used in each reactor for a three-electrode system, and the anode potential was poised at −0.3 V vs. the reference. A minimal media solution of 50 mM acetate,100 mM phosphate buffer (15 mM $Na_2HPO_4$, 85 mM $KH_2PO_4$), 10 mM ammonium chloride,

and trace minerals was prepared in 18 MΩ $DiH_2O$, autoclaved and sparged with $N_2$ gas until anaerobic. 5 mL/L of 4 g/L $FeCl_2 \cdot H_2O$ iron and 1 mL/L of 19.2 g/L sodium sulfide solution was added to the anaerobic medium via syringe. Reactors were inoculated with anaerobic digested sludge and media was continuously fed to the MECs with peristaltic pumps and oxygen resistant norprene tubing to facilitate selection and growth of anode biofilms.

### 6.2.3 Methanogenic and Electrogenic Batch Digestions

Methanogenic batch digestions were conducted in triplicate in anaerobic one-liter bottles that contained 500 mL of inoculum and substrate. Substrate concentration and composition were chosen to be similar to conditions at municipal treatment facilities. The substrate composition included a 50:50 mixture by volume comprised of PS and WAS at a concentration of 1.5% solids. To achieve this, the PS was diluted from 4% solids to 3% solids with DiH2O, to reflect a more typical concentration. The lid on each BMP was made of a rubber stopper with gas and liquid sample lines. The gas was sampled periodically with a gastight syringe (SGE 100 mL, Switzerland). The percentage of $CH_4$, $CO_2$, and $H_2$ in the headspace was measured by injecting 200 μL of headspace gas into a gas chromatograph (GC 2010, Shimadzu Corporation, Columbia, MD) with a CarboxenTM 1010 PLOT column (Supelco, Bellefonte, PA) using a gas-tight syringe (SGE 500 μL, Switzerland). Negligible $H_2$ was measured during the course of the digestions. Triplicate control methanogenic digestions were conducted with ADS only, and $DiH_2O$ instead of PS and WAS to have the same liquid and headspace volume.

To initiate electrogenic batch digestions in MECs the growth media was removed, and ADS inoculum, PS, and WAS substrate were added in the same proportions as used in the BMP experiments to a volume of ~350mL with <10mL of headspace. The current production was recorded in real-time with a potentiostat (Bio-Logic USA, Knoxville, TN) and computer software (Chronoamperometry, EC-Lab software) every 2 minutes for the duration of the digestions. To ensure all COD in electrogenic batch digestions was recovered as charge 10 mM bromoethane sulfonate (BES) was added to inhibit methanogenesis. The COD contribution of BES was subtracted from all results as it is known to be biologically unavailable. Triplicate control electrogenic digestions were conducted with ADS only and Di$H_2O$ instead of PS and WAS to have the same liquid volume.

Sodium bicarbonate was added such that the buffer concentration was 100 mM in methanogenic and electrogenic batch digestions. This was done to mitigate the effect of pH inhibition on methanogens or the anode biofilm. pH values were monitored for all experiments at each sampling point. pH Values remained above 7 for all experimental reactors for the duration of the experiments.

### 6.2.4 Chemical Analysis

Intermediate liquid samples were taken periodically from all digestions for the duration of the experiments. The pH of all samples was measured before dilution with a 1:1 ratio of DI $H_2O$ to increase the analyte volume. Total suspended solids (TSS) and volatile suspended solids (VSS) were measured according to standard methods. Semi-soluble chemical oxygen demand (SSCOD) was measured with the HACH HD COD kit

and HACH DR 2800 spectrophotometer (Genesys 20, Thermo Spectronic, MA) after liquid samples were passed through a glass microfiber filter with 1.2 μM pore size (GF/C, GE Healthcare, Life Sciences). Liquid samples for volatile fatty acid (VFA) analysis were further filtered through a 0.2 μm filter (Acrodisc LC 13 mm Syringe Filter, Pall, Life Sciences) before being analyzed with high performance liquid chromatography (Model LC-2 0AT, Shimadzu, Columbia, MD) equipped with an Aminex HPX-87H (Bio-Rad Laboratories, Hercules, CA, 1997) acids analysis column. Unfiltered samples were frozen for protein and carbohydrate analysis. Total proteins were measured with the BCA assay (Cat# 23225, Thermo Fisher Scientific). Carbohydrates were measured colorimetrically as described in (Dubois et al., 1956).

### 6.2.5 First-Order Kinetic Rate Models

Data was fitted to first order kinetic rate models as described in previous chapters. Analyses were performed in Microsoft Excel using the solver feature to minimize the sum squares of error between measured and modeled data by fitting the first order rate constant, ultimate recovered COD, and, in the case of VSS, the non-biodegradable fraction. Parameters incorporating SSCOD or VFAs included the initial concentration of these COD fractions, $P_{start}$, in the calculations. First-order models were created for methane and circuited electron accumulation, VSS, and for the aggregate parameters methane or circuited electrons + SSCOD, and methane or circuited electrons + VFA.

Representative digestions were also fitted as the sum of three first-order rate curves with different lag phases using the Gompertz Equation:

$$P=P_{max}\cdot\exp\{-\exp[\frac{R_p\cdot e}{P_{max}}\cdot(\lambda-t)+1]\}$$ Equation 6.1

where $P_{max}$ is the ultimate methane or circuited electron recovery, $R_p$ is the maximum rate of product formation [g COD $L^{-1}d^{-1}$], e is the exponent of 1, and λ is the lag phase [d] (Hobbs et al., 2017; Lay et al., 1996).

## 6.3 Results and Discussion

### 6.3.1 Initial SSCOD and VFA Accumulation Persists Longer in Electrogenic Digestions

Methanogenic and electrogenic digestions followed a similar pattern of VSS reduction, SSCDO and VFA accumulation, a recovery as methane or current, as shown in Figure 6.1. While VSS destruction followed a similar pattern in both systems, the recovery was significantly slower in electrogenic digestions. During the first 10 days, a fast accumulation of SSCOD, mostly composed of VFAs, suggested a fast hydrolysis rate that cannot be recovered as methane or current at a fast-enough rate. Nonetheless, pH values did not decrease significantly due to our high bicarbonate concentration (100 mM). At the end of the digestion, total recoveries were similar in both types of digestion, while the electrogenic digestion took longer to consume VFAs produced in the initial hydrolysis event. This slower recovery in electrogenic digestions may be partially attributed to insufficient anode surface area relative to the substrate loading. Previous digestions of sludges in electrogenic systems with greater surface area have not shown this lag (Ki and Torres, unpublished).

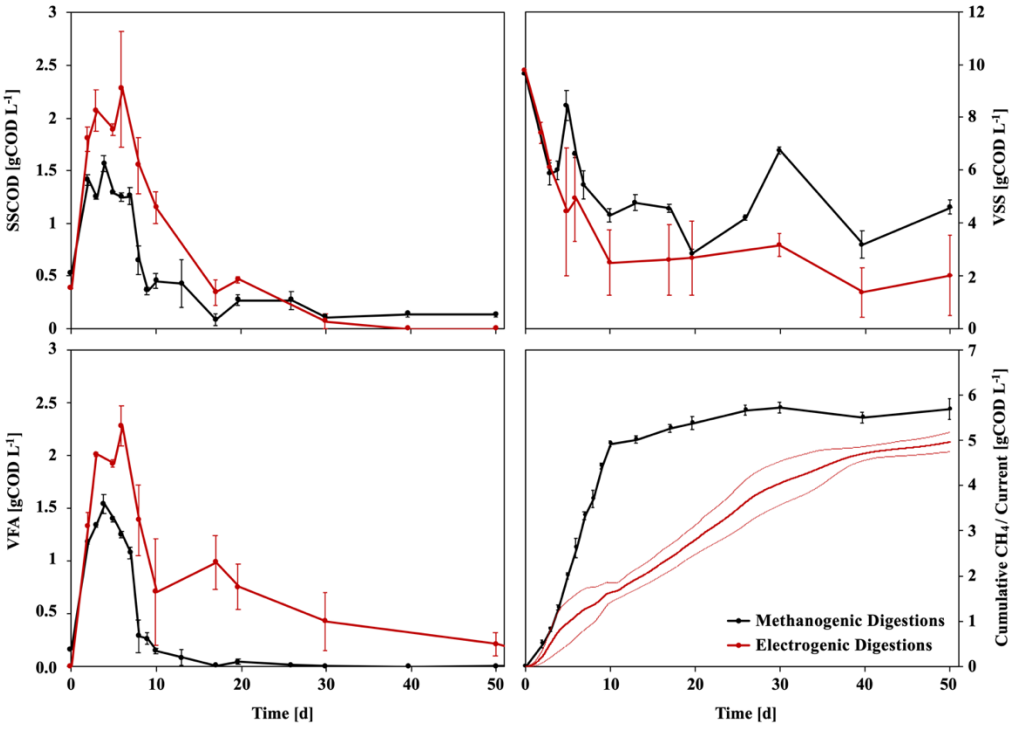


Figure 6.1 VSS, SSCOD, VFA, Methane, and Circuited Electrons recovery. Negative control values have been averaged (n=3) and subtracted for each dataset. Error bars represent one standard error (n=3 for each). The grey region accompanying the cumulative circuited electron graph also represents one standard error; continuous error calculations are possible due to the very high number of data points (n=3 reactors, ≈52,000 points each).

### 6.3.2 Particulate Hydrolysis and SSCOD Hydrolysis Occurred at Similar Rates in Methanogenic and Electrogenic Digestions

A detailed analysis of the kinetics of each system is shown in Figure 6.2, wherein results of first-order rate approximations are shown. The analysis is divided into four parts: VSS, methane or circuited electrons + SSCOD, methane or circuited electrons + VFA, and methane or circuited electrons alone. These were chosen because they represent distinct stages in the anaerobic digestion process. VSS destruction is representative of disintegration and initial hydrolysis to the semi-soluble fraction.

Methane or circuited electrons + SSSCD illustrates the cumulative rate of all hydrolysis to the semi-soluble stage and that which has already been recovered as methane or electrons. Similarly, methane or circuited electrons + VFAs illustrate the cumulative rate of complete hydrolysis and already recovered methane or electrons. Finally, methane or circuited electrons alone are the most analogous to traditional BMP tests, with only the final step of anaerobic digestion being measured in each case.

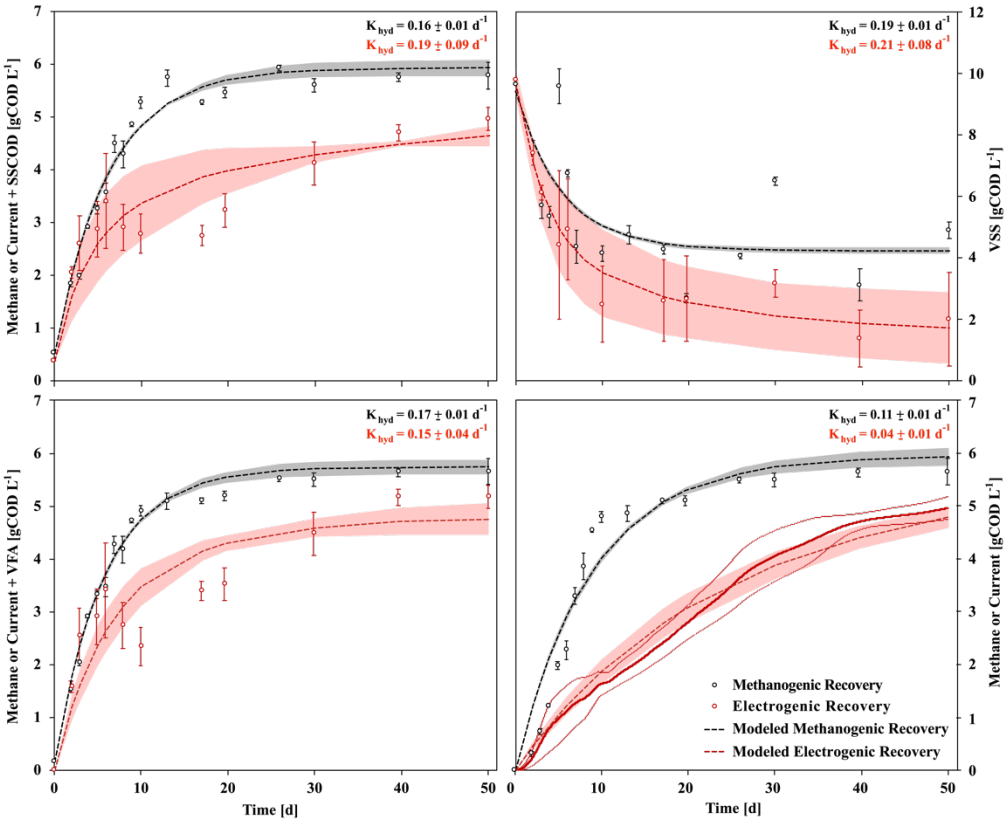


Figure 6.2 Modeled product formation with first-order approximations for batch methanogenic and electrogenic digestions. Fittings are shown for VSS destruction, methane or current accumulation, methane or current + SSCOD, and methane or current + VFAs. Circles represent measured quantities; error bars indicate ± one standard error (n=3). Dashed lines represent modeled first order reactions fitted to the measured data; shaded areas represent ± one standard error of modeled data (n=3).

The calculated first order rate constant ($k_1$) of methane alone was larger than for circuited electrons alone, reflecting the more rapid accumulation of methane (Table 6.1). The values of product formation, however, were the slowest calculated rate constants. This indicates that the rates of methane or electron accumulation alone were not indicative of the rates of upstream digestion processes such as disintegration, hydrolysis, or fermentation. VSS destruction was the fastest modeled process, and similar rates were observed for both systems. Different curves resulted in similar rate constants due to variation in the other of modeled parameters: the ultimate fraction degraded and the non-biodegradable fraction. The similarity of rate constants calculated for VSS and methane or circuited electrons + SSCOD is logical, because the ADS inoculum that contributed to disintegration and hydrolysis was the same in both sets of experiments. Particulate substrates underwent hydrolysis and solubilization at similar rates, while VFA fermentation and methane or electron production proceeded more slowly. Based on these observations, methanogenic and electrogenic methods are both adequate systems for measuring hydrolysis rates as long as intermediate products are tracked.

Table 6.1 Calculated hydrolysis constants and ultimate product recovery for methanogenic and electrogenic digestions. Values are calculated for Methane or Current, Methane or Current + SSCOD, Methane or Current + VFA, and VSS destruction. Error represents ± one standard error (n=3).

| Experiment Type | Measurement | Hydrolysis Constant [$d^{-1}$] | Ultimate Recovery [$gCOD\ L^{-1}$] | $r^2$ |
|---|---|---|---|---|
| BMP | Methane | 0.11 ± 0.01 | 5.95 ± 0.17 | 0.95 |
| | Methane + SSCOD | 0.16 ± 0.01 | 5.93 ± 0.15 | 0.98 |
| | Methane + VFA | 0.17 ± 0.01 | 5.74 ± 0.14 | 0.99 |
| | VSS Consumption | 0.19 ± 0.01 | 5.20 ± 0.19 | 0.54 |
| MEC | Current | 0.04 ± 0.01 | 5.74 ± 0.49 | 0.99 |
| | Current + SSCOD | 0.18 ± 0.09 | 5.01 ± 0.56 | 0.82 |
| | Current + VFA | 0.15 ± 0.04 | 4.80 ± 0.34 | 0.80 |
| | VSS Consumption | 0.21 ± 0.08 | 8.22 ± 1.30 | 0.62 |

### 6.3.3 Patterns of Electrogenic and Methanogenic Hydrolysis Rate Show Multiple Events

While first-order rate approximations are able to provide us with general kinetic parameters for the rate and extent of cumulative methane or charge recovery, they do not accurately represent hydrolysis rates, as shown in Figure 6.4. In Figure 6.4, representative rates for methanogenic and electrogenic digestions were plotted based on methane +VFAs and electrons + VFAs. These represented the major hydrolysis products and considered the fast VFA accumulation during the first few days of digestion. Similar to results presented in Chapter 5, we observed various hydrolysis events, shown as peaks in the rate curve (Figure 6.4, C-D). The peaks suggest a sequential hydrolysis event, in which a sludge component was hydrolyzed and depleted before another component was being hydrolyzed, leading to an increase in rate that forms a new peak. At least three

hydrolysis events were observed in the methanogenic digestions, while 4-6 events were observed in electrogenic digestions. The rate profiles shown in Figure 6.4 cannot be modeled with a single first-order hydrolysis model, since this model would only predict an exponentially decreasing rate (Figure 6.4, green lines).

In order to better describe sludge hydrolysis, it is important to understand the nature of the hydrolysis events observed. O'Rourke et al. was first to suggest a sequential consumption of sludge components: Carbohydrates > proteins > lipids (Parkin and Owen, 1987; Rittmann and McCarty, 2001). Thus, we measured carbohydrate and protein concentrations over time to correlate their consumption to hydrolysis events. Due to limited sampling capacity and volumes, we did not analyze intermediate samples for lipid content. Each digestion had a single hydrolysis event observed in the first 10 days, centered around day 7 in methanogenic and electrogenic digestions. This first hydrolysis event corresponded with the transient accumulation of SSCOD and VFAs, as shown in Figure 6.1, and a reduction in carbohydrate concentrations, seen in Figure 6.3. This was consistent with disintegration and hydrolysis of carbohydrate particulates to fermentable substrates and their subsequent conversion to methane. Initial hydrolysis and fermentation proceeded faster than methanogenesis, resulting in the observed SSCOD and VFA accumulation. Thus, this first hydrolysis event seemed to occur at a much faster rate than the overall rates determined in Figure 6.2.

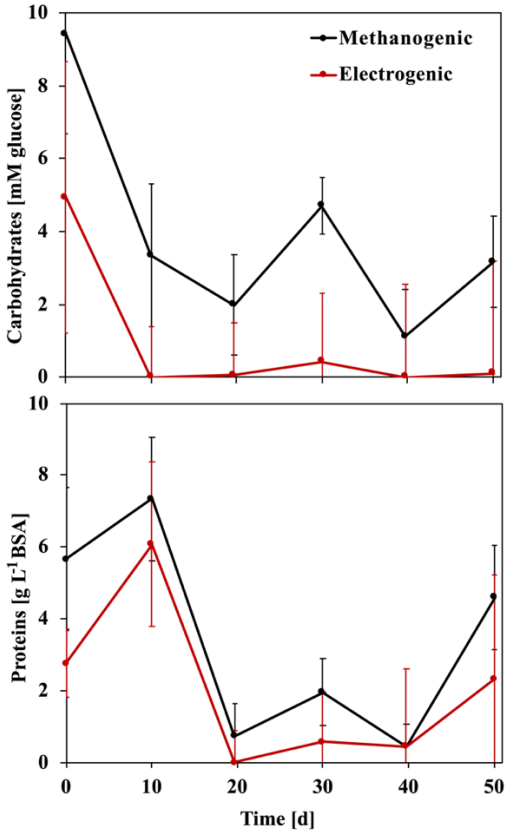


Figure 6.3 Total carbohydrate concentrations from bulk samples of methanogenic and electrogenic digestions. ADS controls are shown with dashed lines. 0.192 g COD/mM carbs as glucose was used to convert to units of COD. Error represents ± one standard error (n=3).

Protein concentration did not decrease during the first 10 days for methanogenic or electrogenic digestions, but did between days 10 and 20 (Figure 6.3). The apparent increase in concentration was due to a decrease in protein concentration in control digestions, possibly due to a lack of other substrates. Figure S7 shows this clearly. Protein digestion began only after carbohydrate concentrations reached a minimum value, suggesting that microorganisms largely focused on carbohydrate hydrolysis in the early digestion stage. This preferential digestion led to the observed rate peaks in Figure 6.4.

Preferential digestion was not observed when the simple substrates casein and cellulose were used (Chapter 5). Protein fractions in PS and WAS were expected to be biochemically more complex and diverse than the model substrate casein, derived from milk. Sequential utilization of distinct fractions of sludge PCOD required a new modeling approach; one that incorporated multiple lag phases specific to substrate classes. Given our limited sampling volumes, we were not able to track other sludge components, such as lipids, DNA/RNA, or humic substances. It is possible that additional rate peaks were associated to these components as shown by O'Rourke for the case of lipids (Parkin and Owen, 1987).

### 6.3.4 Modeling Sludge Hydrolysis Rates Using Multiple Gompertz Kinetic Expressions

Figure 6.4 shows the individual product accumulation (methane + VFAs and electrons + VFAs) and corresponding rates fitted with multiple Gompertz expressions. Hydrolysis rate peaks in the methanogenic and electrogenic digestion were able to be well approximated by subdividing the total recovery into three fractions, each with their own lag phase. In each case there was an initial high rate representative of carbohydrate hydrolysis followed by a second peak after 10 days that corresponded to protein digestion. This was consistent with the protein and carbohydrate concentrations from these individual digestions (Figure 6.4). The initial maximum rate was measured at 1.74 g COD $L^{-1}d^{-1}$ for the electrogenic digestion shown in Figure 6.4, a value that was significantly higher than the rate constant obtained when considering a single hydrolysis event, 0.51 g COD $L^{-1}d^{-1}$. Using multiple Gompertz expressions yielded a similar maximum rate of 1.53 g COD $L^{-1}d^{-1}$, however. While a first-order approximation

predicted the maximum rate well, 0.87 g COD $L^{-1}d^{-1}$ measured and modeled, it did not approximate subsequent recovery events. Estimations of COD values of measured sludge proteins and carbohydrates is not trivial due to the high diversity of these molecules. For this reason, the fittings presented in Figure 6.4 could not be directly correlated to the drop in carbohydrate and protein concentrations observed in Figure 6.3. However, the first modeled event, associated with carbohydrates, represented 75% and 51% of the total recovered COD in methanogenic and electrogenic digestions, respectively. The second, protein-associated, event corresponded to 11% and 13% of the total and the third, unassociated, event corresponded to 14% and 36% of the recovered COD. Understanding this hierarchy is of crucial importance to optimizing energy recovery processes.

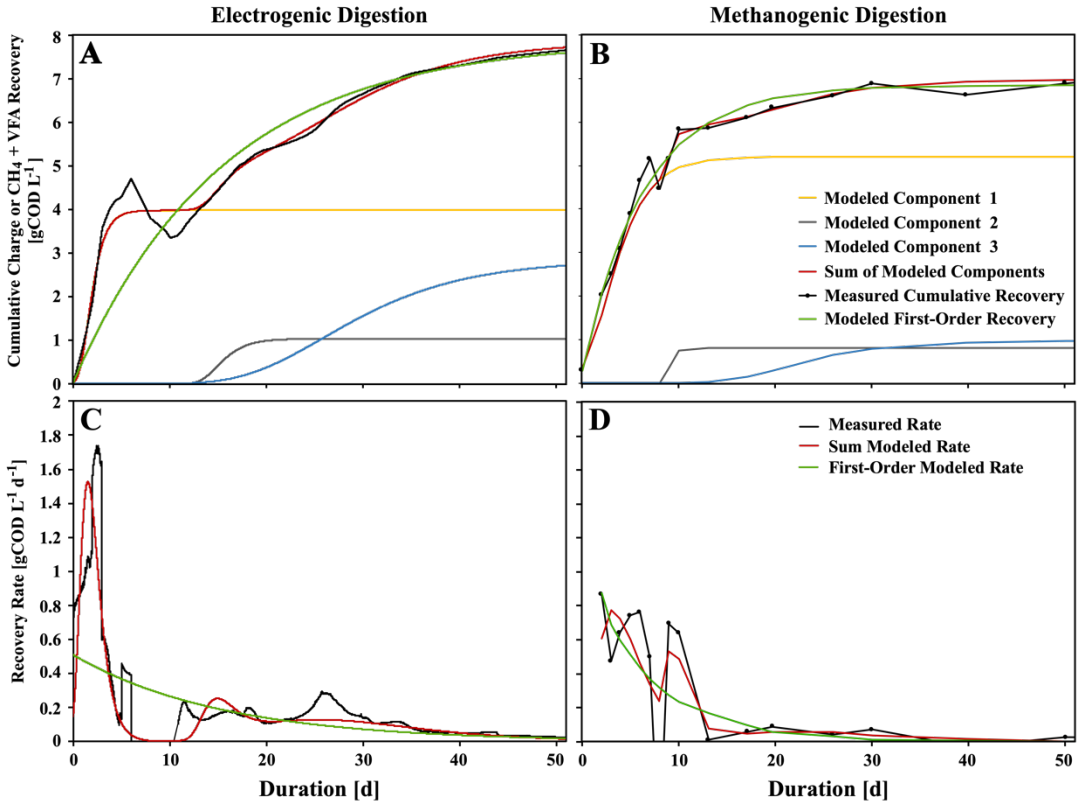


Figure 6.4 Representative model fittings of an individual methanogenic and electrogenic batch digestions from cumulative methane or charge + VFA. Panels A-B show model fittings for cumulative recovery using three Gompertz curves (yellow, gray, blue), the sum of individual fittings (red), and results of single first-order fitting (green). Panels C-D show model fittings for the rates of recovery for $CH_4$ or charge. Shown are measured rates (black), cumulative modeled rates from three components in panels A-B (red), and the modeled rate from a single first-order fitting (green).

## 6.4 Conclusions

Methanogenic and electrogenic batch digestions of mixed PS and WAS exhibited multiple recovery events. Electrogenic recovery of current was slower than methane recovery, likely due to limited anode surface area. Individual fittings of methane and charge recovery events indicated a fast, initial step with subsequent slower steps. Two of these peaks were associated with carbohydrates being selectively digested within the first

10 days, and proteins being digested between days 10-20. This selective delay of protein degradation suggests a hierarchy of particulate preference for digestion. Higher resolution measurements in electrogenic digestions facilitated better fitting of individual events. Understanding this hierarchy is essential to optimizing digester loading, especially in the case of combined waste streams, such as food waste. While a single first-order hydrolysis model can approximate methane or charge accumulation reasonably well, it cannot model the actual rates of product accumulation when multiple events are observed. In both cases, including SSCOD or VFAs allowed a more accurate estimation of hydrolysis rates than when methane or charge alone were used.

# 7 CHALLENGES TO OPTICALLY QUANTIFYING PH GRADIENTS IN GEOBACTER SULFURREDUCENS BIOFILMS


## Abstract

Previous chapters have examined the use of MXCs as sensors for precise measurement of anaerobic digestion kinetics. A limiting factor for current density production in MXCs is the pH gradient that forms during anode respiration. For every electron respired to the anode, a proton is produced which must diffuse out of the biofilm. Kinetic limitations to the diffusion of these protons result in an internal biofilm pH well below the inhibitory level for anode respiring bacteria. The mechanisms and dynamics of pH gradient formation in anode respiring biofilms have yet to be shown. Previous studies have used pH microelectrodes, but these have a limited rate of measurement and are disruptive to biofilm morphology. One previous study has described an alternative method utilizing the fluorescent reporter seminaphorhodafluor-4F 5-(and-6)-carboxylic acid (C-SNARF-4). Here a new design of microbial electrochemical flow cell was used to investigate pH gradients in *Geobacter sulfurreducens spp.* biofilms. Surprisingly, when using C-SNARF-4 with these biofilms, a pH gradient was always detected towards the anode surface, even when the biofilm was inactive. Close analysis of C-SNARF-4 in the presence and absence of biofilm indicated that falsely low pH values were reported when pH > 6. Measured density gradients in *G. sulfurreducens* caused this error to present as a false pH gradient inversely proportional to biofilm density. A promising alternative to C-SNARF-4, HPTS, was examined and while more work is needed to be

able to measure precise pH values, decreasing pH trends closely followed current production.

Acknowledgements

Ethan Howley, Anna Guerrero and César I. Torres contributed to the experimental design, data collection, and analysis of the results presented in this chapter. The authors are deciding whether to publish this chapter as-is, or to perform additional tests with HPTS to develop and confirm an alternative optical pH-sensing technique. Due to the current limitations in beginning new experiments, it is uncertain when these experiments will be performed.

## 7.1 Introduction

### 7.1.1 pH Limitations in Anode Respiring Biofilms

A system of great interest to environmental engineers is the microbial electrochemical cell (Rabaey and Verstraete, 2005). This technology relies on the activity of anode respiring bacteria (ARB) to catalyze the oxidation of organics while generating an electric current. This current may be used to offset the energy used in wastewater treatment, generate valuable products such as hydrogen gas or hydrogen peroxide, or as a real-time measurement of the rate of biological processes occurring in the anode chamber.

Previous chapters have described the use of microbial electrochemical cells as tools for measuring the kinetics of anaerobic digestion. Figure 7.1 shows the results of one such batch digestion. Parallel methanogenic and electrogenic (with ARB instead of methanogens) batch digestions of combined municipal sewage sludges were conducted. Figure 7.1 shows that, while similar volatile suspended solids (VSS) reductions were observed in both systems, volatile fatty acids (VFA) accumulated in the reactors with ARB, but not those with methanogens. Furthermore, while methane was produced, minimal current was observed in all microbial electrochemical cells. These results indicate that, while most of the steps of anaerobic digestion were occurring (disintegration, hydrolysis, acidogenesis, acetogenesis), the activity of ARB was inhibited. One difference in the methanogenic and electrogenic batch systems was the pH of the bulk liquid over the course of the experiment. Both show an initial pH decrease due to the production of volatile fatty acids, but electrogenic reactors show a prolonged

and severe pH depression with the bulk pH decreasing below 6 after the third day. Understanding why this would inhibit current production requires an understanding of the fundamental processes occurring in anode respiring biofilms.

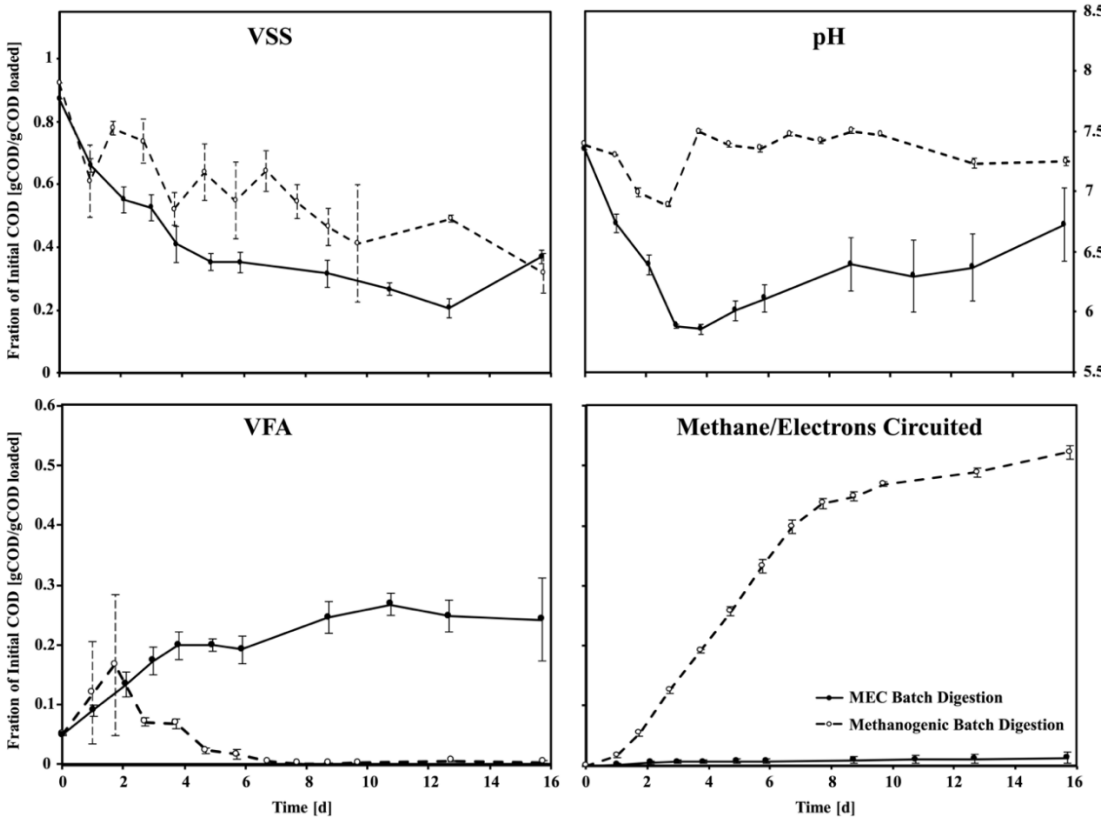


Figure 7.1 Intermediate and final product accumulation in batch methanogenic and inhibited electrogenic reactors.

ARB biofilms are often dominated by microbes of the genus *Geobacter*, known to perform dissimilatory metal-reduction on a wide range of metals found in soils (Tejedor-Sanz et al., 2018). *Geobacter sulfurreducens*, a common ARB, has been shown to grow thick (>100 μm) biofilms on anode surfaces while performing long distance extracellular electron transfer (EET) through an extruded conductive matrix (Torres et al., 2010).

Modeling and experimental observations have shown the diffusion of protons, a product of anode respiration, out of the biofilm to be a rate-limiting processes (Torres et al., 2008). This is because *G. sulfurreducens* and other ARB are inhibited at low pH values (Torres et al., 2008). Stoichiometrically, a proton is produced each time a cell respires an electron to the anode (Equation 7.1). This could explain why, in the experiments described in Figure 7.1, very low current production corresponds to a period of prolonged pH depression.

$$CH_3COO^- + 3H_2O \rightarrow CO_2 + HCO_3^- + 8H^+ + 8e^- \quad \text{Equation 7.1}$$

Figure 7.2 was adapted from (Marcus et al., 2011), and illustrates the expected and modeled pH gradients within respiring ARB biofilms with different buffer concentrations. These analyses predict that the internal pH will decrease as the biofilm grows thicker, or if buffer concentrations decrease. A characteristic non-linear proton concentration gradient is predicted, decreasing asymptotically with depth as cells respire at slower rates due to pH inhibition, and thus produce fewer subsequent protons to further reduce the pH. This model predicts the most active regions of a biofilm would be those furthest away from the surface, assuming the biofilm is conductive enough that there is minimal potential gradient with increased distance from the anode surface (Marcus et al., 2011). Some experimental results have contradicted this, however, reporting the most active region to be the innermost surface (Liu and Bond, 2012; Stephen et al., 2014).

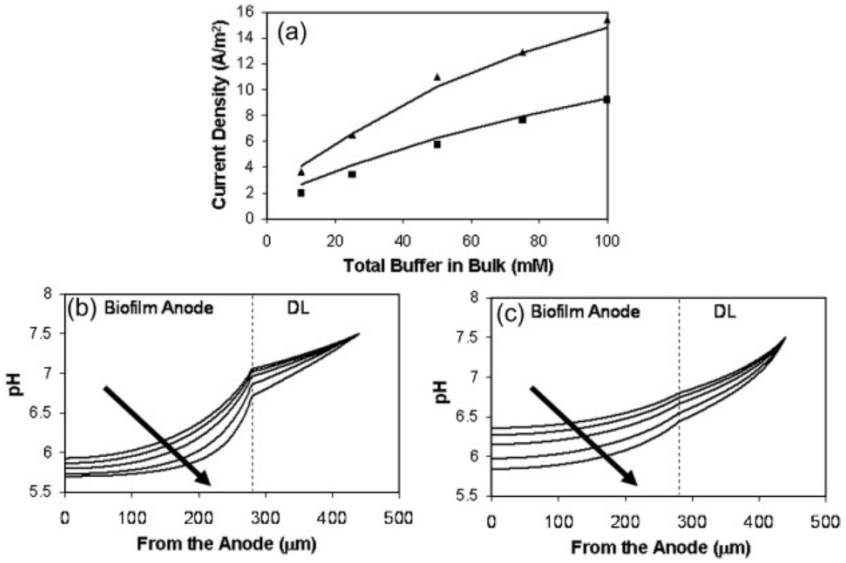


Figure 7.2. Adapted from Marcus et al. 2011. Modeled pH gradients within anode respiring biofilms resulting from decreasing buffer concentrations.

### 7.1.2 Previous Measurements of *Geobacter* Anode Biofilm pH Gradients

Three previous studies have measured pH gradients in *Geobacter* anode biofilms (Babuata et al., 2012; Franks et al., 2009; Hou et al., 2017). Hou et al. utilized a pH microelectrodes to directly measure gradients in an extremely thick anode respiring biofilm (>1000 μm) that are not common in typical *Geobacter* experiments. Even so, Hou et al.'s results appear to confirm expected pH gradient profiles predicted by Marcus et al., 2011. Babuata et al. also utilized a pH microelectrode to measure gradients in ARB biofilms that were200 μm thick. They observed linear decrease in pH from the beginning of the biofilm to the electrode surface. Interestingly, Babuata et al. measured continuously decreasing pH values at the electrode surface, indicating that pH was not limiting when measurements were taken. They conclude that not all ARB biofilms are pH limited. However, microelectrodes are limited in their resolution by size of their tips.

The maximum resolution of pH microelectrodes is approximately 2x the electrode radius (Klusmann and Shultze, 1997). This means the maximum resolution is ~ 20 μm for Babuata et al. and ~50 μm for Hou et al., and finer measurements are an average over this spherical volume. This limits the determination of gradients within active and inactive portions of the biofilm. These probes, even fine-tipped, disrupt the structure of the biofilm as they are being inserted to greater depths, pushing cells out of the way and potentially dragging components from upper layers to lower ones.

Franks et al., 2009, built upon the method described in (Hunter and Beveridge, 2005), which utilized the pH-sensitive fluorophore seminaphorhodafluor-4F 5-(and-6)-carboxylic acid (C-SNARF-4) to report pH at different depths and positions within a biofilm laser scanning microscopy (CLSM). There are numerous advantages to using a small fluorescent reporter for pH, such as the ability to use a closed system for anaerobicity and specificity for pure cultures, the non-disruptive nature of optical measurements, and the possibility of rapid measurements to observe near instantaneous changes in pH gradients. Franks et al. report a linearly decreasing pH gradient as a function of depth within a respiring biofilm. Franks et al. and Hunter et al. both utilized constitutively expressed fluorescent markers (mCherry and GFP, respectively) to identify the specific locations within the biofilm that were being imaged. While this provides needed spatial information, it also has the potential to interfere with the pH signal from C-SNARF-4. This can be partially, but not entirely, mitigated by sequentially exciting each probe and acquiring signals independently, which Franks et al. performed. Franks et

al. is the first publication to report the use of optical measurements to measure ARB biofilm pH gradients.

None of the previous measurements of ARB biofilm pH gradients show the pH profile of an inactive biofilm. This is especially important when using optical pH measurements that have been demonstrated to have interference patterns with biofilm components (Hunter and Beveridge, 2005; Schlafer et al., 2015; 2011; Valli et al., 2005). Franks et al. show a single frame close to the surface of the electrode and report no difference in pH at the electrode surface and in the bulk liquid. They show a similar single frame with a biofilm grown with fumarate as an electron acceptor, which should not demonstrate a pH gradient. None of the pH gradients studies perform time-dependent experiments, instead only presenting static gradients at specified timepoints.

### 7.1.3 C-SNARF-4 as a pH Indicator In and Around Biomass

C-SNARF-4 has a pKa of ~ 6.4, facilitating pH quantification from ~ pH 5.4 to 7.4 ( Liu et al., 2001). Two carboxylic acid functional groups are intended to prevent the dye from crossing cell membranes, facilitating the exclusive measurement of intercellular pH if added to growth medium (Franks et al., 2009; Hunter and Beveridge, 2005; Schlafer et al., 2018), or intracellular pH if injected directly into cells (Valli et al., 2005). As described in detail by (Marcotte and Brouwer, 2005), C-SNARF-4 exhibits a pH-dependent shift in emission spectra. When excited at 514 nM, C-SNARF-4 has emission maxima at 595 and 665 nM, with relative intensities depending on the protonated or deprotonated state of a carbonyl functional group (Marcotte and Brouwer, 2005).

C-SNARF-4 has been used to measure the intracellular pH in yeast cells (Valli et al., 2005), pH gradients in dental biofilms (Schlafer et al., 2015; Schlafer et al.,2011; Schlafer et al., 2018), pH gradients around bacterial cheese colonies (Jeanson et al., 2013), micro-pH environments around drug delivery implants in mice (Schädlich et al., 2014), intercellular pH within fungal biofilms (Schlafer et al., 2018), within *Pseudomonas aeruginosa* biofilms (Hunter and Beveridge, 2005), and anode respiring biofilms (Franks et al., 2009). In many of these experimental conditions, special consideration was taken to understand how C-SNARF-4 interacts with the cellular and extracellular matrix components in each model system. When Valli et al. attempted to measure intracellular yeast pH by injecting C-SNARF-4 directly into cells, they observed that only calibrations conducted within permeabilized cells were reliable. Similarly, Hunter et al. performed the calibration curve in the presence of various "matrix components" (cells, alginic acid, BSA in HEPES) and noted that above pH 7, significant error was observed in C-SNARF-4 pH estimations in the presence of these components. Hunter et al. also noted that this effect was concentration-dependent, with greater deviations occurring at higher matrix component concentrations. Interactions between C-SNARF-4 and cellular and matrix components appear to be case-specific. Jeansen et al. observed no effect on the pH signal from C-SNARF-4 in the presence of proteins and polysaccharides of their model cheese, certainly a complex and dense matrix, at pH 7. Similarly, while Schlafer et al. performed calibrations in the presence of matrix components in their 2015 paper, they report in (Schlafer et al., 2018) no effect of biofilm

presence on the calibration curve. It appears that interactions between C-SNARF-4 and cellular or matrix components must be quantified on a case-by-case basis.

Near neutral pH the carboxylic acid groups of C-SNARF-4 prevent entry into microbial cells, but multiple research groups have reported that the dye is internalized at pH values lower than the pKa (≈6.4), when these same groups may be protonated (Avnir and Barenholz, 2005; Hunter and Beveridge, 2005; Schlafer et al., 2015; Schlafer et al., 2011). In fact, C-SNARF-4 has been noted to accumulate within cells, resulting in increased fluorescence of cellular biomass (Hunter and Beveridge, 2005; Schlafer et al., 2015). Schlafer et al. digitally edit out brighter biomass signals using a thresholding technique to only quantify C-SNARF-4 from intercellular regions (Schlafer and Dige, 2016). While Franks et al. do not mention any possible internalization or interactions of the dye with *Geobacter* cells, the figures they present appear to show this effect. In section 3.3, this effect is measured and quantified to see the effect on calculated pH values.

Here the design for a new and easily constructible microbial electrochemical flow cell (MEFC), compatible with light and fluorescence-based CLSM measurements, is presented. The flow cell was utilized to corroborate and expand upon previous ARB biofilm pH gradient measurements using C-SNARF-4. Based upon repeatable pH measurements in the presence of biofilms in the MEFC and on slides under optimal imaging conditions, a pattern of interference between C-SNARF-4 and *Geobacter sulfurreducens* biomass was identified and quantified. This interference pattern was

shown to result in the measurement of artificial pH gradients under all typically observed conditions. Results presented here indicate that pH gradients have never been accurately quantified using optical measurements in an anode respiring biofilm. A promising alternative measurement technique is presented, utilizing the fluorescent reporter pyranine, also known as HPTS, along with the remaining challenges to implementing this method.

## 7.2 Materials and Methods

### 7.2.1 ARB cultivation in the Microbial Electrochemical Flow Cell (MEFC)

The MEFC was designed to allow the propagation of an anaerobic *Geobacter sulfurreducens* biofilm in such a way as to be observable by CLSM. A schematic of the MEFC is shown in Figure 7.3. Acrylic end plates were layered with rubber gaskets and glass slides to produce the flow chamber. The anode consists of an indium-tin oxide (ITO) doped 0.7-mm thick glass slide (30-60 Ω/sq). The necessity of compression to prevent oxygen intrusion required the use of thicker ITO-coated glass (0.7 mm) than is typically used in light microscope systems (0.17 mm). This increased light diffraction, reduced the signals collected from fluorescent probes, and limited the usable objective lens to 20x or 40x magnification. The slide was etched to have a strip of ITO that was ~ 3 mm x 7 mm at the center of the chamber for *G. sulfurreducens* growth. A reference electrode (BAS Instruments, MF-2052) was connected to the flow cell through a liquid tube connection. A metal syringe at the exit of the flow cell acted as the counter electrode. The chamber was designed to achieve laminar flow, with a volume of approximately 200 μL. Anaerobic conditions were maintained through compression with

six screws positioned around the periphery of the MEFC. A peristaltic pump was used to circulate anaerobic media between the MEFC and a media reservoir with a residence time of approximately one minute. For growth, the reservoir contained 500 mL of *Geobacter sulfurreducens spp.* Media (ATCC 1957). For imaging, a reservoir of 10 mL was substituted to reduce the volume of dye required. Dye was added into the smaller reservoir and allowed to diffuse into the biofilm during recirculation. A portable potentiostat (Ivium Technologies, CompactStat) was used to poise the anode potential.

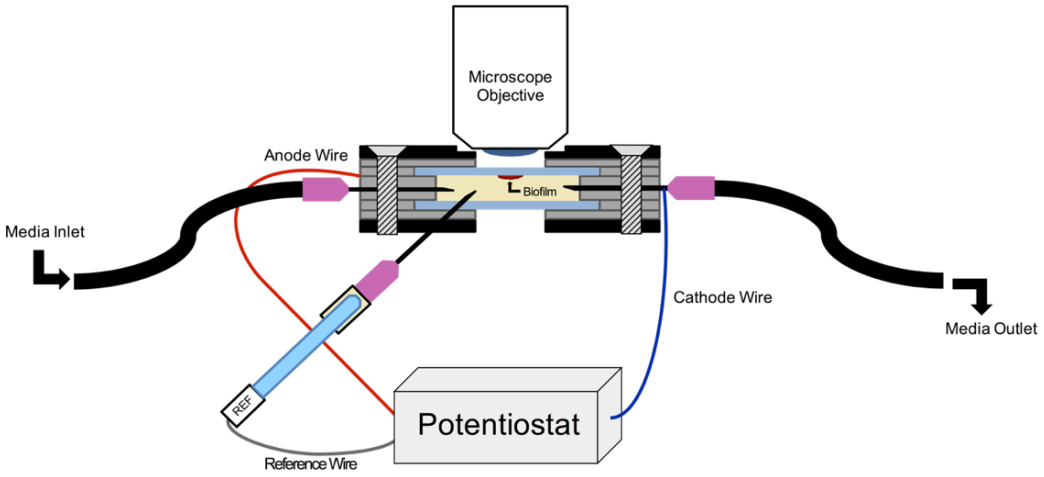


Figure 7.3. Schematic diagram of the microbial electrochemical flow cell (MEFC). A three-electrode system is used. The anode is an Indium Tin Oxide doped glass slide positioned at the top of the flow cell, directly under the microscope objective lens. The stainless-steel needle through which media exits the flow cell is used as the cathode, while an Ag/AgCl reference electrode is ionically connected with the system via another stainless-steel needle. Anode potentials are poised with a potentiostat.

*Geobacter sulfurreducens* growth medium ATCC 1957 was prepared and sparged with 80/20 $N_2/CO_2$ to create anaerobic conditions. A pure culture of *Geobacter sulfurreducens spp.* was first cultivated in tubes with sodium fumarate as an electron

acceptor from a pure freezer stock. The MEFC was inoculated from this culture. An anode potential of -0.15 V vs. Ag/AgCl was poised with a potentiostat (Biologic VMP3) to promote biofilm growth. Current production was observed over the next 20 days as the biofilm grew and matured.

### 7.2.2 Slide Assays

To quantify the effects of *Geobacter sulfurreducens spp.* biomass on pH measurements with C-SNARF-4, fumarate grown pure cultures were imaged in 30 mM phosphate buffers. To prepare each sample, 1 mL of *Geobacter sulfurreducens spp.* culture was centrifuged to pellet the biomass. Cells were resuspended in 0.1 mL of 30 mM phosphate buffers from titrated from pH 5.11 to 7.8. Buffer and cell solutions were mounted on slides and imaged with a Leica SP8 CLSM with a 63x Oil immersion objective.

### 7.2.3 Fluorescent Dyes Used

The pH-sensitive dye seminaphorhodafluor-4F 5-(and-6)-carboxylic acid (C-SNARF-4, Thermo Fisher) was added to *Geobacter* growth medium immediately before imaging at a concentration of 20 μM. C-SNARF-4 was excited at 543 nm and ratiometric signals were collected from 570-610 nm (green) and 620-680 nm (red). After subtraction of blanks, the green/red ratio allows the concentration-independent calculation of pH once a calibration curve is performed. Figure 7.4 shows a representative calibration curve for C-SNARF-4 performed on glass slides. Calibration curves for biofilms were conducted within the MEFC but without biomass. Calibration

curves were created in a similar method as what is described in (Avnir and Barenholz, 2005), but using measured C-SNARF-4 emission ratios.

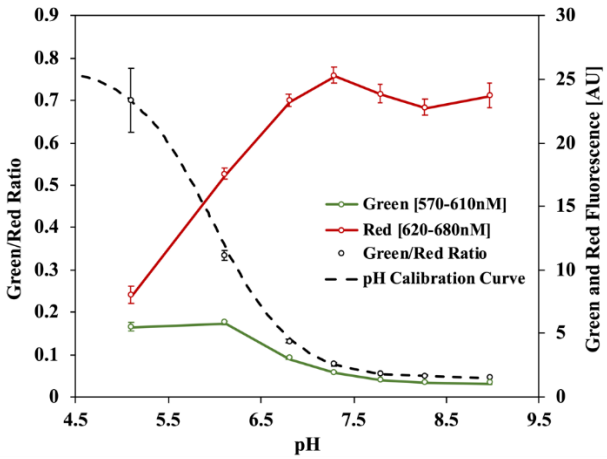


Figure 7.4. Standard curve of the pH-dependent emission shift of C-SNARF-4. Measurements were performed on a Leica SP8 using a 543nm excitation line with a 63x oil-immersion objective. 30 mM phosphate buffers titrated to various pH values were used as standards without any cellular or matrix components present. Error bars represent ± one standard error (n=3). This calibration was used for slide assays (Figure 7.9); a separate calibration was performed in the MEFC, without cellular or matrix components, for biofilm imaging.

8-hydroxypyrene-1,3,6-trisulfonic acid (HPTS, Thermo Fisher), also referred to as pyranine, was added to *Geobacter* growth medium immediately before imaging at a concentration of 0.5mM. To quantify pH, the ratio of fluorescence at 514nm (30nm bandwidth) from excitation with 488nm and 405nm laser lines was measured. The pinhole was set to 1.2µM and images were collected with each line scanned sequentially for distinct signals from each excitation.

### 7.2.4 Microscopic Procedure

The MEFC was used in conjunction with the Leica TCS SP5 AOBS Spectral Confocal system and the Leica SP8 White Light Laser Confocal System in the

Regenerative Medicine Imaging Facility (ASU, Tempe, AZ). The SP5 system used diode and argon lasers for excitation, and AOTF tunable emission filters. A 20x dry objective lens was used for analysis of respiring biofilms. 63x water immersion lenses were used for detailed analysis of grown biofilms, after removal from the MEFC. The SP5 was an upright system. The SP8 system was outfitted with a tunable white light laser, AOTF tunable emission filters, and HyD GaAsP detectors with gating to reduce background interference. The SP8 CLSM was an inverted system. HPTS imaging was conducted in the MEFC on a Nikon C2 confocal system, with LED laser emission lines at 405nm, 488nm, and 640nm (for reflection), in the Biodesign Swette Center for Environmental Biotechnology.

## 7.3 Results and Discussion

### 7.3.1 Geobacter spp. Biofilm Growth and Imaging

*Geobacter sulfurreducens* pure culture biofilms were successfully grown in the MEFC. Current densities of greater than 5 A $m^{-2}$/ were observed. Biofilms have been observed to grow to 20-60 μm thick. Biofilms were imaged when they showed a limitation to increasing current production.

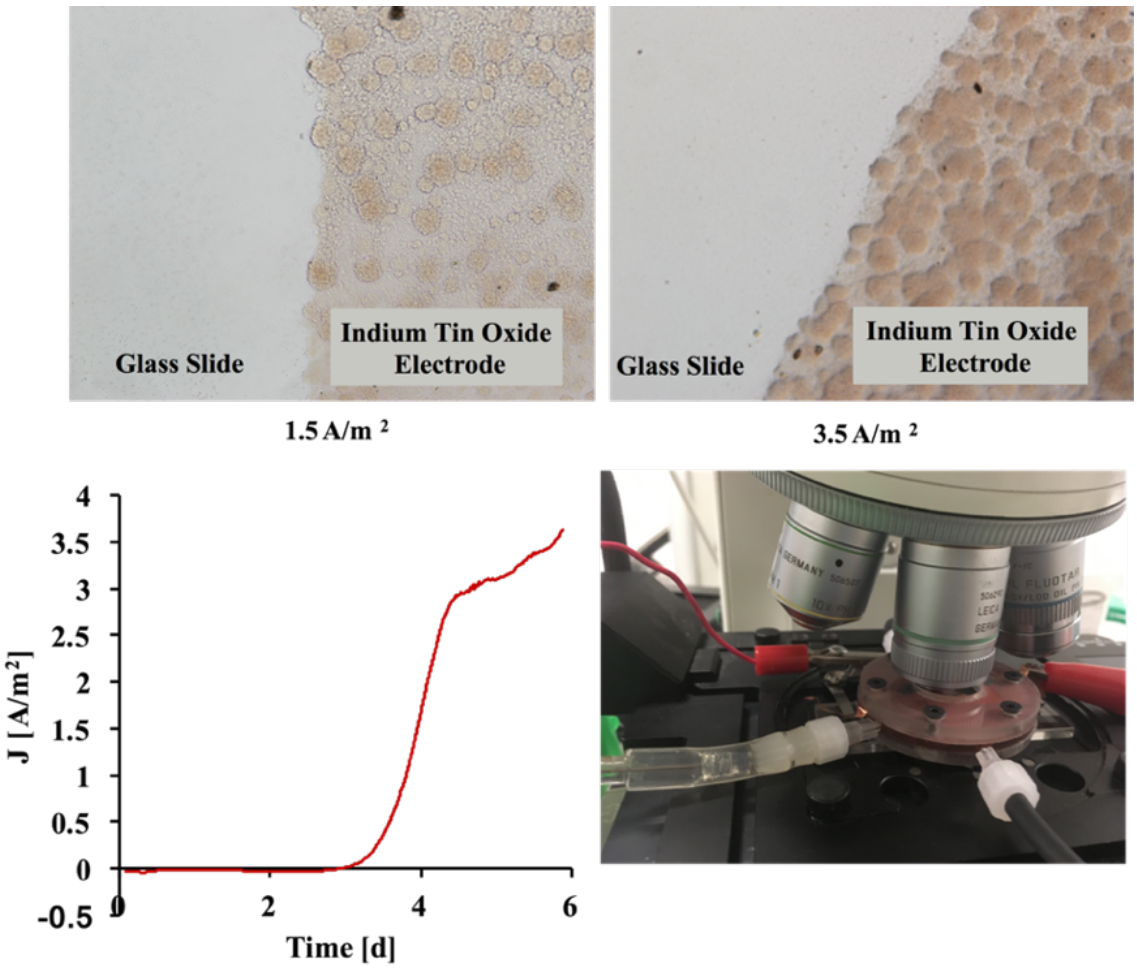


Figure 7.5. Biofilm growth in the microbial electrochemical flow cell. (top) Transmitted light images of *Geobacter sulfurreducens* biofilm growing on an indium tin oxide-coated glass electrode at two different current densities. (bottom left) Current produced during biofilm growth. (bottom right) Imaging biofilms with the Leica TCS SP5 AOBS Spectral Confocal system in the W.C. Keck Bioimaging Lab.

Young *Geobacter sulfurreducens* biofilms showed a characteristic "pillared" morphology as individual colonies on the anode surface merge together during biofilm growth. We observed minimal growth in regions where the ITO has been etched away from the glass surface, shown in Figure 7.5. Detailed images of grown biofilms

confirmed a dense biofilm formed near the glass surface, while more diffuse aggregates occurred as you increase the distance from the surface. The relative density of anode biofilms was measured two ways: 1) by relative intensity of the DNA stain DAPI and 2) from reflected laser light collected during imaging by configuring a detector with emission filters that overlapped with an excitation line. In both cases, mature biofilms (those that have reached maximum current production) demonstrated a regular pattern of exponentially decreasing density with increased distance from the anode surface (Figure 7.7). Reflection was less sensitive than DAPI to lower concentrations of biomass, so while the reflection curve shown in Figure 7.7 followed the same general pattern as DAPI, it decreased more rapidly. This density pattern may be attributed to an increased concentration of cells near the electrode surface and an increase in void spaces nearer the outer surface of the biofilm. Both patterns were visible in the images shown in Figure 7.6.

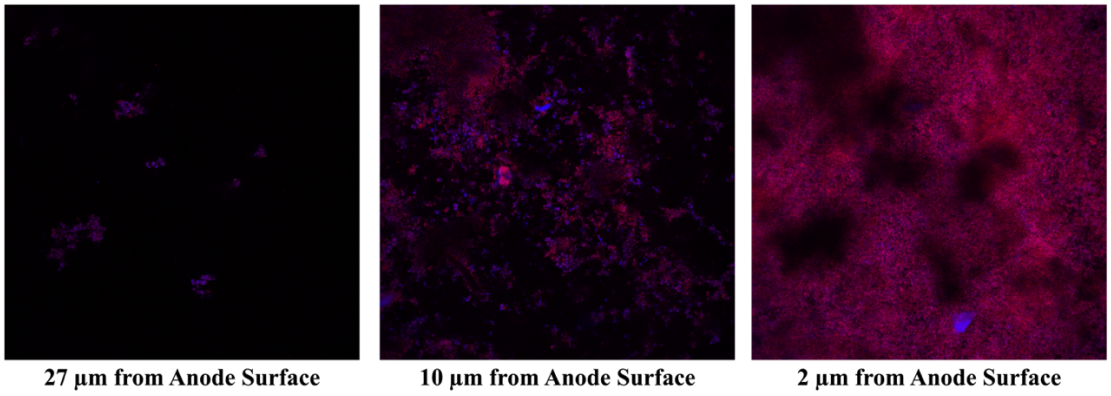


Figure 7.6. High-resolution images of an anode respiring biofilm taken with the Leica TCS SP5 AOBS Spectral Confocal system in the W.C. Keck Bioimaging Lab with 63x a dipping objective at different distances from the anode surface. Fluorescence probes for DNA (DAPI, blue) and plasma membrane (F/M 4-64, red) were used.

Using C-SNARF-4, apparent pH gradients were observed that decrease with depth into the biofilm, as the anode surface is approached. A goal of these experiments was to observe the formation of these gradients in an anode respiring biofilm. We attempted to do this through observations before and after poising the anode potential to allow respiration to occur. In many experiments, we observed little change in the apparent biofilm pHs before and after poising a potential. Figure 7.7 illustrates two data series where poising the anode had minimal effect on the apparent pH gradient reported by C-SNARF-4. Furthermore, the fact that this gradient was linear does not align with current models of pH accumulation in the interior of anode-respiring biofilms. While a linear pH profile could indicate a lack of any pH inhibition, values as low as pH = 5.7 (not shown) were observed, well below what is generally considered to be inhibitory for *G. sulfurreducens* biofilms.

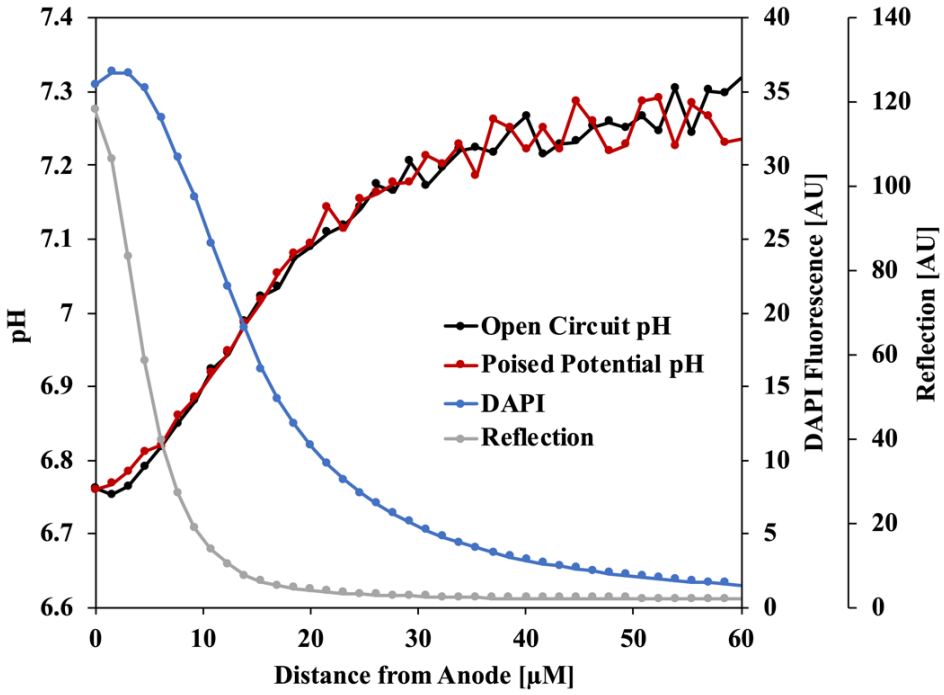


Figure 7.7. Results of a series of pH measurements on a mature *G. sulfurreducens* biofilm. Black and Red lines represent pH values calculated from ratiometric measurements using C-SNARF-4. The glass surface of the electrode is at z=0. Blue and grey lines indicate the DAPI and reflection signals, indications of biomass density. The current density of this biofilm was 4 A $m^{-2}$ at the time of imaging.

We were able to repeat these measurements many times (n=9) with mature *G. sulfurreducens* biofilms using C-SNARF-4 as the pH indicator. Each time, an apparent decreasing pH gradient was always observed towards the glass surface. We have observed this profile after allowing the MEFC to be in open circuit for more than three hours, and after fixing the biofilm with paraformaldehyde. Thus, the change in fluorescence cannot be the result of a change in pH. The single depth profile presented in Franks et al. also showed a linear pH gradient.

## 7.4 *Geobacter sulfurreducens spp.* Biomass Distortion Effects on C-SNARF-4

In the numerous depth profiles measured in the MEFC, fluorescence from C-SNARF-4 was observed to be more intense within the biofilm. This could indicate that C-SNARF-4 was accumulating within cells as previously described (Hunter and Beveridge, 2005; Schlafer et al., 2015). However, if the measured pH within the biofilm was an average of intracellular and intercellular compartments, the apparent pH gradient would be expected to be shallower than the actual extracellular gradient, as *Geobacter sulfurreducens* cells presumably have a circum-neutral internal pH. *Geobacter* biofilms are unlike those previously studied with C-SNARF-4, because they contain components which facilitate long distance extracellular electron transfer. It is conceivable that the unique composition of these biofilms results in new interference patterns.

To quantify any interference between C-SNARF-4 and *Geobacter*, fumarate-grown biomass was imaged on glass slides under optimal optical conditions. Fumarate biomass was used because this metabolic regime was not expected to generate significant pH changes from the surrounding bulk liquid. Figure 7.8 illustrates that, at pH 5.1, *Geobacter* appeared to accumulate C-SNARF-4, resulting in brighter fluorescence than the surrounding bulk liquid. This is seen quantitatively in Figure 7.9, where green and red fluorescence from C-SNARF-4 was greatly increased at pH 5.1. Interestingly, at all pH values above 6, biomass was darker than the surrounding bulk liquid, but only in the red portion of the signal. Figure 7.9 shows the trend for the emissions corresponding to the red peak was essentially reversed in the presence of biomass. Instead of the red fluorescence increasing as pH increases, it stayed roughly the same. Reducing the red

signal resulted in increased Green/Red ratios, and artificially low pH values relative to areas without biomass.

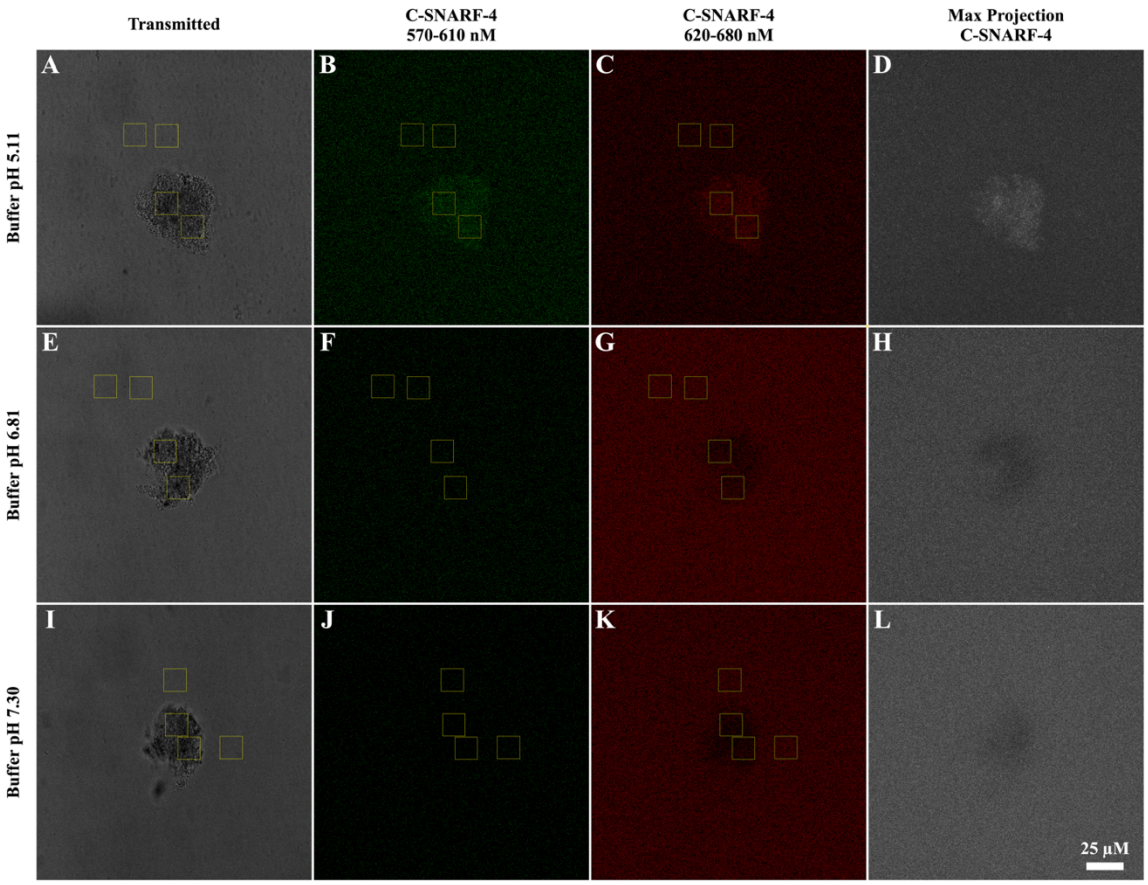


Figure 7.8. Representative images from C-SNARF-4 calibration curve with *Geobacter spp.* biomass grown with fumarate as an electron acceptor. Panels A-C, E-G, I-K are single frames used for pH analysis and have been adjusted for contrast and brightness using the contrast/brightness and "sharpen" functions in ImageJ. Yellow boxes represent measurement areas; two with biomass and two without. Panels D, H, and L are maximum projections of both C-SNARF-4 emission regions from z-stacks taken of the slide volume.

Errors from matrix components have been reported previously from C-SNARF-4, but only above pH 7 (Hunter and Beveridge, 2005). These data indicate that *Geobacter* biomass resulted in artificially low pH measurements at all pH values above 6.

Furthermore, it appears these errors linearly scale from pH 6 to 7.3 with a maximum pH error of -0.4. In 30 mM phosphate buffer with minimal metabolic activity this change in measured pH was an error and not the result of local changes in the actual proton concentration.

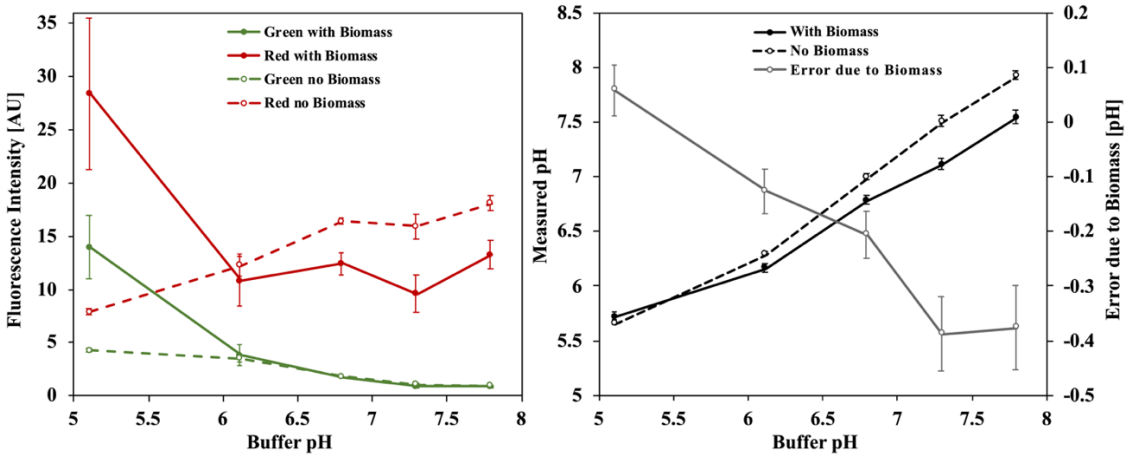


Figure 7.9. pH values measured with C-SNARF-4 in the presence of *Geobacter spp.* biomass and without biomass. Measurements were conducted in 30 mM phosphate buffer at pH values of 5.11 (n=8), 6.12 (n=6), 6.8 (n=6), 7.3 (n=6), and 7.8 (n=6) with and without biomass. Biomass was prepared by growing *Geobacter spp.* planktonically with acetate and fumarate and electron donor and acceptor, pelleting 1 mL of culture in a centrifuge, and resuspending in 0.1mL of buffer with 20 µM C-SNARF-4 before being imaged on slides with a Leica SP8 CLSM. Error due to biomass is the difference between measurement without biomass and measurements with biomass.

The density gradient present in *Geobacter* biofilms would result in variation in the degree of error pH measurement due to biomass. As the fraction of signal attributable to cells increased as the anode surface was approached, so too would the measurement error. Figure 7.10 illustrates an estimation of how this error would be expected to affect the observed pH gradient as a function of depth. The estimated error was calculated from the measured error (Figure 7.9, gray line) and the normalized biomass concentration from

DAPI. The normalized biomass concentration was calculated as the DAPI intensity at a specified distance from the anode divided by the maximum DAPI intensity measured (at the anode surface). To estimate error, the average pH was calculated from the region where no biomass was present, and an error associated with this was scaled with the normalized biomass concentration. This is a conservative estimate, because the biomass in the standard curves was likely less dense than the innermost biofilm regions, but here they are assumed to be the same. This predicted error was subtracted from the measured pH to generate the corrected pH. It is apparent that virtually the entire gradient may be attributed to error from interference between C-SNARF-4 and biomass. This phenomenon explains why C-SNARF-4 indicated pH gradients were present under all conditions: open circuit, after fixation, and in the presence of oxygen. Unfortunately, the low signal to noise ratio of C-SNARF-4 means that this error masked any genuine pH measurements in the biomass.

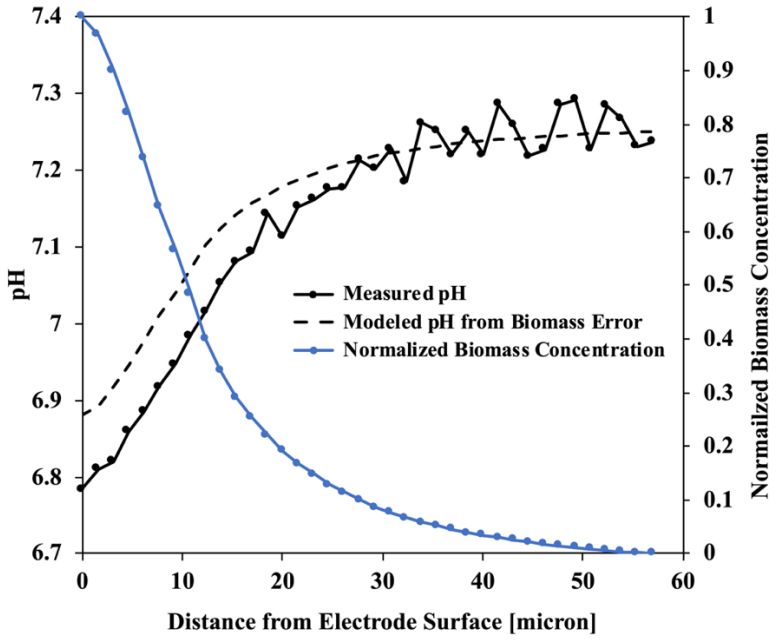


Figure 7.10. Estimated effect of measured pH error due to biomass presence. Black line represents initially measured pH gradient based upon C-SNARF-4 signal. The blue line represents the relative biomass concentration as measured by DAPI. The dashed line is the modeled error, assuming the bulk pH is accurate and the pH error (Figure 7.9) scales with biomass concentration.

The only other reported measurement of *Geobacter* anode biofilm gradients using C-SNARF-4, Franks et al., 2009, show strong indications of containing the same error presented here. C-SNARF-4 figures presented show clear internalization of the dye under certain conditions and dimmer regions near the innermost portion of biofilm pillars. Franks et al. also described that spaces within the biofilm have higher measured pH values than nearby dense zones, as would be expected with biomass-correlated interference described here. Furthermore, control depth profiles from open-circuit biofilms that lack an observed pH gradient were not presented. Neither are the depth profiles of the fumarate controls purported to have no significant pH gradient. As no

individual C-SNARF-4 images were shown, it is unclear how the pH values in single frames close to the electrode surface were calculated. As no method they describe would have removed the effect of this interference, it can be assumed that the gradients they measured have an inherent error. Therefore, it appears that no optical pH measurements of ARB biofilms have been successfully performed to date.

### 7.4.1 HPTS as a potential pH indicator in *Geobacter sulfurreducens* biofilms

A promising alternative to C-SNARF-4 is the dual-excitation dye HPTS (Avnir and Barenholz, 2005). HPTS is more membrane-impermeant than C-SNARF-4 and has not been documented to accumulate within cells. Excitation of HPTS at 488 nm results in pH-dependent emission at 514 nm, while excitation at 405 nm also emits at 514 nm, but with no pH-dependence. Initial results using HPTS with a *Geobacter* biofilm are shown in Figure 7.11. A calibration curve was performed in the MEFC, but without biomass. While HPTS did not appear to accumulate in cells, the ratios measured within biomass were not the same as those in the bulk. This was likely due to the much lower signal form the 405nm excitation due to high concentrations of biomass and relatively small intercellular space, resulting in artificially large ratios. This could potentially be resolved by performing calibration within an inactive *Geobacter* biofilm. Initial observations were promising, however, as the trends show ratios that indicate pH depression highly correlated with current production in the MEFC. Here results are presented as a proof of concept.

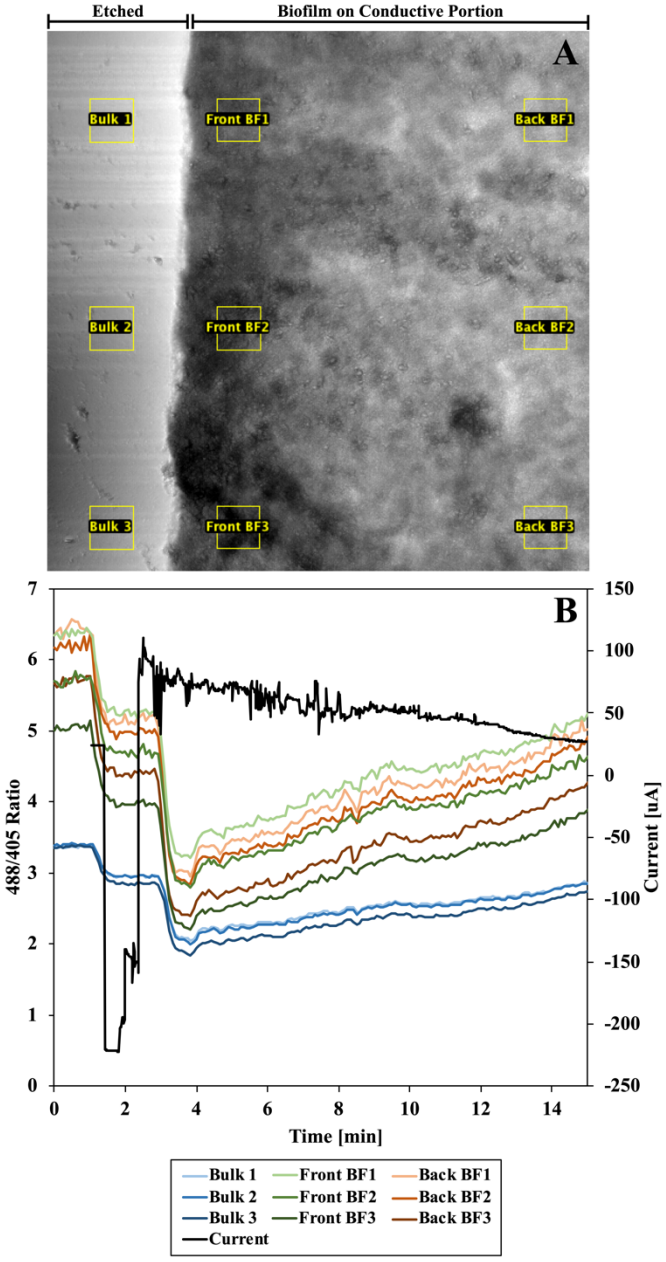


Figure 7.11. Time course of the fluorescence ratio near the anode surface of a *Geobacter sulfurreducens* anode respiring biofilm as calculated from the fluorescent pH indicator HPTS. A) Top-down transmitted light micrograph of the measured biofilm/etched glass region ~5µm from the anode surface. Nine regions of interest are indicated, three without biofilm, three near the edge of the biofilm, and three deeper into the biofilm. Medium flow at the time of imaging is from right to left. B) Fluorescence ratio and current for each region of interest indicated in A.

## 7.5 Conclusions

pH Measurement within *Geobacter sulfurreducens* biofilms using C-SNARF-4 showed an biomass interference that resulted in erroneous pH gradients under commonly measured conditions and controls. There is precedence for this kind of interference with cellular and matrix components, although not on the pH ranges observed in this study. The source of this interference was a reduction in the red portion of the ratiometric C-SNARF-4 emission spectrum. It is possible that this interference was related to the unique composition of electroactive biofilms. As this interference most likely affected a previous study, we believe no reliable optical pH measurements have been successfully conducted in a *Geobacter sulfurreducens* biofilm to date. HPTS is a promising alternative pH reporter, but more work is necessary before accurate pH values may be measured within *Geobacter* biofilms with this dye.

# 8 SUMMARY AND SIGNIFICANCE

## 8.1 Summary of Presented Work

In Chapter 1 I discuss the historical necessity of wastewater treatment before outlining modern practices and regulations in the United States. I explain the general processes of wastewater treatment and solids stabilization by anaerobic digestion. I discuss the strengths and limitations of experimental procedures used to quantify the rates of these reactions.

In chapter 2 I describe the most commonly conducted batch test to measure anaerobic digestion kinetics, the biochemical methane potential test. I also outline an alternative that allows the collection of more highly resolved data, the microbial electrochemical cell. I describe how the series of reactions inherent to anaerobic digestion are often modeled by assuming hydrolysis is the rate-limiting step. The most common kinetic expressions used are first order, Monod, and Gompertz. Each of these expressions are shown to approximate accumulation of products in batch digestions, but not the rates of accumulation when multiple recovery events are observed. I review previous studies that report multiple recovery events.

In chapter 3 I describe modified BMP tests of alkaline and thermally pretreated waste activated sludge. By tracking volatile suspended solids (VSS), semi-soluble chemical oxygen demand (SSCOD), volatile fatty acids (VFAs), and methane production specific rates were able to be calculated for particulate COD hydrolysis, SSCOD hydrolysis, and methanogenesis. I show that accurate estimation of these parameters requires measurement of intermediate products such as SSCOD or VFAs. Results

suggest that pretreatment did not increase the subsequent hydrolysis rate of particulate substrates. Rather, material that had been pre-hydrolyzed by pre-treatment was rapidly utilized for the production of methane while remaining solids degrade at a slower rate.

In chapter 4 I present results of BMPs conducted with combined municipal primary and waste activated sludges approximating the loading of a typical municipal digester. I utilized detailed measurement of the intermediate and final products of to show the effect of selective thermal pretreatment of the waste activated sludge fraction only, a commonly proposed treatment configuration. These results did not support the suggestion that thermal pretreatment of this kind results in increased biodegradability of the remaining solids. While thermal pretreatment was found to increase initial PCOD hydrolysis to SSCOD, subsequent SSCOD hydrolysis occurred at similar rates and remained a possible rate-limiting step.

In Chapter 5 I present the results of casein and cellulose anaerobic digestion conducted in microbial electrolysis cells and BMPs. These single substrate digestions each showed complex current recovery patterns that were previously thought to indicate the stepwise degradation of organic material of different bioavailabilities. These experiments showed, however, that complex signals can arise due to the accumulation and subsequent consumption of intermediate digestion products. Digestions in MECs are compared with traditional BMPs as analytical tools for tracking degradation rates and recovery efficiencies. I show that MECs were able to collect much more time-resolved data of individual recovery events, but that the anode biofilm is susceptible to kinetic

limitations if the surface area is insufficient to consume intermediates produced at high substrate loadings.

In Chapter 6 I describe methanogenic and electrogenic batch digestions performed on mixed primary sludge and waste-activated sludge. I observed multiple recovery events in both systems. Individual fittings of methane and charge recovery events indicated a fast initial step with subsequent slower steps. Results indicated that carbohydrates were competitively degraded before proteins, suggesting a hierarchy of particulate preference for digestion. While a single first-order hydrolysis model can approximate methane or charge accumulation reasonably well, it cannot model the actual rates of product accumulation when multiple events are observed. In both cases, including SSCOD or VFAs allowed a more accurate estimation of hydrolysis rates than when methane or charge alone were used. The multiple observed recovery events were effectively modeled with three Gompertz approximations with different lag phases, indicating that, contrary to the findings from model substrates in chapter 5, sequential degradation of different substrates occurred.

In chapter 7 I show that pH measurement within *Geobacter sulfurreducens* biofilms using C-SNARF-4 result in erroneous pH gradients under commonly measured conditions and controls. The source of this interference is a reduction in the red portion of the ratiometric C-SNARF-4 emission spectrum. As this interference most likely affected a previous study, I believe no reliable optical pH measurements have been successfully conducted in a *Geobacter sulfurreducens* biofilm to date. I show HPTS to

be a promising alternative pH reporter, but more work is necessary before accurate pH values may be measured within *Geobacter* biofilms with this dye.

## 8.2 Significance of Reported Work

The work I present here shows how simple kinetic models may be applied to estimate the kinetics of batch digestions with complex recovery patterns. This is only possible when concentrations of intermediate products are measured, such as semi-soluble chemical oxygen demand, or volatile fatty acids. I show how quantifying these intermediates is especially important after sludge pretreatment, when a large fraction of particulate COD is solubilized or semi-solubilized and present at the start of digestion. One challenge to quantifying the kinetics of anaerobic digestion has been that often multiple recovery events are observed. I show how these events are present during the digestion of simple and complex wastes. For simple wastes, multiple events correspond to the utilization of accumulated VFA intermediates. Complex wastes exhibit this pattern due to selective utilization of certain fractions of particulates, such as carbohydrates before lipids. This is one of the first instances of this delay in utilization of certain fractions being reported. I show a method for accurately modeling these events using multiple Gomperz kinetic expressions that incorporate different lag phases with subsequent first-order-like kinetics.

I compare results from the commonly used methanogenic and, relatively new, electrogenic batch digestion technique. I show that similar digestion rates are able to be measured in both systems when SSCOD or VFAs are incorporated, but while current from electrogenic digestions provides much more highly resolved rate information,

recovery is slower at loadings commonly present in anaerobic digestors and anode surface areas employed here. In instances when sludge pretreatment is performed, $CH_4$ + SSCOD provided the most accurate hydrolysis kinetics. For digestions with high food to microorganism loadings but no pretreatment, as is commonly the case in anaerobic digesters themselves, $CH_4$ + VFA and $CH_4$ + SSCOD yielded similar kinetic parameters, both more accurate than $CH_4$ alone. I show that this delay may also be due to pH inhibition in anode respiring biofilms. While measuring these gradients is essential to understanding limitations of MXC systems, I show that the only previously reported, non-invasive, optical method of measuring these gradients results in false-positives under all conditions when *Geobacter* biomass is present. I present a promising alternative measurement technique that does not appear to have the same drawbacks as the only previously reported method.

WORKS CITED

40 C.F.R. § 403 - General Pretreatment Regulations for Existing and New Sources of Pollution, 1978. 40 C.F.R. § 403 - General Pretreatment Regulations for Existing and New Sources of Pollution, Code of Federal Regulations.

40 C.F.R. § 508 - Standards For the Use or Disposal of Sewage Sludge, n.d. 40 C.F.R. § 508 - Standards For the Use or Disposal of Sewage Sludge, U.S. Code of Federal Regulations.

Aldin, S., Nakhla, G., Ray, M.B., 2011. Modeling the Influence of Particulate Protein Size on Hydrolysis in Anaerobic Digestion. Ind. Eng. Chem. Res. 50, 10843–10849. doi:10.1021/ie200385e

Andrews, J.S., Rolfe, S.A., Huang, W.E., Scholes, J.D., Banwart, S.A., 2010. Biofilm formation in environmental bacteria is influenced by different macromolecules depending on genus and species. Environ Microbiol 12, 2496–2507. doi:10.1111/j.1462-2920.2010.02223.x

Angelidaki, I., Alves, M., Bolzonella, D., Borzacconi, L., Campos, J.L., Guwy, A.J., Kalyuzhnyi, S., Jenicek, P., van Lier, J.B., 2009. Defining the biomethane potential (BMP) of solid organic wastes and energy crops: a proposed protocol for batch assays. Water Science & Technology 59, 927–9. doi:10.2166/wst.2009.040

Appels, L., Baeyens, J., Degrève, J., Dewil, R., 2008. Principles and potential of the anaerobic digestion of waste-activated sludge. Progress in Energy and Combustion Science 34, 755–781. doi:10.1016/j.pecs.2008.06.002

Appels, L., Degrève, J., Van der Bruggen, B., Van Impe, J., Dewil, R., 2010. Influence of low temperature thermal pre-treatment on sludge solubilisation, heavy metal release and anaerobic digestion. Bioresource Technology 101, 5743–5748. doi:10.1016/j.biortech.2010.02.068

Avnir, Y., Barenholz, Y., 2005. pH determination by pyranine: Medium-related artifacts and their correction. Analytical Biochemistry 347, 34–41. doi:10.1016/j.ab.2005.09.026

Babuata, J.T., Nguyen, H.D., Harrington, T.D., Renslow, R., Beyenal, H., 2012. pH, Redox Potential and Local Biofilm Potential Microenvironments Within *Geobacter sulfurreducens* Biofilms and Their Roles in Electron Transfer. Biotechnology and Bioengineering 109, 2651–2662. doi:10.1002/bit.24538/abstract)

Batstone, D.J., Keiler, J., Angelidaki, I., Kalyuzhnyi, S.V., Pavlostathis, S.G., Rozzi, A., Sanders, W.T.M., Siegrist, H., Vavilin, V.A., 2002. The IWA Anaerobic Digestion Model No 1 (ADM1). Water Science & Technology 45, 65–73.

Batstone, D.J., Puyol, D., Flores-Alsina, X., Rodríguez, J., 2015. Mathematical modelling of anaerobic digestion processes: applications and future needs. Rev Environ Sci Biotechnol 14, 595–613. doi:10.1007/s11157-015-9376-4

Bolzonella, D., Fatone, F., Pavan, P., Cecchi, F., 2005. Anaerobic Fermentation of Organic Municipal Solid Wastes for the Production of Soluble Organic Compounds. Ind. Eng. Chem. Res. 44, 3412–3418. doi:10.1021/ie048937m

Bougrier, C., Delgenès, J.P., Carrère, H., 2008. Effects of thermal treatments on five different waste activated sludge samples solubilisation, physical properties and anaerobic digestion. CHEMICAL ENGINEERING JOURNAL 139, 236–244. doi:10.1016/j.cej.2007.07.099

Burger, G., Parker, W., 2013. Investigation of the impacts of thermal pretreatment on waste activated sludge and development of a pretreatment model. Water Research 47, 5245–5256. doi:10.1016/j.watres.2013.06.005

Cai, M., Liu, J., Wei, Y., 2004. Enhanced Biohydrogen Production from Sewage Sludge with Alkaline Pretreatment. Environ. Sci. Technol. 38, 3195–3202. doi:10.1021/es0349204

Cano, R., Pérez-Elvira, S.I., Fdz-Polanco, F., 2015. Energy feasibility study of sludge pretreatments: A review. Applied Energy 149, 176–185. doi:10.1016/j.apenergy.2015.03.132

Carlsson, M., Lagerkvist, A., Morgan-Sagastume, F., 2012. The effects of substrate pre-treatment on anaerobic digestion systems: A review. Waste Management 32, 1634–1650. doi:10.1016/j.wasman.2012.04.016

Carrère, H., Dumas, C., Battimelli, A., Batstone, D.J., Delgenès, J.P., Steyer, J.P., Ferrer, I., 2010. Pretreatment methods to improve sludge anaerobic degradability: A review. Journal of Hazardous Materials 183, 1–15. doi:10.1016/j.jhazmat.2010.06.129

Chang, C.-N., Lin, J.-G., Huang, S.-J., 1997. Alkaline and ultrasonic pretreatment of sludge before anaerobic digestion. Water Science & Technology 36, 155–162.

Chen, C.-C., Chuang, Y.-S., Lin, C.-Y., Lay, C.-H., Sen, B., 2012. Thermophilic dark fermentation of untreated rice straw using mixed cultures for hydrogen production. International Journal of Hydrogen Energy 37. doi:10.1016/j.ijhydene.2012.01.036

Chosterton, J.W., Geesey, G.G., Cheng, K.J., 1978. How Bacteria Stick. Scientific American 238, 86–95.

Chynoweth, D.P., Turick, C.E., Owens, J.M., Jerger, D.E., 1993. Biochemical Methane Potential of Biomass and Waste Feedstocks. Biomass and Bioenergy 5, 95–111.

Clesceri, L.S., Greenberg, A.E., Eaton, A.D., 1998. Standard Methods for the Examination of Water and Wastewater, 20th Edition.

Dandikas, V., Heuwinkel, H., Lichti, F., Eckl, T., Drewes, J.E., Koch, K., 2018. Correlation between hydrolysis rate constant and chemical composition of energy crops. Renewable Energy 118, 34–42. doi:10.1016/j.renene.2017.10.100

De Feo, G., Antoniou, G., Fardin, H., El-Gohary, F., Zheng, X., Reklaityte, I., Butler, D., Yannopoulos, S., Angelakis, A., 2014. The Historical Development of Sewers Worldwide. Sustainability 6, 3936–3974. doi:10.3390/su6063936

Debabov, V.G., 2008. Electricity from microorganisms. Microbiology 77, 123–131. doi:10.1134/S002626170802001X

Donlan, R.M., 2002. Biofilms: Microbial Life on Surfaces. Emerging Infectious Diseases 8, 881–890.

Donoso-Bravo, A., Ortega, V., Lesty, Y., Bossche, H.V., Olivares, D., 2019. Addressing the synergy determination in anaerobic co-digestion and the inoculum activity impact on BMP test. Water Science & Technology 80, 387–396. doi:10.2166/wst.2019.292

Dubois, M., Gilles, K.A., Hamilton, J.K., Rebers, P.A., Smith, F., 1956. Colorimetric Method for Deterimination of Sugars and Related Substances. Anal. Chem. 28, 350–356.

Eastman, J.A., Ferguson, J.F., 1981. Solubilization of Particulate Organic Carbon during the Acid Phase of Anaerobic Digestion. Water Pollution Control Federation 1–16.

Eskicioglu, C., Kennedy, K.J., Droste, R.L., 2006. Characterization of soluble organic matter of waste activated sludge before and after thermal pretreatment. Water Research 40, 3725–3736. doi:10.1016/j.watres.2006.08.017

Franks, A.E., Nevin, K.P., Jia, H., Izallalen, M., Woodard, T.L., Lovely, D.R., 2009. Novel strategy for three-dimensional real-time imaging of microbial fuel cell communities: monitoring the inhibitory effects of proton accumulation within the anode biofilm. Energy Environ. Sci. 2, 113–119. doi:10.1016/S0162-0908(08)79352-8

Girault, R., Bridoux, G., Nauleau, F., Poullain, C., Buffet, J., Steyer, J.P., Sadowski, A.G., Béline, F., 2012. A waste characterisation procedure for ADM1 implementation based on degradation kinetics. Water Research 46, 4099–4110. doi:10.1016/j.watres.2012.04.028

Gompertz, B., 1825. On the Nature of the Function Expressive of the Law of Human Mortality, and on a New Mode of Determining the Value of Life Contingencies. Philosophical Transactions of the Royal Society of London 115, 513–583.

Gonzalez, A., Hendriks, A.T.W.M., van Lier, J.B., de Kreuk, M., 2018. Pre-treatments to enhance the biodegradability of waste activated sludge: Elucidating the rate limiting step. Biotechnology Advances 36, 1434–1469. doi:10.1016/j.biotechadv.2018.06.001

Hansen, T.L., Schmidt, J.E., Angelidaki, I., Marca, E., Jansen, J.L.C., Mosbæk, H., Christensen, T.H., 2004. Method for determination of methane potentials of solid organic waste. Waste Management 24, 393–400. doi:10.1016/j.wasman.2003.09.009

Hobbs, S.R., Landis, A.E., Rittmann, B.E., Young, M.N., Parameswaran, P., 2017. Enhancing anaerobic digestion of food waste through Biochemical Methane Potential Assays at different substrate: inoculum ratios. Journal of Industrial Microbiology & Biotechnology 1–33.

Holliger, C., Alves, M., Andrade, D., Angelidaki, I., Astals, S., Baier, U., Bougrier, C., Buffiere, P., Carballa, M., de Wilde, V., Ebertseder, F., Fernandez, B., Ficara, E., Fotidis, I., Frigon, J.-C., de Laclos, H.F., Ghasimi, D.S.M., Hack, G., Hartel, M., Heerenklage, J., Horvath, I.S., Jenicek, P., Koch, K., Krautwald, J., Lizasoain, J., Liu, J., Mosberger, L., Nistor, M., Oechsner, H., Oliveira, J.V., Paterson, M., Pauss, A., Pommier, S., Porqueddu, I., Raposo, F., Ribeiro, T., Pfund, F.R., Stromberg, S., Torrijos, M., van Eekert, M., van Lier, J., Wedwitschka, H., Wierinck, I., 2016. Towards a standardization of biomethane potential tests. Water Science & Technology 74, 2515–2522. doi:10.2166/wst.2016.336

Hou, J., Liu, Z., Zhou, Y., Chen, W., Li, Y., Sang, L., 2017. An experimental study of pH distributions within an electricity-producing biofilm by using pH microelectrode. Electrochimica Acta 251, 187–194. doi:10.1016/j.electacta.2017.08.101

Hunter, R.C., Beveridge, T.J., 2005. Application of a pH-Sensitive Fluoroprobe (C-SNARF-4) for pH Microenvironment Analysis in Pseudomonas aeruginosa Biofilms. Applied and Environmental Microbiology 71, 2501–2510. doi:10.1128/AEM.71.5.2501-2510.2005

Ingenieure, D.V.D., 2006. VDI 4630. Fermentation of organic materials - characterisation of the substrate, sampling, collection of material data, fermentation tests.

Jeanson, S., Floury, J., Issulahi, A.A., Madec, M.-N., Thierry, A., Lortal, S., 2013. Micrograd ients of pH Do Not Occur around Lactococcus Colonies in a Model Cheese. Applied and Environmental Microbiology 79, 6516–6518. doi:10.1128/AEM.01678-13

Kim, J., Park, C., Kim, T.-H., Lee, M., Kim, S., Kim, S.-W., Lee, J., 2003. Effects of various pretreatments for enhanced anaerobic digestion with waste activated sludge. Journal of Bioscience and Bioengineering 95, 271–275. doi:10.1016/S1389-1723(03)80028-2

Klusmann, E., Shultze, J.W., 1997. pH-microscopy-theoretical and experimental investigations. Electrochimica Acta 42, 3123–3134.

Koch, K., Drewes, J.E., 2014. Alternative approach to estimate the hydrolysis rate constant of particulate material from batch data. Applied Energy 120, 11–15. doi:10.1016/j.apenergy.2014.01.050

Koch, K., Helmreich, B., Drewes, J.E., 2015a. Co-digestion of food waste in municipal wastewater treatment plants: Effect of different mixtures on methane yield and hydrolysis rate constant. Applied Energy 137, 250–255. doi:10.1016/j.apenergy.2014.10.025

Koch, K., Helmreich, B., Drewes, J.E., 2015b. Co-digestion of food waste in municipal wastewater treatment plants: Effect of different mixtures on methane yield and hydrolysis rate constant. Applied Energy 137, 250–255. doi:10.1016/j.apenergy.2014.10.025

Koch, K., Helmreich, B., Drewes, J.E., 2014. Co-digestion of food waste in municipal wastewater treatment plants: Effect of different mixtures on methane yield and hydrolysis rate constant. Applied Energy 137, 250–255. doi:10.1016/j.apenergy.2014.10.025

Lay, C.-H., Chang, F.Y., Chu, C.Y., Chen, C.-C., Chi, Y.C., Hsieh, T.T., Huang, H.H., Lin, C.-Y., 2011. Enhancement of anaerobic biohydrogen/methane production from cellulose using heat-treated activated sludge. Water Science & Technology.

Lay, J.-J., Li, Y.-Y., Noike, T., 1996. Effect of Moisture Content and Chemical Nature on Methane Fermentation Characteristics of Municipal Solid Wastes. J. Environ. Syst. and Eng. 101–108.

Lee, H.-S., Parameswaran, P., Kato Marcus, A., Torres, C.I., Rittmann, B.E., 2008. Evaluation of energy-conversion efficiencies in microbial fuel cells (MFCs) utilizing fermentable and non-fermentable substrates. Water Research 42, 1501–1510. doi:10.1016/j.watres.2007.10.036

Lee, I.-S., Parameswaran, P., Alder, J.M., Rittmann, B.E., 2010. Feasibility of Focused-Pulsed Treated Waste Activated Sludge as a Supplemental Electron Donor for Denitrification. Water Environment Research 82, 1–10. doi:10.2175/10614301

Li, Y., Jin, Y., Li, J., Li, H., Yu, Z., 2016. Effects of thermal pretreatment on the biomethane yield and hydrolysis rate of kitchen waste. Applied Energy 172, 47–58. doi:10.1016/j.apenergy.2016.03.080

Liu, J., Diwu, Z., Leung, W.-Y., 2001. Synthesis and Photophysical Properties of New Fluorinated Benzo[c]xanthene Dyes as Intracellular pH Indicators. Bioorganic Medicinal Chemistry Letters 11, 2903–2905.

Liu, Y., Bond, D.R., 2012. Long-Distance Electron Transfer by G. sulfurreducens Biofilms Results in Accumulation of Reduced c-Type Cytochromes. ChemSusChem 5, 1047–1053. doi:10.1002/cssc.201100734

Llabrés-Luengo, P., Mata-Alvarez, J., 1987. Kinetic Study of the Anaerobic Digestion of Straw-Pig Manure Mixtures. Biomass 14, 129–142.

Lusk, B.G., Colin, A., Parameswaran, P., Rittmann, B.E., Torres, C.I., 2017. Simultaneous fermentation of cellulose and current production with an enriched mixed culture of thermophilic bacteria in a microbial electrolysis cell. Microb. Biotechnol. 11, 63–73. doi:10.1111/1751-7915.12733

Madigan, M.T., Martinko, J.M., Bender, K.S., Buckley, D.H., Stahl, D.A., 2015. Brock Biology of Microorganisms. Pearson Education.

Marcotte, N., Brouwer, A.M., 2005. Carboxy SNARF-4F as a Fluorescent pH Probe for Ensemble and Fluorescence Correlation Spectroscopies. J. Phys. Chem. B 109, 11819–11828. doi:10.1021/jp0510138

Marcus, A.K., Torres, C.I., Rittmann, B.E., 2011. Analysis of a microbial electrochemical cell using the proton condition in biofilm (PCBIOFILM) model. Bioresource Technology 102, 253–262. doi:10.1016/j.biortech.2010.03.100

Marcus, A.K., Torres, C.I., Rittmann, B.E., 2010. Evaluating the impacts of migration in the biofilm anode using the model PCBIOFILM. Electrochimica Acta 55, 6964–6972. doi:10.1016/j.electacta.2010.06.061

McCarty, P.L., Bae, J., Kim, J., 2011. Domestic Wastewater Treatment as a Net Energy Producer–Can This be Achieved? Environ. Sci. Technol. 45, 7100–7106. doi:10.1021/es2014264

miron, Y., zeeman, G., van lier, J.B., lettinga, G., 2000. The role of sludge retention time in the hydrolysis and acidification of lipids, carbohydrates and proteins during digestion of primary sludge in CSTR systems. Water Research 34, 1705–1713.

Monod, J., 1949. The Growth of Bacterial Cultures. Annu. Rev. Microbiol. 3, 371–394.

Morgenroth, E., Kommedal, R., Harremoës, P., 2002. Processes and modeling of hydrolysis of particulate organic matter in aerobic wastewater treatment - a review. Water Science & Technology 45, 25–40.

Nagler, M., Aichinger, P., Kuprian, M., Pümpel, T., Insam, H., Ebner, C., 2016. A case study for a cost-benefit-based, stepwise optimization of thermo-chemical WAS pre-treatment for anaerobic digestion. Journal of Material Cycles and Waste Management 20, 266–273. doi:10.1007/s10163-016-0577-x

Nazari, L., Yuan, Z., Santoro, D., Sarathy, S., Ho, D., Batstone, D., Xu, C.C., Ray, M.B., 2017. Low-temperature thermal pre-treatment of municipal wastewater sludge: Process optimization and effects on solubilization and anaerobic degradation. Water Research 113, 111–123. doi:10.1016/j.watres.2016.11.055

Neves, L., Oliveira, R., Alves, M.M., 2006. Anaerobic co-digestion of coffee waste and sewage sludge. Waste Management 26, 176–181. doi:10.1016/j.wasman.2004.12.022

North East Biosolids and Residuals Association, 2007. A National Biosolids Regulation, Quality, End Use & Disposal Survey.

Owen, W.F., Stuckey, D.C., Healy, J.B., Jr, Young, L.Y., McCarty, P.L., 1979. Bioassay for Monitoring Biochemical Methane Potential and Anaerobic Toxicity. Water Research 13, 485–492.

Parameswaran, P., Rittmann, B.E., 2012. Feasibility of anaerobic co-digestion of pig waste and paper sludge. Bioresource Technology 124, 163–168. doi:10.1016/j.biortech.2012.07.116

Parameswaran, P., Torres, C.I., Lee, H.-S., Krajmalnik-Brown, R., Rittmann, B.E., 2009. Syntrophic interactions among anode respiring bacteria (ARB) and Non-ARB in a biofilm anode: electron balances. Biotechnology and Bioengineering 103, 513–523. doi:10.1002/bit.22267

Parameswaran, P., Zhang, H., Torres, C.S.I., Rittmann, B.E., Krajmalnik-Brown, R., 2010. Microbial community structure in a biofilm anode fed with a fermentable substrate: The significance of hydrogen scavengers. Biotechnology and Bioengineering 105, 69–78. doi:10.1002/bit.22508

Parkin, G.F., Owen, W.F., 1987. Fundamentals of Anaerobic Digestion of Wastewater Sludges. Journal of Environmental Engineering 867–920.

Pavlostathis, S.G., Giraldo Gomez, E., 1991. Kinetics of anaerobic treatment: A critical review. Critical Reviews in Environmental Control 21, 411–490. doi:10.1080/10643389109388424

Pavlostathis, S.G., Gossett, J.M., 1988. Preliminary Conversion Mechanisms in Anaerobic Digestion of Biological Sludges. J. Environ. Eng. 114, 575–592.

Peces, M., Pozo, G., Koch, K., Dosta, J., Astals, S., 2020. Exploring the potential of co-fermenting sewage sludge and lipids in a resource recovery scenario. Bioresource Technology 300, 122561. doi:10.1016/j.biortech.2019.122561

Pečar, D., Pohleven, F., Goršek, A., 2020. Kinetics of methane production during anaerobic fermentation of chicken manure with sawdust and fungi pre-treated wheat straw. Waste Management 102, 170–178. doi:10.1016/j.wasman.2019.10.046

Popat, S.C., Ki, D., Young, M.N., Rittmann, B.E., Torres, C.I., 2014. Buffer pKa and Transport Govern the Concentration Overpotential in Electrochemical Oxygen Reduction at Neutral pH. CHEMELECTROCHEM 1, 1909–1915. doi:10.1002/celc.201402058

Rabaey, K., Verstraete, W., 2005. Microbial fuel cells: novel biotechnology for energy generation. Trends in Biotechnology 23, 291–298. doi:10.1016/j.tibtech.2005.04.008

Rincón, B., Banks, C.J., Heaven, S., 2010. Biochemical methane potential of winter wheat (*Triticum aestivum L.*): Influence of growth stage and storage practice. Bioresource Technology 101, 8179–8184. doi:10.1016/j.biortech.2010.06.039

Rittmann, B.E., 2008. Opportunities for renewable bioenergy using microorganisms. Biotechnology and Bioengineering 100, 203–212. doi:10.1002/bit.21875

Rittmann, B.E., Lee, H.-S., Zhang, H., Alder, J., Banaszak, J.E., Lopez, R., 2008. Full-scale application of focused-pulsed pre-treatment for improving biosolids digestion and conversion to methane. Water Science & Technology 58, 1895–7. doi:10.2166/wst.2008.547

Rittmann, B.E., McCarty, P.L., 2001. Environmental biotechnology. McGraw-Hill Science/Engineering/Math.

Rivera-Cancel, G., Sanders, J.M., Hay, A.G., 2012. Kinetics of hydrolysis and mutational analysis of N,N-diethyl-m-toluamide hydrolase from Pseudomonas putida DTB. FEBS Journal 279, 1044–1053. doi:10.1111/j.1742-4658.2012.08495.x

Salerno, M.B., Lee, H.-S., Parameswaran, P., Rittmann, B.E., 2009. Using a Pulsed Electric Field as a Pretreatment for Improved Biosolids Digestion and Methanogenesis. Water Environment Research 81, 831–839. doi:10.2175/106143009X407366

Sanders, W.T.M., Geerink, M., Zeeman, G., Lettinga, G., 2000. Anaerobic hydrolysis kinetics of particulate substrates. Water Science & Technology 41, 17–24.

Schädlich, A., Kempe, S., Mäder, K., 2014. Non-invasive in vivo characterization of microclimate pH inside in situ forming PLGA implants using multispectral fluorescence imaging. Journal of Controlled Release 179, 52–62. doi:10.1016/j.jconrel.2014.01.024

Schlafer, S., Baelum, V., Dige, I., 2018a. Improved pH-ratiometry for the three-dimensional mapping of pH microenvironments in biofilms under flow conditions. Journal of Microbiological Methods 152, 194–200. doi:10.1016/j.mimet.2018.08.007

Schlafer, S., Dige, I., 2016. Ratiometric Imaging of Extracellular pH in Dental Biofilms. JoVE 1–7. doi:10.3791/53622

Schlafer, S., Garcia, J.E., Greve, M., Raarup, M.K., Nyvad, B., Dige, I., 2015. Ratiometric Imaging of Extracellular pH in Bacterial Biofilms with C-SNARF-4. Applied and Environmental Microbiology 81, 1267–1273. doi:10.1128/AEM.02831-14

Schlafer, S., Kamp, A., Garcia, J.E., 2018b. A confocal microscopy based method to monitor extracellular pH in fungal biofilms. FEMS Yeast Research 1–8. doi:10.1093/femsyr/foy049

Schlafer, S., Raarup, M.K., Meyer, R.L., Sutherland, D.S., Dige, I., Nyengaard, J.R., Nyvad, B., 2011. pH Landscapes in a Novel Five-Species Model of Early Dental Biofilm. PLoS ONE 6, e25299–12. doi:10.1371/journal.pone.0025299

Shizas, I., Bagley, D.M., 2004. Experimental Determination of Energy Content of Unknown Organics in Municipal Wastewater Streams. Journal of Energy Engineering 45–53.

Sosa-Hernández, O., Parameswaran, P., Alemán-Nava, G.S., Torres, C.I., Parra-Saldívar, R., 2016. Evaluating biochemical methane production from brewer's spent yeast. Journal of Industrial Microbiology & Biotechnology 43, 1195–1204. doi:10.1007/s10295-016-1792-0

Stanley, N.R., Lazazzera, B.A., 2004. Environmental signals and regulatory pathways that influence biofilm formation. Molecular Microbiology 52, 917–924. doi:10.1111/j.1365-2958.2004.04036.x

Stephen, C.S., LaBelle, E.V., Brantley, S.L., Bond, D.R., 2014. Abundance of the Multiheme c-Type Cytochrome OmcB Increases in Outer Biofilm Layers of Electrode-Grown Geobacter sulfurreducens. PLoS ONE 9, e104336–10. doi:10.1371/journal.pone.0104336

Stromberg, S., Nistor, M., Liu, J., 2014. Towards eliminating systematic errors caused by the experimental conditions in Biochemical Methane Potential (BMP) tests. Waste Management 34, 1939–1948. doi:10.1016/j.wasman.2014.07.018

Stuckey, D.C., McCarty, P.L., 1984. The effect of thermal pretreatment on the anaerobic biodegradability and toxicity of waste activated sludge. Water Research 18, 1343–1353.

Sun, H., Angelidaki, I., Wu, S., Dong, R., & Zhang, Y. (2019). The Potential of Bioelectrochemical Sensor for Monitoring of Acetate During Anaerobic Digestion: Focusing on Novel Reactor Design. *Frontiers in Microbiology*, *9*, 1–10. http://doi.org/10.3389/fmicb.2018.03357

Tandukar, M., Pavlostathis, S.G., 2015. Co-digestion of municipal sludge and external organic wastes for enhanced biogas production under realistic plant constraints. Water Research 87, 432–445. doi:10.1016/j.watres.2015.04.031

Tchobanoglous, G., Stensel, H.D., Tsuchihashi, R., Burton, F., 2014. Wastewater Engineering: Treatment and Resource Recovery, Metcalf and Eddy, Fifth Edition. ed. McGraw Hill.

Tejedor-Sanz, S., Fernández-Labrador, P., Hart, S., Torres, C.I., Esteve-Núñez, A., 2018. Geobacter Dominates the Inner Layers of a Stratified Biofilm on a Fluidized Anode During Brewery Wastewater Treatment. Front. Microbiol. 9, 1919–12. doi:10.3389/fmicb.2018.00378

Thauer, R.K., Kaster, A.-K., Seedorf, H., Buckel, W., Hedderich, R., 2008. Methanogenic archaea: ecologically relevant differences in energy conservation. Nat Rev Micro 6, 579–591. doi:10.1038/nrmicro1931

Tong, X., Smith, L.H., McCarty, P.L., 1990. Methane Fermentation of Selected Lignocellulosic Materials. Biomass 239–255.

Torres, C., 2012. Improving microbial fuel cells. Membrane Technology 2012, 8–9. doi:10.1016/S0958-2118(12)70165-9

Torres, C.I., Kato Marcus, A., Rittmann, B.E., 2008. Proton transport inside the biofilm limits electrical current generation by anode-respiring bacteria. Biotechnology and Bioengineering 100, 872–881. doi:10.1002/bit.21821

Torres, C.I., Kato Marcus, A., Rittmann, B.E., 2007. Kinetics of consumption of fermentation products by anode-respiring bacteria. Appl Microbiol Biotechnol 77, 689–697. doi:10.1007/s00253-007-1198-z

Torres, C.I., Krajmalnik-Brown, R., Parameswaran, P., Marcus, A.K., Wanger, G., Gorby, Y.A., Rittmann, B.E., 2009. Selecting Anode-Respiring Bacteria Based on Anode Potential: Phylogenetic, Electrochemical, and Microscopic Characterization. Environ. Sci. Technol. 43, 9519–9524. doi:10.1021/es902165y

Torres, C.I., Marcus, A.K., Lee, H.-S., Parameswaran, P., Krajmalnik-Brown, R., Rittmann, B.E., 2010. A kinetic perspective on extracellular electron transfer by anode-respiring bacteria. FEMS Microbiol Rev 34, 3–17. doi:10.1111/j.1574-6976.2009.00191.x

Toutian, V., Barjenbruch, M., Unger, T., Loderer, C., Remy, C., 2020. Effect of temperature on biogas yield increase and formation of refractory COD during thermal hydrolysis of waste activated sludge. Water Research 171, 115383–11. doi:10.1016/j.watres.2019.115383

Trzcinski, A.P., Stuckey, D.C., 2012. Determination of the Hydrolysis Constant in the Biochemical Methane Potential Test of Municipal Solid Waste. Environmental Engineering Science 29, 848–854. doi:10.1089/ees.2011.0105

U.S. Environmental Protection Agency, 2015. Clean Watersheds Needs Survey 2012 Report to Congress 1–41.

U.S. Environmental Protection Agency, 2004. Primer for Municipal Wastewater Treatment Systems.

U.S. Environmental Protection Agency, 1999. Biosolids Generation, Use, and Disposal in The United States.

U.S. Federal Government, 2011. Federal Water Pollution Control Act.

United Nations, 2018. World Urbanization Prospects: The 2018 Revision.

Valli, M., Sauer, M., Branduardi, P., Borth, N., Porro, D., Mattanovich, D., 2005. Intracellular pH Distribution in Saccharomyces cerevisiae Cell Populations, Analyzed by Flow Cytometry. Applied and Environmental Microbiology 71, 1515–1521. doi:10.1128/AEM.71.3.1515-1521.2005

Vavilin, V.A., Angelidaki, I., 2004. Anaerobic degradation of solid material: Importance of initiation centers for methanogenesis, mixing intensity, and 2D distributed model. Biotechnology and Bioengineering 89, 113–122. doi:10.1002/bit.20323

Vavilin, V.A., Fernandez, B., Palatsi, J., Flotats, X., 2008. Hydrolysis kinetics in anaerobic degradation of particulate organic material: An overview. Waste Management 28, 939–951. doi:10.1016/j.wasman.2007.03.028

Vavilin, V.A., Rytov, S.V., Lokshina, L.Y., 1996. A Description of Hydrolysis Kinetics in Anaerobic Degradation of Particulate Organic Matter. Bioresource Technology 56, 229–237.

Veeken, A., Hamelers, B., 1999. Effect of temperature on hydrolysis rate of selected biowaste components. Bioresource Technology 249–254.

Veeken, A., Kalyuzhnyi, S., Scharff, H., Hamelers, B., 2000. Effect of pH and VFA on hydrolysis of organic solid waste. Journal of Environmental Engineering 126, 1076–1081.

Velasquez-Orta, S.B., Yu, E., Katuri, K.P., Head, I.M., Curtis, T.P., Scott, K., 2011. Evaluation of hydrolysis and fermentation rates in microbial fuel cells. Appl Microbiol Biotechnol 90, 789–798. doi:10.1007/s00253-011-3126-5

Vlyssides, A., 2004. Thermal-alkaline solubilization of waste activated sludge as a pre-treatment stage for anaerobic digestion. Bioresource Technology 91, 201–206. doi:10.1016/S0960-8524(03)00176-7

Wang, X., Feng, Y., Wang, H., Qu, Y., Yu, Y., Ren, N., Li, N., Wang, E., Lee, H., Logan, B.E., 2009. Bioaugmentation for Electricity Generation from Corn Stover Biomass Using Microbial Fuel Cells. Environ. Sci. Technol. 43, 6088–6093. doi:10.1021/es900391b

Xu, Y., Lu, Y., Zheng, L., Wang, Z., Dai, X., 2020. Effects of humic matter on the anaerobic digestion of sewage sludge: New insights from sludge structure. Chemosphere 243, 125421. doi:10.1016/j.chemosphere.2019.125421

Yasui, H., Goel, R., Li, Y.Y., Noike, T., 2008. Modified ADM1 structure for modelling municipal primary sludge hydrolysis. Water Research 42, 249–259. doi:10.1016/j.watres.2007.07.004

Young, M.N., Marcus, A.K., Rittmann, B.E., 2013. A Combined Activated Sludge Anaerobic Digestion Model (CASADM) to understand the role of anaerobic sludge recycling in wastewater treatment plant performance. Bioresource Technology 136, 196–204. doi:10.1016/j.biortech.2013.02.090

Zhang, H., Banaszak, J.E., Parameswaran, P., Alder, J., Krajmalnik-Brown, R., Rittmann, B.E., 2009a. Focused-Pulsed sludge pre-treatment increases the bacterial diversity and relative abundance of acetoclastic methanogens in a full-scale anaerobic digester. Water Research 43, 4517–4526. doi:10.1016/j.watres.2009.07.034

Zhang, H., Banaszak, J.E., Parameswaran, P., Alder, J., Krajmalnik-Brown, R., Rittmann, B.E., 2009b. Focused-Pulsed sludge pre-treatment increases the bacterial diversity and relative abundance of acetoclastic methanogens in a full-scale anaerobic digester. Water Research 43, 4517–4526. doi:10.1016/j.watres.2009.07.034

Zhang, L., Gao, R., Naka, A., Hendrickx, T.L.G., Rijnaarts, H.H.M., Zeeman, G., 2016. Hydrolysis rate constants at 10-20 C can be more than doubled by a short anaerobic pre-hydrolysis at 35 C. Water Research 104, 283–291. doi:10.1016/j.watres.2016.07.038

Zwietering, M.H., Jongenburger, I., Rombouts, F.M., Riet, K.V., 1990. Modeling of the Bacterial Growth Curve. Applied and Environmental Microbiology 56, 1875–1881.

# APPENDIX A

# SUPPLIMENTARY FIGURES

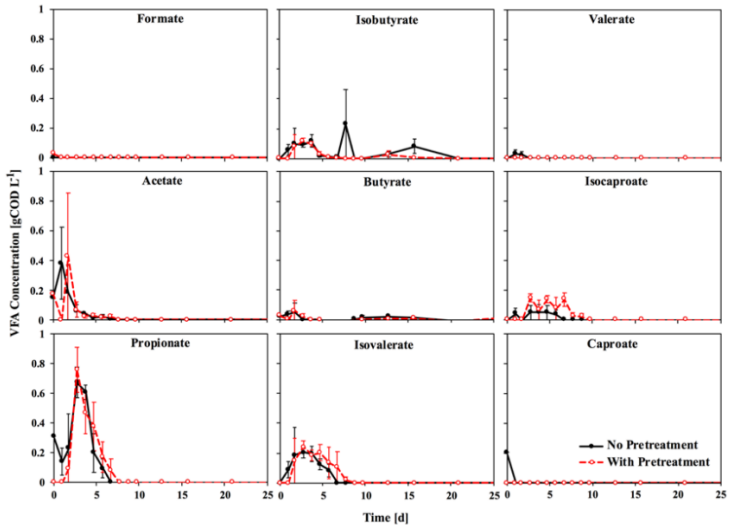


Figure S1 Individual VFA accumulation for all batch methanogenic digestions from chapter 4 as measured by HPLC. Red lines represent digestions without pretreatment; black lines represent digestions with thermally pretreated WAS. Error bars represent ± one standard error (n=3).

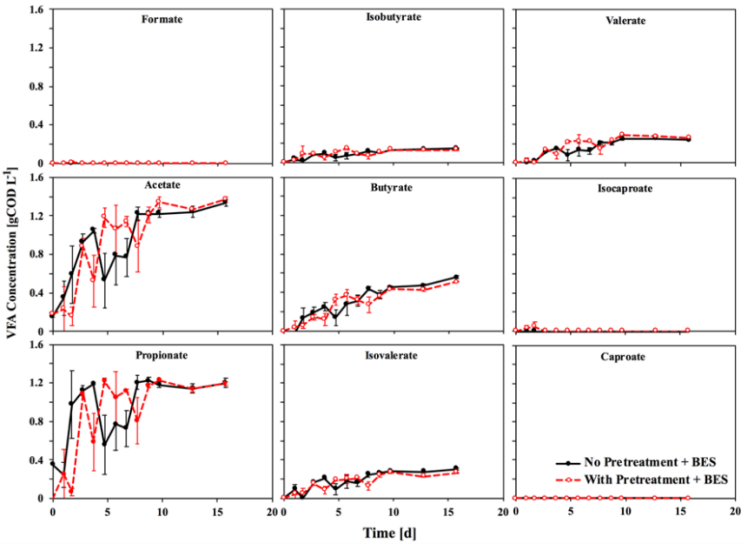


Figure S2 Individual VFA accumulation for all batch methanogenic digestions with BES from chapter 4 as measured by HPLC. Red lines represent digestions without pretreatment; black lines represent digestions with thermally pretreated WAS. Error bars represent ± one standard error (n=3).

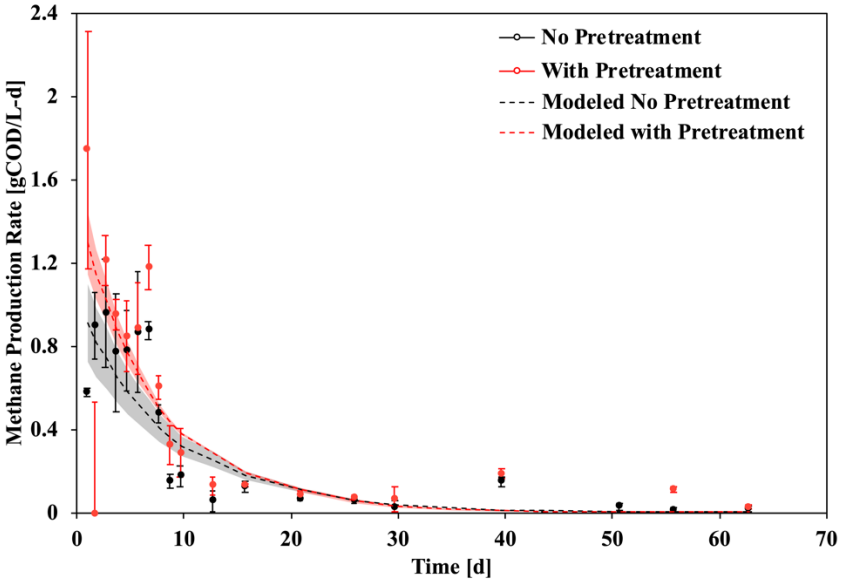


Figure S3 Methane recovery rates in batch methanogenic digestions from chapter 4. Solid points represent measured values from digestions with pretreatment (black) and without (red). Dashed lines represent modeled recovery rates from fitted parameters (Table 4.1). Error bars and shaded regions represent ± one standard error.

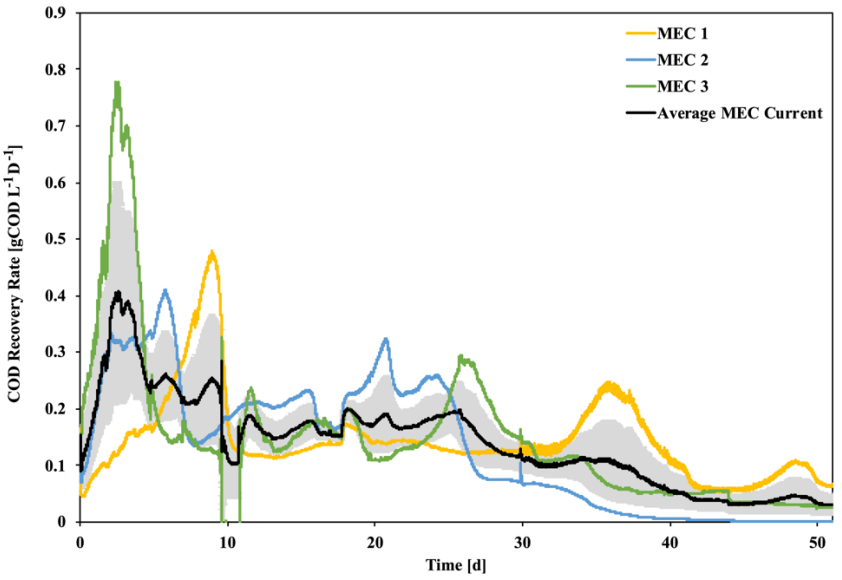


Figure S4 Individual current measured in each MEC reactor from chapter 6. The black line represents the average of three MECs, and the gray shaded area represents ± one standard error.

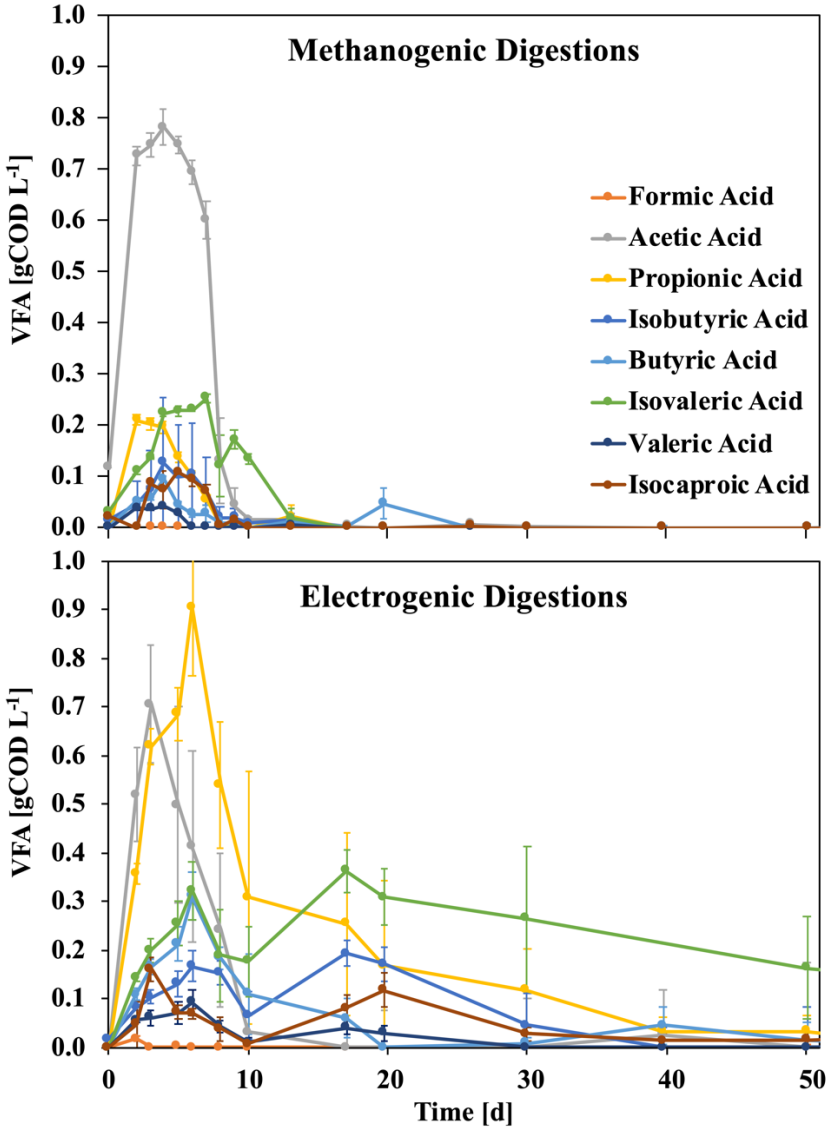


Figure S5 Average accumulations of individual VFAs from methanogenic (top) and electrogenic (bottom) digestions in chapter 6. Error bars represent ± one standard error.

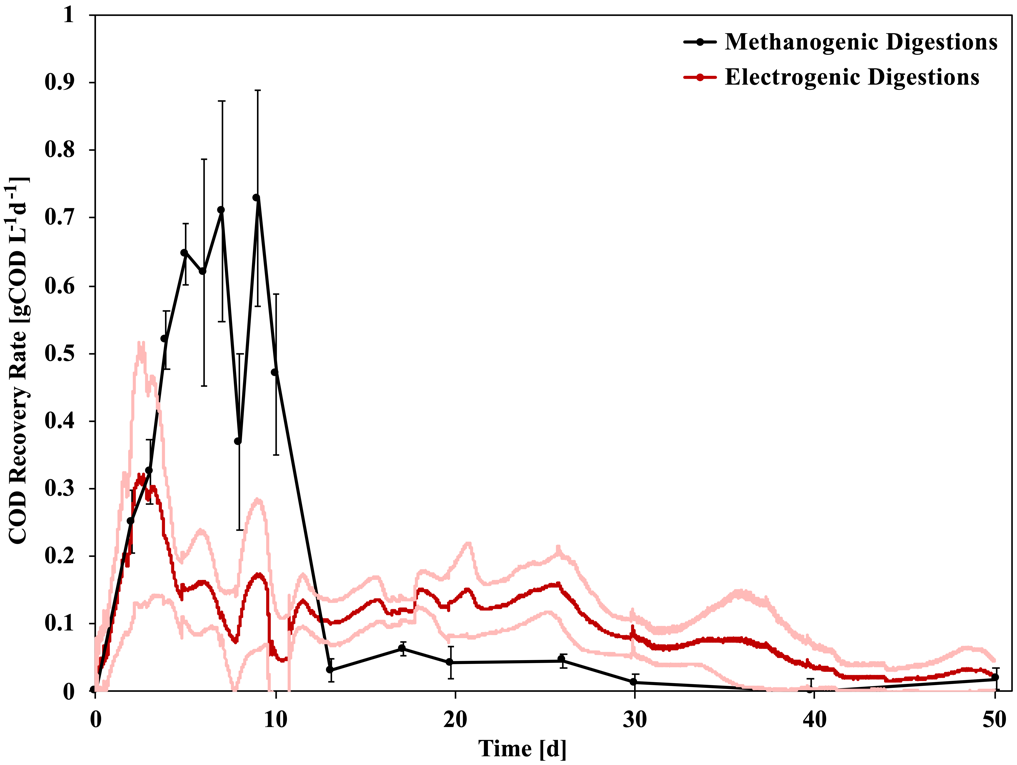


Figure S6 Average recovery rate of methane or circuited electrons from methanogenic and electrogenic batch digestions in chapter 6. Error bars and light red lines represent ± one standard error.

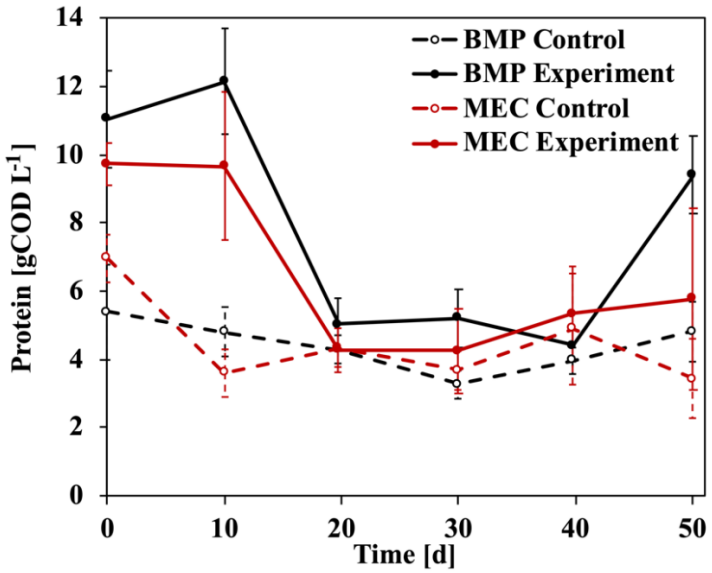


Figure S7 Protein concentrations in methanogenic and electrogenic digestions in chapter 6. Solid lines represent digestions with PS and WAS substrate and ADS inoculum; dashed lines represent control digestions with only ADS inoculum. Error bars represent ± one standard error.

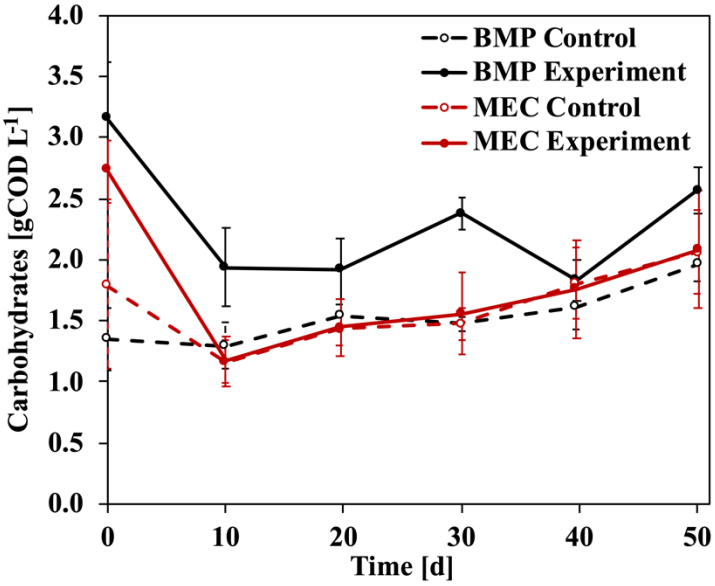


Figure S8 Carbohydrate concentrations in methanogenic and electrogenic digestions in chapter 6. Solid lines represent digestions with PS and WAS substrate and ADS inoculum; dashed lines represent control digestions with only ADS inoculum. Error bars represent ± one standard error.

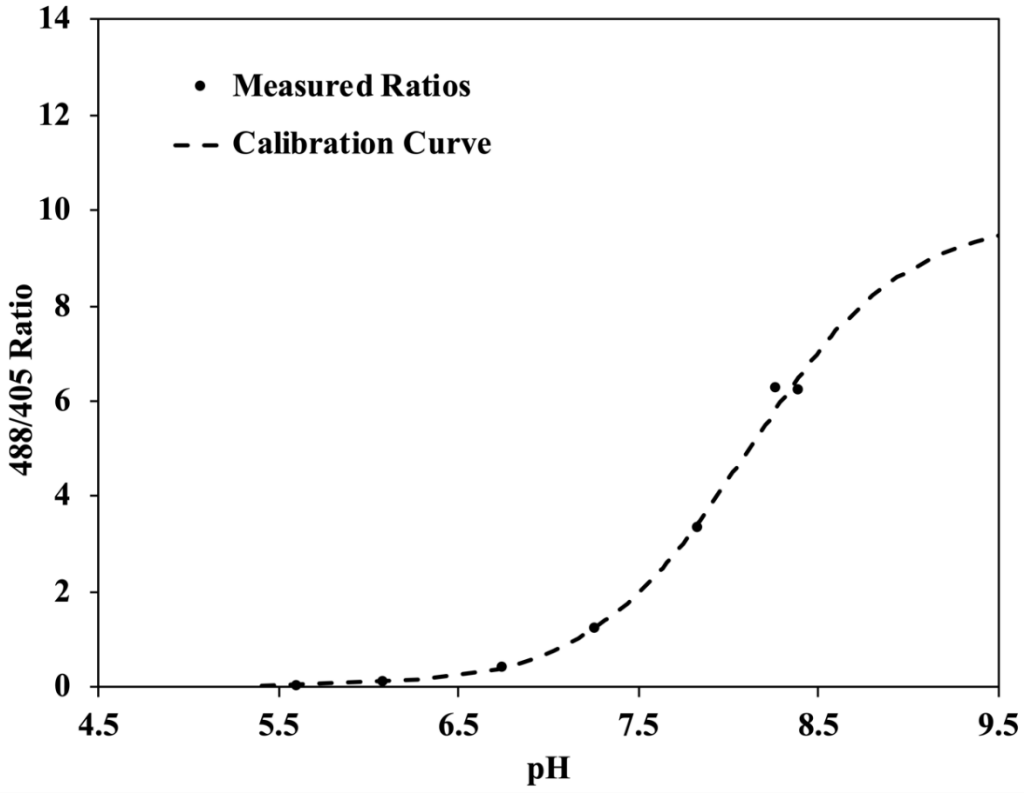


Figure S9 Calibration curve of HPTS in 30mM phosphate buffers at various pH values without biomass. Calibration was conducted in the MEFC with an ITO coverslip in place, but without any biomass. Points represent the average ratio from the bulk region of a z-stack. Dashed line represents the calibration curve fitted by the least squares technique.